

Structural Studies of Large Architectural Nucleoporins and Coat Proteins

by

James Richardson Ross Whittle

A.B., Chemistry
Harvard College, 2003

SUBMITTED TO THE DEPARTMENT OF BIOLOGY
IN PARTIAL FULFILLMENT OF THE REQUIREMENT FOR THE DEGREE OF
DOCTOR OF PHILOSOPHY
AT THE
MASSACHUSETTS INSTITUTE OF TECHNOLOGY
MAY 2010

© 2010 James Richardson Ross Whittle. All Rights Reserved.

The author hereby grants to MIT permission to reproduce and to distribute
publicly paper and electronic copies of this thesis document in whole or in part
in any medium now known or hereafter created.

Signature of Author _____
Department of Biology
May, 2010

Certified by _____
Thomas U. Schwartz
Associate Professor of Biology
Thesis Supervisor

Accepted by _____
Stephen P. Bell
Professor of Biology
Co-Chair, Biology Graduate Committee

Structural Studies of Large Architectural Nucleoporins and Coat Proteins

by
James R.R. Whittle

Abstract

The Nuclear Pore Complex (NPC) is a ~50 MDa protein complex that forms the sole conduit for macromolecular transport across the nuclear envelope. It assembles from ~30 proteins, termed nucleoporins or nups, symmetrically arranged about a central 8-fold axis. Some nucleoporins also contribute to other structures or perform diverse other functions. A subset forms a stably-associated core scaffold for the NPC, organized into two large subcomplexes, the Y-complex and the Nic96-complex. Studies using electron microscopy and X-ray crystallography have begun to elucidate the architecture of the NPC scaffold. To better understand the NPC and related proteins, two studies were performed:

1. The crystal structure of the C-terminal α -helical domain of Nup133 in complex with the C terminus of Nup107 revealed (with a prior structure of the N-terminal β -propeller domain of Nup133) the complete structure of Nup133 and its connection to the Y-complex. This contributes to a nearly complete molecular model of the Y-complex. Nup107•Nup133 forms the distal half of the stalk of the Y-complex. Sequence similarity between Nup133 and another nucleoporin, Nup170, was detected, and structural similarity proven by solving the structure of the α -helical domain of Nup170. Nup170 is a member of the Nic96-complex. Similarity between Nup133 and Nup170 suggests that the Y-complex and the Nic96-complex employ the same architectural principles.
2. Four nucleoporins contain an α -helical domain structurally related to the COPII coat protein Sec31. This domain is called the ancestral coatomer element 1 (ACE1). Sec13•Sec31 and Nup84•Nup145C•Sec13 complexes form analogous edge elements for the COPII coat and the NPC. A sequence-based search for other ACE1s identified the COPII accessory protein Sec16. Sec16 and Sec13 were shown to form a 2:2 heterotetramer. A crystal structure of Sec13•Sec16 revealed similarities to the Sec13•Sec31 edge element. Together with other structural and *in vivo* data, this result suggests that Sec13•Sec16 is a template for the Sec13•Sec31 coat.

These studies demonstrate that duplication of multiple classes of architectural proteins occurred in the evolution of the NPC and COPII coat, and support the hypothesis that these systems evolved from a common, ancestral membrane-coating complex.

Thesis Supervisor: Thomas U. Schwartz
Title: Associate Professor of Biology

Table of Contents

Abstract	3
Table of Contents	4
Figures and Tables	6
Acknowledgments	7
CHAPTER 1 Introduction	9
Overall structure of the Nuclear Pore Complex	10
Nucleocytoplasmic Transport	12
<i>Regulation of Nucleocytoplasmic Transport</i>	12
<i>Models of Selective Permeability of the Nuclear Pore Complex</i>	15
Composition of the NPC	18
<i>β-Propellers</i>	19
<i>α-Helical Domains</i>	20
Structures of Vesicle Coats	21
<i>Clathrin</i>	21
<i>COPI</i>	23
<i>COPII</i>	24
<i>Comparison of Clathrin and COPII</i>	26
Modularity as a Basis for Structural Characterization of the NPC	26
<i>A Hybrid Approach for Determining the Architecture of the NPC</i>	28
<i>An Alternative Computational Method</i>	28
Towards a Multiscale Model for the NPC	29
<i>The Y-complex</i>	29
<i>The Nic96-complex</i>	31
Specific Functions of Nucleoporins Nup133 and Nup170	33
<i>Nup133</i>	33
<i>Nup170</i>	34
Evidence for a Specific Relationship between COPII and NPC	36
Outlook	37
Figures	38
CHAPTER 2 Architectural nucleoporins Nup157/170 and Nup133 are structurally related and descend from a second ancestral element	47
Abstract	48
Introduction	48
Results	52
<i>Structure of the α-helical domain of Nup170</i>	52
<i>Nup133₅₁₇₋₁₁₅₆ adopts a quadripartite domain</i>	53
<i>Comparison to minimal interacting complex hNup107₆₅₈₋₉₂₅•hNup133₉₃₄₋₁₁₅₆</i>	54
<i>Structural comparison of Nup170 and Nup133</i>	55
<i>yNup170₉₇₉₋₁₅₀₂ has two conserved surface features</i>	55

<i>Comparison of Nup170 to Nup157</i>	57
Discussion	57
Methods	63
<i>Protein Expression and Purification</i>	63
<i>Protein Crystallization</i>	64
<i>Data Collection, Structure Solution and Refinement</i>	64
<i>Structure Analysis</i>	66
Figures	67
CHAPTER 3 Structure of the Sec13•Sec16 edge element, a template for assembly of the COPII vesicle coat	77
Abstract	78
Introduction	78
Results	81
<i>Structure of the Sec13•Sec16 tetramer</i>	81
Structural comparison of ACE1 edge elements	84
<i>Central Angle of the Edge Element</i>	85
<i>Domain-swapping of the Edge Element</i>	86
<i>Interlocking of the Edge Element</i>	87
Structure-based mutants of Sec31	88
<i>Solution behavior of Sec31 mutants Sec31EE and Sec31ΔL</i>	88
<i>Crystal structure of Sec13•Sec31ΔL</i>	89
<i>Complementation of sec16Δ or sec31Δ by structure-based mutants</i>	90
Discussion	92
<i>Sec16 as a template for the COPII coat</i>	95
<i>Model for the function of Sec16 in the COPII coat</i>	96
Methods	98
<i>Sequence Analysis</i>	98
<i>Protein Expression Constructs</i>	98
<i>Protein Preparation and Crystallization</i>	98
<i>Data Collection and Structure Solution</i>	99
<i>Analytical Ultracentrifugation and Size Exclusion Chromatography</i>	100
<i>Complementation Assay</i>	101
Figures	102
CHAPTER 4 Prospectus	119
Summary	120
Future Directions	120
<i>Nup107•Nup133 and Nup170</i>	120
<i>Sec16 in Assembly of the COPII coat</i>	123
Conclusion	125
References	127

Figures and Tables

Figure 1-1 Electron Microscopy of the NPC	38
Figure 1-2 Nucleocytoplasmic Transport mediated by Ran	39
Figure 1-3 Inventory of the NPC	40
Figure 1-4 β -Propeller	41
Figure 1-5 α -Helical Solenoid	41
Figure 1-6 Structure of Clathrin	42
Figure 1-7 COPII Cage or Outer Coat	43
Figure 1-8 Subcomplex Map of the NPC	45
Figure 2-1 Nup170 ₉₇₉₋₁₅₀₂ forms a bipartite, irregular α -helical stack	67
Figure 2-2 Model and Electron Density for Nup170 ₉₇₉₋₁₅₀₂	68
Figure 2-3 Nup133 ₅₁₇₋₁₁₅₆ in complex with Nup107 ₆₅₈₋₉₂₅	69
Figure 2-4 Model and Electron Density for Novel Portion of Nup133 ₅₁₇₋₁₁₅₆	70
Figure 2-5 Topology of Nup170 and Nup133 α -helical domains is conserved	71
Figure 2-6 Surface conservation of Nup170 suggests two protein-protein interfaces	72
Figure 2-7 Schematic Representation of the Heptameric Nup84-complex, or Y-complex	73
Figure 2-8 Representative Nucleoporin α -Helical Stack Domains	74
Table 2-1 Proteins of the NPC Core Structural Scaffold	75
Table 2-2 Data Collection and Refinement Statistics	76
Figure 3-1 Summary of Ancestral Coatmer Element 1 (ACE1) Proteins	102
Figure 3-2 Multiple Sequence Alignment of the CCD of Sec16 Homologs	104
Figure 3-3 Hydrodynamic Characterization of Sec13•Sec16	105
Figure 3-4 Structural Comparison of Sec16 and Sec31	107
Figure 3-5 Structural Consequences of Temperature-Sensitive Alleles of Sec16	108
Figure 3-6 Interactions Formed by the ACE1 Crown	110
Figure 3-7 SA-omit Map of Sec16 Swap Loop	111
Figure 3-8 Solution Behavior and Crystal Structure of Sec13•Sec31 mutants	112
Figure 3-9 Electron Density at Sec31 Δ L Swap Hinge	113
Figure 3-10 Complementation of Sec16 or Sec31 by Structure-Based Mutations	115
Figure 3-11 Model for Assembly of the COPII Coat Complex	116
Table 3-1 Data Collection and Refinement Statistics	117

Acknowledgments

My friends and colleagues at M.I.T. have smoothed my way through this doctorate, and I owe them great gratitude.

Professor Thomas Schwartz has been a superb advisor. The collegial atmosphere he generates in lab has made this a great place to do research. I have fond memories of fishing crystals for the first time, trips to the synchrotron, and countless hours in the computer room troubleshooting programs (and trying to conquer our most challenging crystal—“the virus”).

Professors Chris Kaiser and Robert Sauer were on my committee, and consistently provided sound guidance. I was fortunate to have Professor Kaiser to consult, when our research on nucleoporins led me to study the COPII protein Sec16. Eric Spear and Darcy Morse in his lab were kind to teach me yeast techniques and often let me share their bench space. Professor Sauer takes a strong interest in graduate students. I’ve several times gone to him for advice, and he was always welcoming and thoughtful in providing it. His strong sense of which experiments to do—and which to skip—has helped speed me to publication and graduation.

Professor Iain Cheeseman let me briefly be part of his lab at the Whitehead Institute to do cell culture and imaging experiments. Julie Welburn in his lab has been a good friend.

James Partridge, Steve Brohawn and I started graduate school together. They’ve made the lab a lively place to be, and made doing research much easier and more fun. Sandra Jeudy and Thomas Böhmer, as well as Thomas Neiland, were post-docs and good friends. Nina Leksa, Silvija Bilokapi, Brian Sosa, and several new additions to the lab have helped make this experience enjoyable. Upstairs, Bob Grant and Steven Glynn often helped with crystallography.

My parents, Richard and Faye, continue to be the foundation for my success. My fiancée, Lauren, helped me steer the course to the finish, and is an unfailing source of encouragement.

Für Henning Friedrich.

Er war ein wahrer Freund.

CHAPTER 1 Introduction

Overall structure of the Nuclear Pore Complex

Eukaryotic cells segregate their genetic material in a nucleus. The nucleus is an organelle enclosed by a double lipid bilayer called the nuclear envelope (NE). The NE is fenestrated at discrete intervals where inner nuclear membrane (INM) and outer nuclear membrane (ONM) fuse, forming nuclear pores. The number of nuclear pores ranges from ~200 per nucleus in yeast to ~5,000 in proliferating human cells (Cordes et al., 1995; Rout and Blobel, 1993; Winey et al., 1997). Ions, metabolites and other small molecules diffuse freely across the NE through nuclear pores (a process called passive transport). Macromolecules greater than 30 kDa cross only when bound to dedicated nuclear transport receptors, termed importins and exportins, or karyopherins (a process called facilitated transport) (Görlich and Kutay, 1999). The nuclear pore is selectively permeable: most macromolecules are excluded, though others (some much larger) pass freely. This selective permeability barrier is established by the Nuclear Pore Complex (NPC), which form the sole conduit for nucleocytoplasmic transport. The NPC is formed by ~30 proteins, termed nucleoporins or nups (Rout et al., 2000a). Each nucleoporin is present in 8·n copies per NPC. In total, each NPC consists of ~480 polypeptides (Alber et al., 2007). At ~50 MDa in *S.cerevisiae*, or possibly up to ~125 MDa in vertebrates, the NPC is one of the largest complexes in the non-dividing cell (as reviewed in (Brohawn et al., 2009)).

The overall structure of the NPC has been studied by electron cryomicroscopy (cryoEM) and tomography (cryoET). The current best reconstructions are based on cryoET of the vertebrate NPC (Figure 1-1) (Beck et al., 2007; Elad et al., 2009). Unlike other transporters, the NPC is not imbedded in a membrane; most nucleoporins are soluble or peripheral (rather than integral) membrane proteins. Rather, the NPC forms a proteinaceous coat for the NE membrane, which is highly curved at the nuclear pore. This coat stabilizes toroidal membrane curvature at the pore. The dimensions of the

NPC have been estimated by electron microscopy. Its diameter is similar in all eukaryotes, about 90-120 nm (Beck et al., 2007; Elad et al., 2009; Fahrenkrog et al., 2000; Hinshaw et al., 1992; Stoffler et al., 2003). Its height is more uncertain (because of a technical limitation of ET, the missing angle problem), but is ~20-50 nm (Alber et al., 2007; Elad et al., 2009). A central channel along the vertical axis of the NPC is the primary conduit for transport. Around this central channel, electron dense units are arranged with 8-fold symmetry to form the core scaffold of the NPC. This scaffold is also called the spoke ring, because it appears as alternating thick and thin regions in electron micrographs (Akey and Rademacher, 1993; Hinshaw et al., 1992). From this scaffold, cytoplasmic filaments extend towards the cytoplasm, and a nuclear basket sits, suspended by filaments, into the nucleoplasm (Kiseleva et al., 2004; Kiseleva et al., 2000).

The central channel is less electron dense than the scaffold, and is filled by natively unfolded FG repeat domains, contributed by several nucleoporins. FG repeat domains are long polypeptides characterized by repeated phenylalanine-glycine (FG) dipeptides interspersed amongst otherwise hydrophilic sequence (Denning et al., 2003; Denning and Rexach, 2007; Hurt, 1988). FG repeat domains are essential for viability and establish the permeability barrier of the NPC (Strawn et al., 2004). Several models for the function of this barrier have been proposed and are detailed below. Specific interactions between nuclear transport receptors (NTRs) and representative FG peptides have been shown, and allow cargo to transit the pore. Mutant NTRs that are defective in binding FG repeat domains are also defective in NPC passage (Bayliss et al., 2000; Bayliss et al., 1999; Bednenko et al., 2003; Iovine et al., 1995; Ribbeck and Görlich, 2001).

Although the central channel is the primary transport conduit, peripheral channels are also visible near the NE in cryoET images of the NPCs of *Xenopus* and *Dictyostelium* (Beck et al., 2007; Elad et al., 2009). These peripheral channels might

transport small proteins or ions (Kramer et al., 2007), or integral membrane proteins (Powell and Burke, 1990; Zuleger et al., 2008).

Nucleocytoplasmic Transport

Passive diffusion across the NE is fast for small molecules, but becomes slower as macromolecules approach a size limit of 20-40 kDa (Bonner, 1975; Paine et al., 1975). The NPC provides this permeability barrier, which allows select, very large macromolecules to enter or exit the nucleus, though preventing most other macromolecules from passing (Mohr et al., 2009; Newmeyer et al., 1986). The nucleocytoplasmic transport system has separate stationary and mobile phases. The stationary phase, contributed by the NPC, creates the selectively permeable barrier. The mobile phase provides the means to pass this barrier, thereby regulating nucleocytoplasmic transport.

Regulation of Nucleocytoplasmic Transport

Regulation of nucleocytoplasmic transport has been studied extensively. Proteins are synthesized in the cytoplasm. Those destined for import expose nuclear localization signals (NLSs). A classical NLS, typified by the SV40 T antigen, binds importin α , which acts as an adaptor for importin β (Görlich et al., 1995). The use of importin α as adaptor is exceptional, however. Most cargoes bind directly a single importin (importin β or a functional equivalent) (Görlich et al., 1996a; Weis et al., 1996). Cargo•importin complexes have a more hydrophobic surface than many cytoplasmic proteins, a property that helps them to cross the NPC (Ribbeck and Görlich, 2002). Specific interaction of importins with FG repeat domains further enables cargo•importin complexes to transverse the NPC. Such an interaction can be seen in the structure of importin β bound to an FG repeat peptide (Bayliss et al., 2000).

Nuclear import is a vectorial process. In other words, it is driven in one direction. Directionality of transport is achieved by action of another soluble factor, the small GTPase Ran (Figure 1-2) (Görlich et al., 1996b). In the nucleus, Ran binds primarily guanosine triphosphate (GTP), rather than guanosine diphosphate (GDP). A guanosine exchange factor (GEF) for Ran, RCC1, is present in the nucleus in high concentration, tethered to chromatin. As a consequence, the nuclear concentration of Ran•GTP is about 200-fold greater than the concentration in the cytoplasm (Kalab et al., 2002). Once the cargo•importin complex reaches the nucleus, Ran•GTP displaces importin from the cargo. The structure of an importin in complex with Ran•GTP shows that Ran and cargo bind importin mutually exclusively, so that when Ran•GTP is present, importin must release the cargo (Fontes et al., 2000). The complex of importin and Ran•GTP is then free to diffuse back to the cytoplasm, but the cargo is left stranded in the nucleus, unable to cross the NPC.

In vertebrate cells, the vertebrate-specific nucleoporin Nup153 holds most cargo•importin complexes at the nuclear rim until a Ran•GTP releases the complex, though some cargo•importin complexes bypass Nup153 (Wohlwend et al., 2007). The transport of integral membrane proteins across the NPC into the nucleus is less well understood than transport of soluble proteins, but some INM proteins may use the same importin/Ran system (Lusk et al., 2007).

Once importin releases its cargo in the nucleus, the complex of importin and Ran•GTP returns to the cytoplasm, where Ran encounters a Ran-specific GTPase activating protein (Ran-GAP). Ran-GAP stimulates the GTPase activity of Ran, causing hydrolysis of GTP to GDP. Ran•GDP releases the importin, which can enter a second round of transport. Since concentration of import cargo in the nucleus occurs against a chemical activity gradient, energy is required to achieve vectorial transport. Successive rounds of GTP hydrolysis provide this energy, driving nucleocytoplasmic transport.

Protein export also depends on Ran (Figure 1-2). Proteins present in the nucleus but designated for export expose nuclear export signals (NESs) (Fornerod et al., 1997; Fukuda et al., 1997; Ossareh-Nazari et al., 1997; Stade et al., 1997). These bind an exportin to form a ternary complex with Ran•GTP, the predominant species in the nucleus. Once the ternary cargo•exportin•Ran complex crosses the NPC to the cytoplasm, hydrolysis of GTP by Ran to form Ran•GDP causes dissociation of the export complex. Structures of the exportin Cse1 have shown the mechanism of this export cycle in detail (Cook et al., 2005; Matsuura and Stewart, 2004).

Because each complete cycle of import or export transfers one Ran molecule to the cytoplasm, the nuclear pool of Ran must be replenished. A separate dedicated transport system uses NTF2 to return Ran to the nucleus (Ribbeck et al., 1998; Smith et al., 1998).

Recent structural studies have shown that other classes of macromolecules cross the NE by similar mechanisms. Spliceosomal UsnRNPs are imported by a mechanism similar to classical importin α/β -mediated import. Having been synthesized in the nucleus, UsnRNAs are exported to the cytoplasm (Will and Lührmann, 2001). Assembly of the UsnRNP core leads to hypermethylation of the 5' cap to form a m₃G cap. The mature UsnRNP then is imported back to the nucleus. The m₃G cap (as well as the first nucleotide of the stacked RNA) is recognized by the protein snuportin1 (Strasser et al., 2005). Like importin α , snuportin1 acts as an adaptor for importin β . Other studies have used snuportin1 as a model cargo for studying protein export. After it releases the UsnRNP cargo in the nucleus, cargo-free snuportin1 forms a ternary complex with the exportin Crm1 and Ran•GTP, which facilitates its re export to the cytoplasm (Monecke et al., 2009). Although UsnRNPs use snuportin1 as an adaptor for importin β , other RNAs employ dedicated NTRs. Recently a structure has been reported of tRNA bound to the exportin Xpot and Ran•GTP (Cook et al., 2009). This structure shows how Xpot recognizes properly processed 3' and 5' ends to distinguish pre-tRNAs from mature

tRNAs. Similarly, pre-microRNAs are bound directly by a dedicated NTR, exportin-5, which enables their export from the nucleus (Okada et al., 2009). Interestingly, though exportin-5 is structurally similar to other exportins—it is an α -helical repeat (HEAT repeat) protein—because exportin-5 transports RNA rather than protein, its binding surface is positively, rather than negatively, charged. Exportins that recognize the typical, basic NES of protein cargos form a negatively charged binding pocket. The positively charged surface of Exportin-5 instead complements the negative phosphate backbone of pre-microRNA cargo. This electrostatic interaction allows exportin-5 to bind pre-microRNAs in a sequence independent fashion, allowing this exportin to transport diverse pre-microRNAs.

Export of messenger RNAs (mRNAs) from the nucleus occurs by an entirely different pathway, which is tightly coupled to splicing, processing, and quality control steps, (as reviewed in (Carmody and Wentz, 2009)). Although a subset of mRNAs do use the Ran-dependent exportin Crm1, bulk mRNA transport does not depend on Ran. Instead a heterodimer of Nxf1 and Nxt1 is recruited to the mRNA particle (mRNP) by an active mechanism involving the ATPase UAP56. The complex interacts with FG repeat domains as it passes through the NPC. At the cytoplasmic face of the NPC, the essential mRNA export factors Dpb5 and Gle1 sit tethered by Nup214 and hCG1. Gle1, with the cofactor inositol hexakisphosphate (IP6), stimulates the ATPase activity of Dpb5, triggering the removal of proteins from the transiting mRNP. This remodeling makes the export process directional, as the remodeled mRNP cannot pass back through the NPC.

Models of Selective Permeability of the Nuclear Pore Complex

Several theories have been proposed to explain the selective permeability of the NPC. The barrier excludes most macromolecules >30 kDa, but allows passage of select macromolecules, some much greater in mass (Bonner, 1975; Paine et al., 1975).

It is accepted that FG repeat domains of the NPC act as a selective permeability barrier. How exactly they do so remains disputed (Frey and Görlich, 2009; Lim et al., 2007; Peters, 2009; Rout et al., 2003).

The virtual gating model proposes that natively unstructured FG repeat domains form an entropic barrier (Rout et al., 2003). In this model, the FG repeat domains do not form a solid barrier. Instead, they leave gaps large enough for transport complexes to pass. Motion of the FG repeat domains (together with transport complexes bound to them) creates an entropic penalty for entering the NPC. This entropic penalty is sufficient to exclude most macromolecules from the NPC. The authors propose that binding of transport complexes to FG repeat domains overcomes the entropic cost of entering the NPC—the enthalpy of binding counteracts the entropic penalty. Transport complexes do not become stuck at the point they enter the NPC, because they are able, by binding two or more FG region simultaneously, to pass sequentially from one FG nucleoporin to the other and thereby transit the pore. The authors propose considering transport as if it were a reaction pathway, with low Gibbs free energy on either side of the NPC and higher Gibbs free energy in the central channel, in analogy to the transition state of a reaction. They claim the NPC is a catalyst for transport, because for transport complexes the enthalpy of binding lowers the Gibbs free energy of this transition state.

There are arguments against this model. Foremost, it is unclear whether the mechanism proposed could sustain the high rates of nucleocytoplasmic transport observed. Claiming catalytic activity for NPC implies that the NPC can specifically recognize certain cargos, but specific recognition implies strong binding, and strong binding should slow transport, not accelerate it. Furthermore, the authors draw a smooth energetic pathway, where in fact the pathway would have to be much more rugged—it should have discrete transition states for each FG region bound and released during passage. The authors themselves acknowledge that on- and off-rates

for binding pose a kinetic problem for the model. In subsequent work, this model was adapted to a diffusion based theory for transport (Zilman et al., 2007). The transition state was reformulated as an energy potential well. In this paper, the authors claim that mathematical modeling proves that affinity for FG repeats is appropriately tuned to allow selective transport, but allow transport to be rapid.

The reversible collapse model proposes considering the FG repeat domains as a “polymer brush” that excludes macromolecules. This polymer brush is proposed to collapse upon binding an importin or exportin, thereby opening a cavity through which the transport complex can pass, and actively pulling the transport complex into the NPC (Lim et al., 2007). This model is based on a specific experimental system: When the FG region of Nup153 is expressed, purified, and covalently attached to a glass slide, the bulk protein forms an object, which can be measured by atomic force microscopy. This object collapses towards the glass slide, when karyopherin β 1 is added to the solution, and collapse can be reversed by adding of Ran•GTP.

There are several weaknesses in the reversible collapse model. First, it is obvious that Nup153 itself cannot form the primary component of the permeability barrier, because it is absent in yeast. The relevance of this experiment to actual transport is therefore unclear. Second, if the FG repeat domains functioned as proposed, they would make a very leaky barrier—collapse of the barrier due to entry of *bona fide* cargo would allow other macromolecules pass through as well. The authors counter the later argument by claiming that stochastic collapse and recovery of distinct groups of FG repeat domains could be fast enough to maintain an effective seal.

The selective phase model proposes that FG repeat domains collectively form a meshwork barrier for the NPC, into which transport complexes partition more favorably than other macromolecules. Specifically, the authors propose that FG repeat domains on adjacent nucleoporins crosslink themselves into a sieve like FG hydrogel, and that the mesh size of this gel defines the ~30 kDa size limit for passive diffusion through the

NPC (Ribbeck and Görlich, 2001; Ribbeck and Görlich, 2002). Large cargos are able to pass through the gel, because specific interactions with FG repeat domains locally disrupt the meshwork. However, the meshwork remains impermeable to other macromolecules because these interactions also serve to seal the meshwork around the cargo in transit, preventing other molecules from entering. This theory is buttressed by a series of experiments in which isolated FG repeat domains of several nucleoporins have been shown *in vitro* to form gelatinous solids, called hydrogels. These hydrogels reprise, on a macroscopic scale, many characteristics of microscopic transport through the NPC (Frey and Görlich, 2007; Frey et al., 2006; Ribbeck and Görlich, 2002). The relevance of this experimental system to the biophysics of transport through the actual NPC is still not firmly established, but it is the best system so far available for studying the transport properties of FG repeat domains *in vitro*.

Composition of the NPC

A complete structural characterization of the NPC will help elucidate how the complex is assembled, how it contributes to forming nuclear pores, how transport is regulated, and how the NPC arose in evolution. Although cryoEM and cryoET have revealed its overall architecture, they do not reveal where individual proteins sit within the NPC. At the achieved resolution, the boundaries between macromolecules are not visible. Structural characterization of the NPC must rely therefore on complementary techniques, in particular X-ray crystallography.

Proteomic characterization of the NPC (in the yeast *S. cerevisiae* (Rout et al., 2000b) and rat hepatocytes (Cronshaw et al., 2002)) provided an inventory of ~30 nucleoporins, and approximate locations within the NPC for each (Figure 1-3). To form the full structure, each nucleoporin is provided in multiple copies per NPC. A subset of nucleoporins is stably associated with the NPC, rather than dynamically associated

(Rabut et al., 2004a). Among the most stably associated are the so-called architectural nucleoporins of the core scaffold. The scaffold is defined as the central part of the NPC, situated co-planar with the NE, which consists of proteins that (1) are predicted to have defined tertiary structure (in contrast to the FG repeat domains), (2) are stably associated to the NPC during interphase (residence time > 40 hours), and (3) are required for proper assembly of the NPC. The scaffold of the NPC can be considered a docking site for FG repeat domain nucleoporins and for more mobile nucleoporins, some of which have roles far from the NPC (Kalverda and Fornerod, 2007). In total, the scaffold comprises about 55% of the total mass of the NPC (Brohawn et al., 2009).

The proteins of the NPC are formed from a limited set of structural elements, as shown in Figure 1-3 and reviewed in (Brohawn et al., 2009). The diversity of the scaffold is even more limited. Two types of protein domain compose most of the scaffold: β -propellers and α -helical domains. Other than β -propellers and α -helical domains, there are unstructured regions at the N termini of several scaffold nucleoporins and a coiled-coil domain in Nic96, which tethers the Nsp1•Nup57•Nup49 complex to the NPC (Grandi et al., 1993). Nup53/59 is predicted to lack defined secondary structure, except for an α/β domain in its middle, whose structure was solved by X-ray crystallography (Handa et al., 2006). Nup145C is also unusual, in that it is formed by autoproteolytic processing of the precursor protein Nup145 into N- and C-terminal fragments (Wente and Blobel, 1994).

β -Propellers

The β -propeller (~25% of the mass of the scaffold) (Figure 1-4) is a common class of protein, especially abundant in eukaryotes, which has diverse functions (Chaudhuri et al., 2008; Paoli, 2001). In the NPC scaffold, Sec13 and Seh1 were recognized as β -propellers when they were discovered, by the presence of characteristic WD-40 motifs (Pryer et al., 1993). The other β -propellers in the NPC, which lack the WD-40

motif, were identified only after the crystal structure of the Nup133 N-terminal domain prompted further investigation (Berke et al., 2004). Additionally, Nup85 and Nup145C each have a single β -blade at its N terminus. Crystal structures have shown that this β -blade completes *in trans* the open, six-bladed β -propeller of Seh1 or Sec13, respectively (Brohawn et al., 2008; Debler et al., 2008; Hsia et al., 2007). This compound β -propeller arrangement is so far unique to Seh1 and Sec13. Sec13 also binds the COPII coat protein Sec31 (Fath et al., 2007) or Sec16 (this work) using the same mode of interaction.

α -Helical Domains

The α -helical domains of the NPC (~70% of the mass of the scaffold) (Figure 1-5) were initially classified as α -helical solenoids. α -helical solenoids are made up from 2- or 3-helix bundles stacked to form elongated, often superhelical domains (Kobe and Kajava, 2000). Such regular α -helical structures are found in tandem with β -propeller domains in clathrin (Edeling et al., 2006). It was predicted that the same the β -propeller/ α -helical tandem occurs in some nucleoporins and in the COPII vesicle coat protein Sec31. On the basis of this shared domain composition (β -propellers, α -helical domains, and β -propeller/ α -helical tandems), it was proposed that the NPC and vesicle coats arose from a common evolutionary ancestor (Devos et al., 2004). Structural studies of the α -helical domains of the NPC and the COPII coat, (including those in this work), have shown that this classification is overly simplistic (Brohawn et al., 2008; Debler et al., 2008; Hsia et al., 2007; Jeudy and Schwartz, 2007; Leksa et al., 2009). Indeed, α -helical domains in NPC fall into three classes, none of which is α -solenoidal in the canonical sense: the ancestral coatomer element 1 (ACE1), Nup120 (a unique fold), and Nup133/Nup170 (detailed in this work). The ACE1 is a unique class of α -helical fold, in which the helical stack folds back on itself to form a J-shape with three distinct modules called crown, trunk, and tail. The ACE1 is found in both NPC

and COPII—this cements the ancestral relationship between these complexes—but the ACE1 is distinct in structure from clathrin or other truly α -solenoidal proteins. The N-terminal 70 kDa domain of Nup120 forms a structure that fully integrates its α -helical portion with its β -propeller into a single 3D domain. The tight integration between these parts could not have been predicted by sequence-based methods. Nup133 and Nup170 each form an α -helical stack that is significantly more irregular than the predicted α -solenoid, and structurally distinct from clathrin, COPI, COPII or other known proteins (as described in Chapter 2). In addition, two further α -helical proteins, Nup188 and Nup192, are found in the NPC. Although they may form regular α -solenoidal structures, their structures more likely hold new surprises.

Structures of Vesicle Coats

Devos et al. proposed that the NPC might be related to vesicle coat proteins (Devos et al., 2004). Clathrin, COPI, and COPII coats each employ β -propeller, α -helical, and β -propeller/ α -helical tandem domain architectures, like the NPC scaffold. The hypothesis that the NPC and vesicle coats are related implies they evolved from some common protocoatomer. In an ancestral eukaryote, a simpler membrane-coating complex may have served both as a vesicle coat and as primitive NPC. Since understanding the structure of the NPC is aided by comparison to vesicle coats, and Chapter 3 is devoted to describing a novel ACE1 in the COPII system, it is useful to review what is known structurally about these coats.

Clathrin

Clathrin coats stabilize membrane patches at which protein and lipid cargos are concentrated, deform the membrane, and eventually pinch it off to form vesicles. Clathrin coated vesicles are employed in many intracellular transport steps, and are the

most extensively studied class of transport vesicle (Edeling et al., 2006). The clathrin coat is formed by assembly of three clathrin heavy chains (CHC, 1,675 residues, 190 kDa) and three clathrin light chains (CLC, 25-29 kDa). It forms a triskelion, a spider-like assembly with three long legs meeting at a central vertex (Figure 1-6). The CHC contributes most of the structure of this triskelion, which is then decorated by CLC. The three CHC molecules are held together by a helical tripod at the hub where they meet, which is also the binding site for auxilin and Hsc70, proteins involved in disassembly of the coat (Fotin et al., 2004a; Xing et al., 2010). Each leg of the triskelion extends 475 Å, and ends at a terminal domain provided by the CHC N-terminal domain. The CHC terminal domain is a seven-bladed β -propeller (residues 1-330). Most of the remaining CHC forms helical α zigzags that extend from the terminal domain towards the hub of the triskelion, near the C terminus. At the C terminus, residues 1589-1630 form a helical rod, which trimerizes to make the helical tripod. Residues 1631-1675 form a proline-rich C-terminal segment, the binding site for auxilin (Fotin et al., 2004a; Fotin et al., 2004b).

The legs of the clathrin triskelion (made of CHC) have characteristic bends that divide them into segments. A crystal structure and sequence analysis of these segments shows that the helical α zigzag is made of short, regularly stacked α -helices (Ybe et al., 1999). Because each helix in the stack is so short, the resulting helical stack is quite long, causing each leg to extend much further than if the helical repeats were formed from longer α -helices or were more irregular (as in Nup133 and Nup170). Each leg of the triskelion spans more than one edge of the assembled coat. Three types of interaction propagate the clathrin coat: interdigitation of the C termini at the helical tripod of each vertex, layering of three proximal legs along the edge adjacent to this vertex, and layering of three distal legs along the edge that is one vertex removed from this vertex. There is substantial overlap between adjacent triskelia of the coat. The clathrin cage can adapt to vesicles of different sizes by changing the angle at which the

leg segments overlap. The terminal domain β -propeller, whose structure has been solved (ter Haar et al., 2000; ter Haar et al., 1998), projects inward and binds peptides contributed by adaptor molecules, thereby linking the clathrin coat to an adaptor layer that separates it from the membrane. The adaptor layer is formed by “assembly polypeptides” (APs), also called adaptor proteins or adaptins, which form heterotetrameric protein complexes essential for coat assembly under physiological conditions.

COPI

COPI coated vesicles act in the early secretory pathway. Their best characterized function is retrograde transport of luminal and membrane proteins amongst compartments of the Golgi and the endoplasmic reticulum (ER). The molecular mechanisms of COPI function have been well studied (Beck et al., 2009; Hsu and Yang, 2009). The F-subcomplex of COPI is analogous to the AP adaptors of clathrin, and has sequence homology to it. The B-subcomplex consists of α , β' , and ϵ subunits, which are not similar in sequence to any proteins of the clathrin system. The small GTPase Arf1 regulates COPI coat assembly, as well as several other aspects of cellular physiology, including clathrin assembly (D'souza-Schorey and Chavrier, 2006). Like other coat complexes, COPI proteins have β -propeller, α -helical and β -propeller/ α -helical tandem domain architectures (Devos et al., 2004), but though much is known about COPI and factors that regulated it, less is known about the architecture of the coat. No assembled coat has been structurally characterized at high resolution. The COPI system is more complicated than the clathrin system, but homology between AP complexes and the F-subcomplex of COPI suggests some structural commonality.

COPII

COPII, despite its name, is structurally unrelated to COPI. In the secretory pathway, cargo proteins translocated into the ER are trafficked to other compartments by vesicles that bud from the ER membrane. The COPII coat complex mediates formation of these transport vesicles (Bonifacino and Glick, 2004; Hughes and Stephens, 2008; Tang et al., 2005). The COPII coat complex consists of an inner coat and an outer coat. Crystal structures of all five component proteins have been solved (Bi et al., 2002; Bi et al., 2007; Fath et al., 2007). The inner coat is formed by a dimer of Sec23 and Sec24 (structurally related proteins with distinct functions) and the GTPase Sar1. Sar1 has sequence similarity to Arf1. Sar1 in the GTP-bound state interacts with membranes by insertion of an N-terminal amphipathic α -helix into the outer leaflet of the ER lipid bilayer (Lee et al., 2005). Sec23 binds Sar1, and forms part of a ternary GTPase activating complex (with Sec31) (Bi et al., 2007). Sec24 acts as a cargo adaptor (Miller et al., 2002; Mossessova et al., 2003). The inner coat organizes assembly of an outer coat composed of Sec13 and Sec31 (Figure 1-7) (Fath et al., 2007; Stagg et al., 2008; Stagg et al., 2006). Conceptually, the inner coat corresponds to the adaptor layer of the clathrin system, and the outer coat to clathrin itself, but the component proteins (and how they assemble) are unrelated. Both clathrin and the COPII outer coat contain β -propeller/ α -helical tandem domain architectures, but otherwise their structures are entirely different.

The structure of the COPII outer coat has been elucidated by an elegant combination of cryoEM and X-ray crystallography (Fath et al., 2007; Stagg et al., 2008; Stagg et al., 2006). Sec31 (1273 residues, 139 kDa) has a β -propeller domain, a β -blade, and an α -helical domain that together make up the N-terminal 60% of the protein. A proline-rich extension, predicted as unstructured, then connects to a smaller, predicted, α -helical domain at the C terminus. Sec13 (297 residues, 33 kDa) forms a β -propeller. A purified complex of human Sec31 and Sec13 self-assembles into

polyhedral cages, when dialyzed against a buffered solution containing 700 mM KOAc (Stagg et al., 2006). The structure of this cage by cryoEM at 30 Å resolution revealed a cubo-octahedral geometry. For X-ray crystallography, Sec31 was split into fragments (Fath et al., 2007). First, the structure of its β -propeller and β -blade domains in complex with Sec13 was solved, and termed the “vertex element.” Second, the structure of the β -blade and α -helical domains, also in complex with Sec13, was solved, and termed the “edge element.” The structure of the rest of Sec31 is not solved, but because this part is mostly unstructured, it is not needed to interpret the contribution of the Sec13•Sec31 complex to the architecture of the COPII cage.

Using the overlapping portions of the vertex element and the edge element to combine the two, the structure of the complete assembly unit was revealed (Fath et al., 2007). It forms a straight rod, 30 Å in diameter and 280 Å in length. The α -helical domains of Sec31 homodimerize to form the central element of the assembly unit. Flanking them, the six β -blades of the Sec13 β -propeller clasp a seventh β -blade provided by Sec31, which allows Sec31 to pass through Sec13, placing the N-terminal β -propeller of Sec31 at the ends of the rod. As their names suggest, the vertex element (β -propeller of Sec31 in complex with Sec13) forms the vertex of the COPII cage, and the edge element (dimerized Sec31 α -helical domains in complex with Sec13) forms the edges of the cage. Contrary to predictions (and the description of Fath et al.), the α -helical domain of Sec31 is not an α -solenoid. Instead, the N terminus of the domain folds against the middle of the domain to form a J-shape. Furthermore, a 50 residue loop connecting the N-terminal four α -helices to the rest of the domain causes the two molecules of Sec31 to interlock with each other. Because of this interlocking, the structure suggests that dimerization must be coordinated with folding of the α -helical domain. A full description of this architecture and comparison to a related protein, Sec16, is provided in Chapter 3.

At each vertex, four copies of the Sec13•Sec31 vertex element come together, asymmetrically, to propagate the cage. EM reconstruction of a second, larger COPII cage suggests that the cage adapts to vesicles of different size by changing the angles at which the vertex elements meet, rather than bending of the edges elements (Stagg et al., 2008).

Comparison of Clathrin and COPII

The clathrin coat has 3-fold vertices formed by assembly of helical segments into a tripod. The coat is propagated by extensive interactions between overlapping legs, which are 475 Å long α -helical domains, made from regular, short helical repeats. Each leg spans two edges of the cage. The β -propeller terminal domain of clathrin is important for interactions with adaptors, but does not itself form significant interactions with other triskelia. By contrast, the vertices of the COPII outer coat are 4-fold assemblies of adjacent β -propeller domains. The α -helical domains of Sec31 form interlocked edge elements, but each Sec31 molecule contributes to only one edge of the cage. The clathrin coat adapts to vesicle size by changing the angles at which the legs overlap, but the COPII coat adapts by varying the angles at which the vertex elements meet. A similarly detailed description of the core scaffold is a principle aim of current structural efforts on the NPC.

Modularity as a Basis for Structural Characterization of the NPC

In clathrin and COPII, two proteins are sufficient to self-assemble complete cages. The NPC is more complex. At least 30 proteins compose the complete structure. Even the scaffold alone is 14 proteins (in *S. cerevisiae*). Fortunately for the structural biologist, one characteristic of the NPC is that it is highly modular (Schwartz,

2005). First, the NPC is organized with 8-fold rotational symmetry around its central axis, and the scaffold possesses 2-fold pseudosymmetry about an axis in the plane of the NE. Second, though it has ~30 proteins, these nucleoporins are built from a limited set of domain topologies. ~10 contain disordered N or C termini that are rich in FG repeats. Three have coiled-coil domains, and three others have transmembrane domains. 14 nucleoporins form the scaffold, where two domain topologies predominate: β -propellers and α -helical domains. Third, only a fraction of the NPC is stably attached at all times. Fourth, the stably attached nucleoporins segregate into distinct subcomplexes, which assemble in multiple copies to build the complete NPC (Figure 1-8).

The subcomplexes are defined as sets of nucleoporins that co-purify from cellular extracts. They also are found as stable entities in mitotic extracts of higher eukaryotes, in which the NPC disassembles when breakdown of the NE occurs during open mitosis (Matsuoka et al., 1999). After mitosis, these subcomplexes reassemble in a defined order (Dultz et al., 2008). The scaffold of the NPC is formed from two major subcomplexes: the heptameric Y-complex (or Nup84-complex), and the heteromeric Nic96-complex. Additionally, a subcomplex of three integral membrane proteins interfaces with the Nic96-complex, anchoring it to the NE.

The modularity of the NPC opens the possibility of reconstructing the structure of the full ~50 MDa complex from the structures of isolated components. In clathrin and COPII, as well as other molecular machines (Chiu et al., 2006), a hybrid approach combining cryoEM and X-ray crystallography has proven fruitful. The aim is to bridge the gaps between light microscopy, electron microscopy, and X-ray crystallography or nuclear magnetic resonance. The best cryoET images of the NPC provide ~5.8 nm resolution (Beck et al., 2004). At this resolution, individual subcomplexes cannot be discerned. An EM reconstruction of the isolated Y-complex at 3.8 nm resolution is sufficiently detail to allow tentative fitting of crystal structures, but does not provide by

itself the resolution to see the boundaries between proteins or to see secondary structure elements (Beck et al., 2004). X-ray crystallography is currently the principle method for determining structures of large macromolecular complexes at atomic or near atomic resolution; we and others have begun to apply this method to the NPC.

A Hybrid Approach for Determining the Architecture of the NPC

A strategy for determining the structure of the NPC is: (1) define binary or ternary interactions among nucleoporins (or fragments of nucleoporins), express these nucleoporins, or nucleoporin complexes recombinantly, and purify them in quantities sufficient for structural studies, (2) solve their structures by X-ray crystallography, (3) fit these structures together, using biochemical data on specific interactions, alignment of overlapping structures, or fitting of structures into EM images of assembled units, (4) assemble a complete structure of the NPC in silico, using tomographic reconstructions of the entire NPC, its known 2- and 8-fold symmetry operators, and other imaging data (such as immunogold labeling or subnanometer light microscopy) to position molecular models of subcomplexes.

An Alternative Computational Method

In the interim, an alternative approach has been used to make a draft model of the NPC. A computational algorithm was used to integrate several (non-structural) sources of data: volumetric and stoichiometric data, the 2- and 8-fold symmetry of the complex, and distance restraints obtained from comprehensive coimmunoprecipitation analysis of all nucleoporins. The algorithm produced a low (~5 nm) resolution model of the NPC optimally consistent with these sources of data (Alber et al., 2007). The model has severe limitations (notably, the Y-complex morphs into a straight rod), but at least suggests some gross features of the NPC. According to this computed model, eight Y-complexes self-assemble into symmetric cytoplasmic and nucleoplasmic rings that

sandwich two central rings, composed of Nup157/Nup170, Nup188, and Nup192. The remaining nucleoporins (except the cytoplasmic filaments and nuclear basket) are positioned in the model as well, and decorate this main scaffold.

Towards a Multiscale Model for the NPC

The Y-complex

The Y-complex (or Nup84-complex) is the best characterized subcomplex of the NPC. It forms about 20% of the NPC, or one-third the scaffold. It is essential for assembly of the NPC in several organisms (Boehmer et al., 2003; Fabre and Hurt, 1997; Galy et al., 2003; Harel et al., 2003; Walther et al., 2003). It has seven universally conserved components: Nup84, Nup85, Nup120, Nup133, Nup145C, Sec13, and Seh1. These components assemble stoichiometrically to form a Y shape in electron micrographs (Kampmann and Blobel, 2009; Lutzmann et al., 2002; Siniosoglou et al., 2000). In many eukaryotes, excluding *S. cerevisiae*, the complex includes three other proteins: Nup37, Nup43, and ELYS/MEL 28. Their architectural role is unclear (Cronshaw et al., 2002; Franz et al., 2007; Rasala et al., 2006).

The Y-complex was reconstituted for EM studies from recombinantly expressed dimeric and trimeric components (Lutzmann et al., 2002). Two short arms of the Y are made from a Seh1•Nup85 dimer and from Nup120. A Sec13•Nup145C dimer forms the proximal portion of the long stalk. A Nup84•Nup133 dimer forms the distal portion of the stalk, which has a pronounced bend in the middle, with Nup133 at the bottom of the stalk. In this study, none of the components were expressed at high enough yield for crystallographic characterization. In subsequent work, fragments of these proteins have been expressed alone or in complex with others at higher yield. Crystallographic analysis of nearly entire Y-complex (except the hub where arms and stalk meet) is now complete:

The crystal structure of the N-terminal domain of Nup133 revealed a β -propeller, prompting the realization that several nucleoporins have β -propeller or β -propeller/ α -helical domain tandem architectures (Berke et al., 2004). Since Nup120 and Nup133 were both predicted to have this tandem architecture, it was thought they might have similar structures. One segment of the Nup133 β -propeller, which is unstructured in the crystal structure, contains an ALPS motif, which binds liposomes of specific curvature. It thereby acts as a curvature sensor (Drin et al., 2007). This result suggests that the β -propeller of Nup133 directly contacts the membrane. The binding interface for Nup107 (the human ortholog of Nup84) was mapped to a C-terminal fragment of Nup133, and the crystal structure of this Nup133 fragment in complex with the C terminus of Nup107 was solved (Boehmer et al., 2008). This structure made clear that neither Nup133 nor Nup107(Nup84) forms regular α -solenoidal helical repeats. Solving the structure of the remaining, middle portion of Nup133 proved challenging but was eventually achieved (Chapter 2). These structures revealed the molecular basis for the sharp bend in the stalk seen in EM images. Nup107 meets the C-terminal domain of Nup133 at an obtuse angle; a flexible connection between the middle and C-terminal domains of Nup133 allows the distal segment of the stalk to actuate with respect to the rest of the Y.

The structure of the proximal segment of the stalk was solved in two parts. First, Blobel and colleagues solved the structure of Nup145C (minus a C-terminal portion) in complex with Sec13 (Hsia et al., 2007). Nup145C was found to insert a β -blade domain into the open six-bladed β -propeller of Sec13, completing it *in trans*—the same mode of interaction seen in the Sec13•Sec31 complex. Second, Nup145C and Sec13 in complex with Nup84 (also minus a C-terminal fragment) was solved (Brohawn and Schwartz, 2009b). This proximal stalk of the Y-complex is structurally analogous to the edge element of the COPII coat, as discussed further below. Together with the structures of the Nup133 N-terminal domain and the Nup107(Nup84)•Nup133

interaction complex, these structures provide a complete model of the stalk of the Y-complex.

One arm of the Y-complex contains the Nup85•Seh1 complex, and the other contains Nup120. The structure of Nup85•Seh1 proved similar to that of Nup145C•Sec13, as well as Sec13•Sec31 (Brohawn et al., 2008). The structure of Nup120 was unexpected (Leksa et al., 2009): it proved entirely unrelated to that of Nup133. Instead of separate β -propeller and α -helical domains, as predicted, four α -helices inserted between the sixth and seventh β -blades of the β -propeller make intimate contacts with the rest of the helical portion of the structure. In effect, Nup120 folds into a single compact unit.

The crystal structures of all these parts were fit into an improved EM reconstruction of the Y-complex (Kampmann and Blobel, 2009). Although a small fraction of the structure of the Y-complex has not yet been solved, most of it is hence known at near-atomic resolution. It is still not clear, though, how the Y-complex is oriented within the NPC. It has been suggested, by analogy with the COPII edge element, that the proximal segment of the stalk (Nup84•Nup145C•Sec13) follows the convex curvature of the NE parallel to the central axis of the pore, with symmetric Y-complexes arranged so that the stalks with Nup133 at the end face out towards either face of the NPC, and the arms of the Y face inward (Brohawn and Schwartz, 2009b).

The Nic96-complex

The Nic96-complex is not as well defined as the Y-complex. Its proposed components associate less stably, making it more difficult to characterize. It forms about 35% of the NPC, or two-thirds of the scaffold. Nic96 interacts directly with Nup53 and Nup59 (Hawryluk-Gara et al., 2005), and co-immunoprecipitates with Nup188 (Nehrbass et al., 1996) and Nup192 (Kosova et al., 1999). Nup53 and Nup59

also interact with Nup157 and Nup170, as well as with the transmembrane nucleoporin Ndc1 (Makio et al., 2009; Onischenko et al., 2009). It is therefore likely that the Nic96-complex provides the scaffold's principle attachment to the membrane, via Ndc1 and associated integral membrane nucleoporins. Additionally, the N-terminal coiled-coil domain of Nic96 tethers the Nsp1 complex to the NPC (Grandi et al., 1995), so Nic96 also recruits a set of FG repeat nucleoporins to the NPC. The well established whole genome duplication in yeast (Scannell et al., 2007) left some proteins of the Nic96-complex duplicated. Nup157/Nup170 and Nup53/Nup59 are paralogous gene pairs, each with one homolog in metazoa: Nup155 and Nup35, respectively. A database of gene duplications in *Saccharomyces* yeast shows that other yeast have two genes encoding Nic96 homologs (Byrne and Wolfe, 2005).

The structure of the C-terminal domain of Nic96 showed that it forms an irregular helical domain that folds to form a J-shape (Jeudy and Schwartz, 2007; Schrader et al., 2008). The N-terminal coiled-coils project out from the center of this folded-back domain. The C terminus has hydrophobic, conserved residues on its surface that may form a protein-protein interface. When the structure of Nic96 was solved, it was a unique fold, but it has since proved to be the founding member of the ancestral coatmer element 1 (ACE1) class. The structure of Nup170 was solved next. As described in Chapter 2, sequence analysis suggested a β -propeller/ α -helical domain tandem architecture and remote homology to Nup133, which was confirmed by the crystal structure of the α -helical domain of Nup170. The structures of two further large, α -helical proteins, Nup188 and Nup192, are not yet known. Homology between members of the Y- and Nic96-complexes, leads us to suggest that the Nic96-complex, like the Y-complex, will be shown to form an elongated, branched structure.

Specific Functions of Nucleoporins Nup133 and Nup170

Many nucleoporins have specific functions attributed to them. Since this work characterizes Nup133 and Nup170, it is appropriate to review specific functions attributed to them.

Nup133

Nup133 was first discovered in *S. cerevisiae* as a gene whose deletion causes accumulation of poly(A)⁺ RNA in the nucleus and clustering of NPCs to one area (or a few areas) of the NE (Doye et al., 1994; Li et al., 1995). Localization of an NLS reporter construct in this deletion mutant suggests that protein import is not impaired by deletion of Nup133. Other genes of the Y-complex, as well as Nup159 and Gle2, have the same phenotype (Doye and Hurt, 1997). Overexpression of a fragment of Nup133 (or of Nup160—the metazoan homolog of Nup120) has a dominant negative effect—it likewise impairs mRNA export (Vasu et al., 2001). Only Nup133 residues 587-936 (the middle domain of Nup133), not full length Nup133, causes this dominant negative. Since this fragment lacks the Nup107 binding interface, it cannot be targeted to the NPC or block endogenous Nup133 from integrating into the NPC. Therefore, this fragment of Nup133 must exert its effect elsewhere. How it does so is not clear. In HeLa cells, depletion of Nup133 or Nup107 by RNAi reduces the cellular levels of multiple nucleoporins and decreases the number of NPCs in the NE. In a nuclear assembly assay performed with *Xenopus* egg extracts, immunodepletion of Nup133, and hence the Y-complex along with it, leads to assembly of nuclei with a closed NE, but no NPCs (Walther et al., 2003). Nup133, Nup107, and Nup96 (human ortholog of Nup145C) are phosphorylated during mitosis; this phosphorylation may regulate release of the Y-complex from the NPC during NE breakdown (Glavy et al., 2007). Nup133 is found to associate with chromatin, as part of the Y-complex, early during the

process of recovery from mitosis (Walther et al., 2003). Indeed, recruitment of the Y-complex is an early step in assembly of new NPCs (Dultz et al., 2008).

Nup133, along with the Y-complex, is observed to partially localize to kinetochores during mitosis (Belgareh et al., 2001; Loiodice et al., 2004). What purpose the Y-complex has at the kinetochore is still unclear. The Y-complex may promote or stabilize spindle assembly (Mishra et al., 2010; Orjalo et al., 2006). A yeast-two-hybrid screen with Nup133 and mass spectrometry of proteins affinity-purified with CENP-F together suggest a direct interaction between Nup133 and CENP-F, a component of the kinetochore (Zuccolo et al., 2007). How the Y-complex is recruited to the kinetochore and whether it indeed influences spindle assembly remain open areas of inquiry.

Nup133 has a specific developmental phenotype: in mice, a point mutation called *merm*, which causes C-terminal truncation of Nup133, leads to a defect in neuronal differentiation (Lupu et al., 2008).

Nup170

Nup170 is homologous to mammalian Nup155, which was first identified in extracts of rat liver (Radu et al., 1993). Nup170 and Nup157 were then identified in *S. cerevisiae* as redundant genes complemented by rat Nup155 (Kenna et al., 1996). Nup155 homologs are essential for growth in various species (Franz et al., 2005; Galy et al., 2003; Gigliotti et al., 1998; Kiger et al., 1999). Deletion of Nup170 (or Nup188) increases how quickly a nuclear GFP reporter diffuses out to the cytoplasm once *S. cerevisiae* cells are shifted to 0°C, suggesting that loss of Nup170 increases the passive permeability of the NPC (Shulga et al., 2000). A mutation in Nup170 causes a chromosome transmission fidelity (*ctf*) phenotype related to kinetochore integrity, which can be suppressed by overexpression of Nup157 (Kerscher et al., 2001). Similarly, in *C. elegans*, depletion of Nup155 leads to defects in chromosome segregation (Franz et

al., 2005). In a *S. cerevisiae* strain where Nup157 is deleted and Nup170 can be selectively downregulated, assembly of the NPC is impaired, a set of nucleoporins accumulates in cytoplasmic foci and a precursor complex is observed on the nuclear face of the NE (Makio et al., 2009). In other words, loss of Nup170 and Nup157 together impairs the fusion of INM and ONM to form pores, and prevents proper assembly of downstream nucleoporins to form a functional NPC. Nup170 is implicated in INM protein import, as deletion of the gene in *S. cerevisiae* causes the INM proteins Heh1 and Heh2 to be mislocalized (King et al., 2006). The human homolog of Nup170, Nup155, also contributes to holding the mRNA export factor Gle1 at the NPC (Rayala et al., 2004).

Purified Nup170 was shown by EM to assume a crescent shape, with a large lobe at one end (the β -propeller domain), a central arch, and a smaller lobe at the C terminus (Flemming et al., 2009). Chapter 2 of this work demonstrates that the C-terminal half of the protein forms an α -helical domain similar to Nup133. This part of Nup170 is necessary for recruitment to the NPC (Flemming et al., 2009). GFP-Nup170C, but not GFP-Nup170N, localizes to nuclear rim. Furthermore, overexpression of Nup170C is lethal, suggesting this C-terminal domain can compete with and exclude full length Nup170 from the NPC. Nup157 also adopts a crescent shape in electron micrographs, and seems to interact with members of the Y-complex, in particular Nup120 (Lutzmann et al., 2005).

Nup155 (the homolog of Nup170) has recently been implicated in human disease. A point mutation in Nup155 was identified as the cause of an autosomal recessive inherited disorder that results in atrial fibrillation (AF) (Zhang et al., 2008). Since AF causes 15% of strokes and occurs in 8% of persons 80-89 years old, the study of genetic causes of AF has important potential clinical relevance. This mutation causes the single amino acid substitution R391H in the N-terminal β -propeller, which in some way disables Nup155. Nup155^{-/-} has a similar AF phenotype in mice, showing that

Nup155 has an effect on the development of cardiac tissue in both mice and men. It remains to be determined whether this effect is specific to cardiac cells, or whether AF is simply the most visible manifestation of a general defect in NPC assembly.

Evidence for a Specific Relationship between COPII and NPC

The protocoatmer hypothesis has proven partially correct: Nup133 and Nup157/Nup170 (this work), and Nup120 (Leksa et al., 2009) are less closely related to vesicle coat proteins than originally proposed; Nup84, Nup85, Nic96, and Nup145C, however, show strong structural similarity in their α -helical domains to the COPII coat protein Sec31. Hence, this group of four nucleoporins has been termed the ancestral coatmer element 1 (ACE1) (Brohawn et al., 2008). Chapter 3 of this work identifies one further member of this family, Sec16, another component of the COPII system. Structural similarity between COPII proteins and nucleoporins is strong evidence that the NPC and COPII evolved from a common ancestor.

The ACE1 is composed of three structural units. The N terminus folds against the middle of the domain to form a trunk. The U-turn between these two parts is called the crown. Nucleoporins have an additional C-terminal helical part called the tail. In Nup84 (human Nup107) this tail is the interaction site for Nup133, and part of the Nup107•Nup133 crystal structure presented in Chapter 2. Dimerization of the crown units of Sec31 creates the central rod of the Sec13•Sec31₂•Sec13 edge element of the COPII coat. Nup84 and Nup145C similarly dimerize through their crowns to form a Nup84•Nup145C•Sec13 edge element for the NPC (the proximal stalk of the Y-complex) (Brohawn et al., 2008). This edge element likely plays a structural role in the NPC similar to the Sec13•Sec31 edge element in the COPII coat. Unlike the COPII coat, where the vertex elements of Sec13•Sec31 join adjacent edges, it is still not clear

how the scaffold subcomplexes of the NPC connect to one another. The vertex element for the NPC has not been identified.

Outlook

Structural studies such as those presented in this work are rapidly revealing the molecular architecture of the NPC. Major challenges include (1) determining the connections among proteins of the Nic96-complex and that complex's overall architecture, (2) defining the interactions used to connect the subcomplexes of the NPC scaffold to one another, (3) placing molecular models of these subcomplexes into the overall structure of the NPC, (4) using these structures to probe the mechanism by which the NPC assembles from its component parts and disassembles during mitosis. In particular, understanding how the structure shapes the membrane of the NE and how INM and ONM fuse to form new pores are areas of broad interest in the field. Integration of structural (particularly crystallographic) data into computational models integrating various types of data would provide useful information, as would developments in super-resolution light microscopy of the NPC. If the rate of progress in the field is sustained, a complete structure of the NPC scaffold is not far off.

Figures

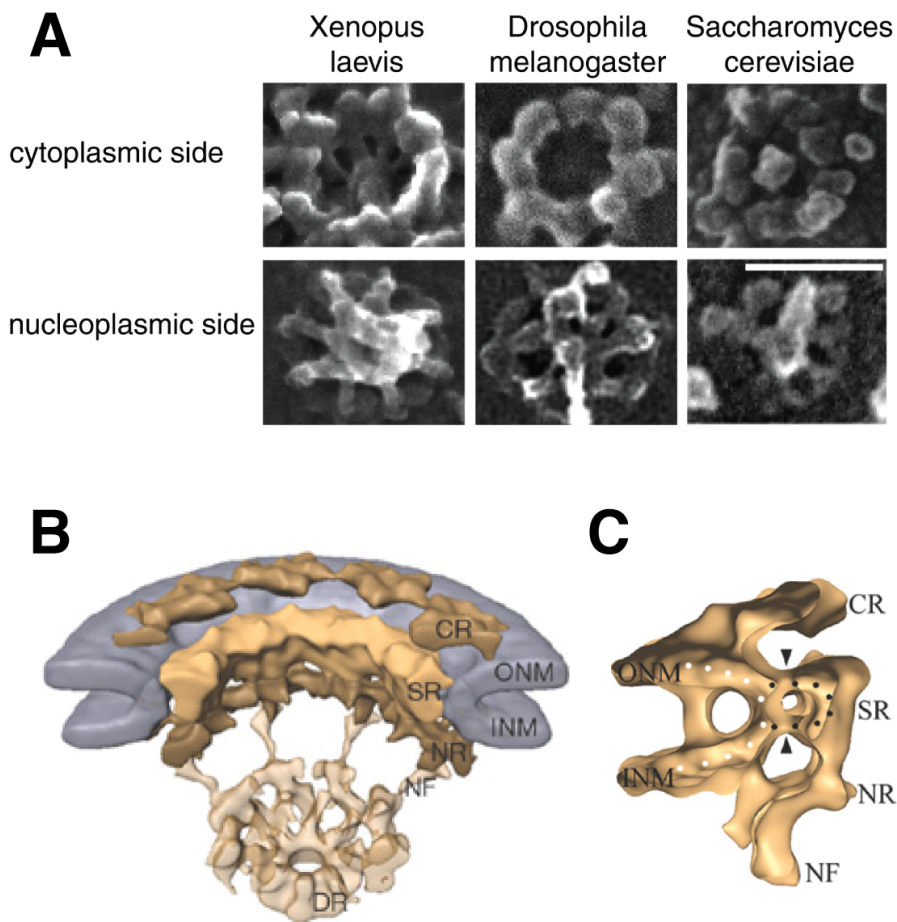


Figure 1-1 Electron Microscopy of the NPC

- (A) Scanning electron micrographs of NPCs from diverse eukaryotes. The surface features that differentiate cytoplasmic and nucleoplasmic faces of the NPC are conserved, as are the overall dimensions in the plane of the nuclear envelope. Scale bar indicates 100 nm.
- (B) Cut away view of cryo-electron tomographic (cryoET) reconstruction of the *Dictyostelium discoideum* NPC (Beck et al., 2007). Structural features are labeled as cytoplasmic (CR), spoke (SR) and nuclear rings (NR) in shades of yellow, and the inner (INM) and outer nuclear membrane (ONM) in bluish grey. For clarity, the center plug or transporter is omitted. The central 8-fold symmetry is apparent from the four sections shown.
- (C) A single section of the NPC. The fused INM and ONM are marked by white dots and the spoke structure with black dots.

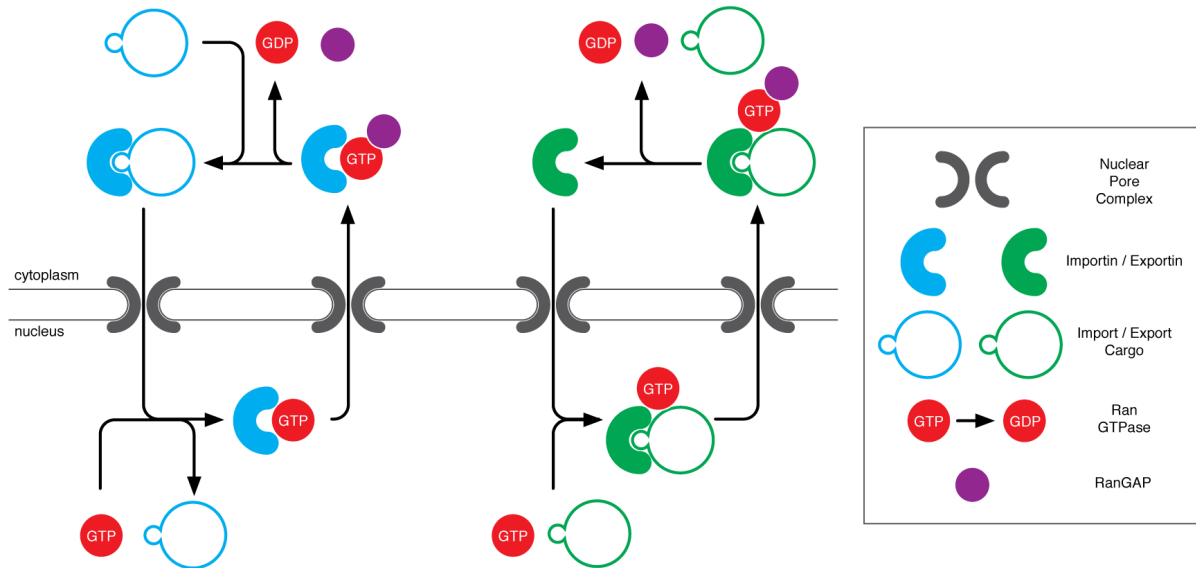


Figure 1-2 Nucleocytoplasmic Transport mediated by Ran

The mechanism of Ran mediated nucleocytoplasmic transport is diagramed. For import (left), cargoes are brought into the nucleus in complex with a specific importin. Ran•GTP causes release of the cargo and allows importin to return to the cytoplasm with Ran•GTP-bound to it. Ran–GAP promotes hydrolysis of GTP by Ran, releasing Ran•GDP from the importin. For export (right), Ran•GTP and the export cargo form a trimeric complex with a specific exportin. On reaching the cytoplasm, Ran encounters Ran–GAP and hydrolyzes GTP, releasing the ternary complex. Both import and export cycles lead to a net export of one molecule of Ran and hydrolysis of a single molecule of GTP.

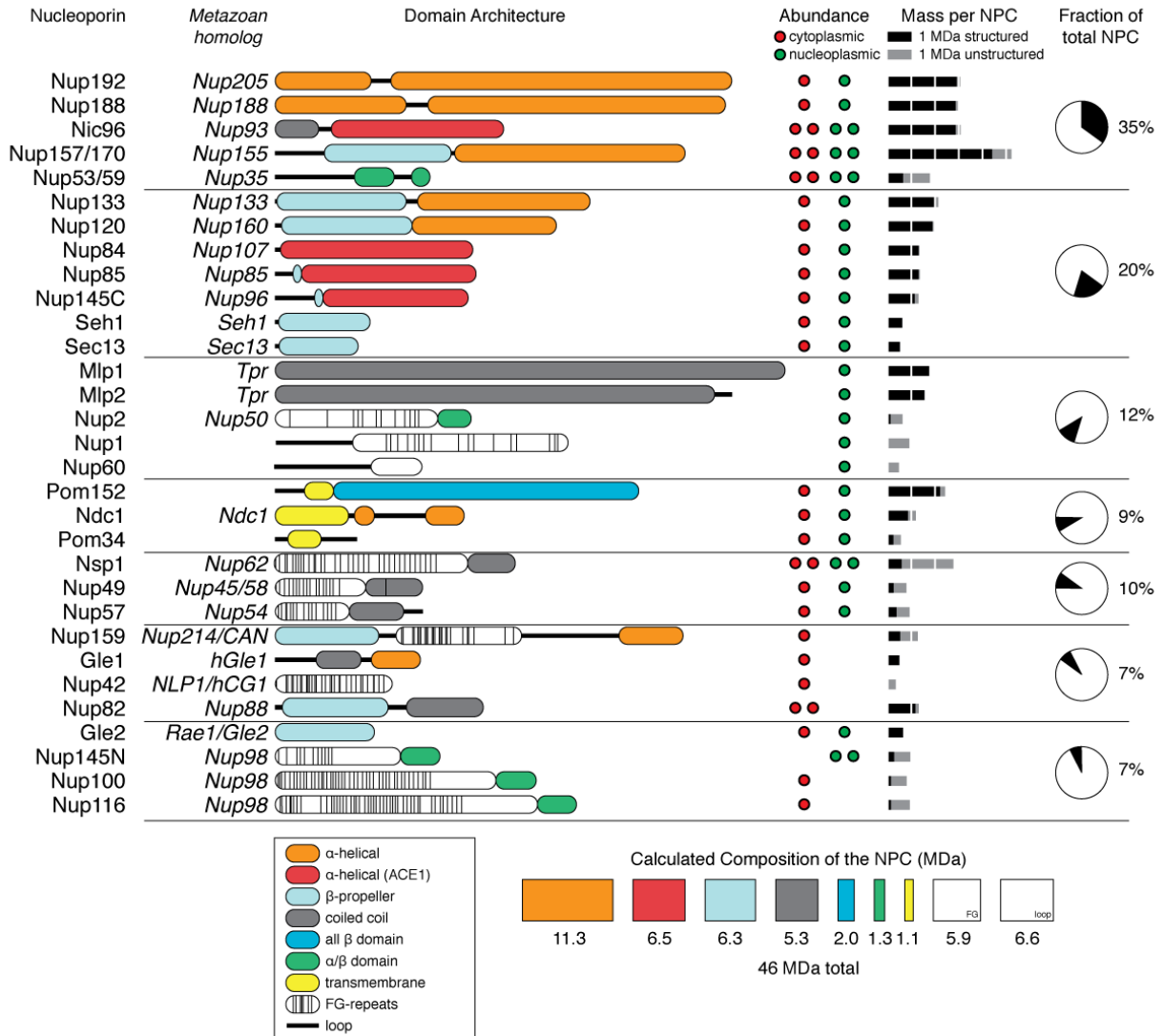


Figure 1-3 Inventory of the NPC

Summary of the nucleoporins that compose the NPC. Domain architecture of nucleoporins from *S. cerevisiae* are as determined by X-ray crystallography or prediction. Abundance and mass for each nucleoporin are derived from published stoichiometries (Cronshaw et al., 2002; Rout et al., 2000b). Nucleoporins specific to metazoa are italicized. Colored dots represent the number of nucleoporins per spoke of the 8-fold symmetric complex, on the cytoplasmic (red) or nucleoplasmic (green) face of the NPC. Bar graphs show the mass contributed by each nucleoporin to the total NPC in structured (black) or unstructured (grey) domains. Pie charts show the fraction by mass contributed by each subcomplex to the total NPC.

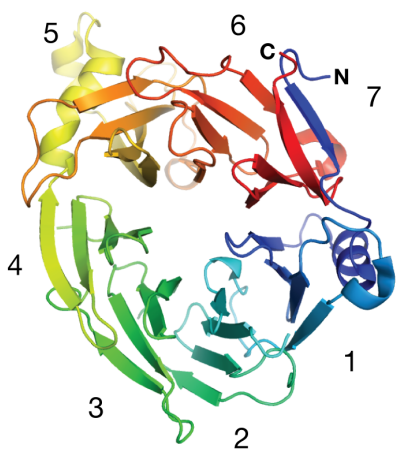


Figure 1-4 β -Propeller

An example of a β -propeller, the N-terminal domain of Nup133 (PDB ID: 1XKS). The seven β -blades of the domain are labeled. Each β -blade is composed of four β -strands, decorated by loops and intervening α -helical segments. The structure is colored blue to red from N to C terminus. Termini are labeled N and C. The first β -blade at the N terminus forms a “velcro closure” for the last β -blade, a common feature of β -propellers.

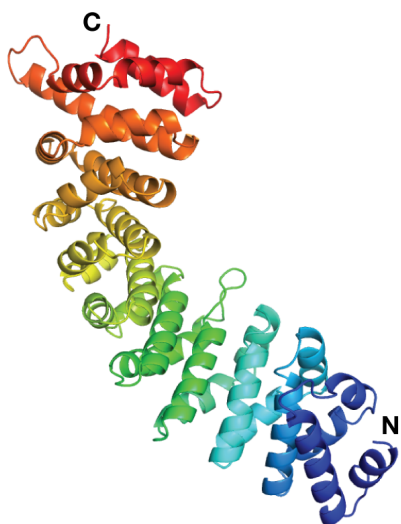


Figure 1-5 α -Helical Solenoid

An example of an α -helical solenoid, importin α from *S. cerevisiae* (PDB ID: 1BK5). The domain is colored blue to red from N to C terminus. Termini are labeled N and C. Importin α forms a regular α solenoid in which stacked, regular 2- or 3-helix repeats impart superhelical twist. The α -helical domains of nucleoporins were initially predicted to be regular α -solenoids, such as shown here, but in fact have been shown to assume more irregular topologies, as described in Chapter 2.

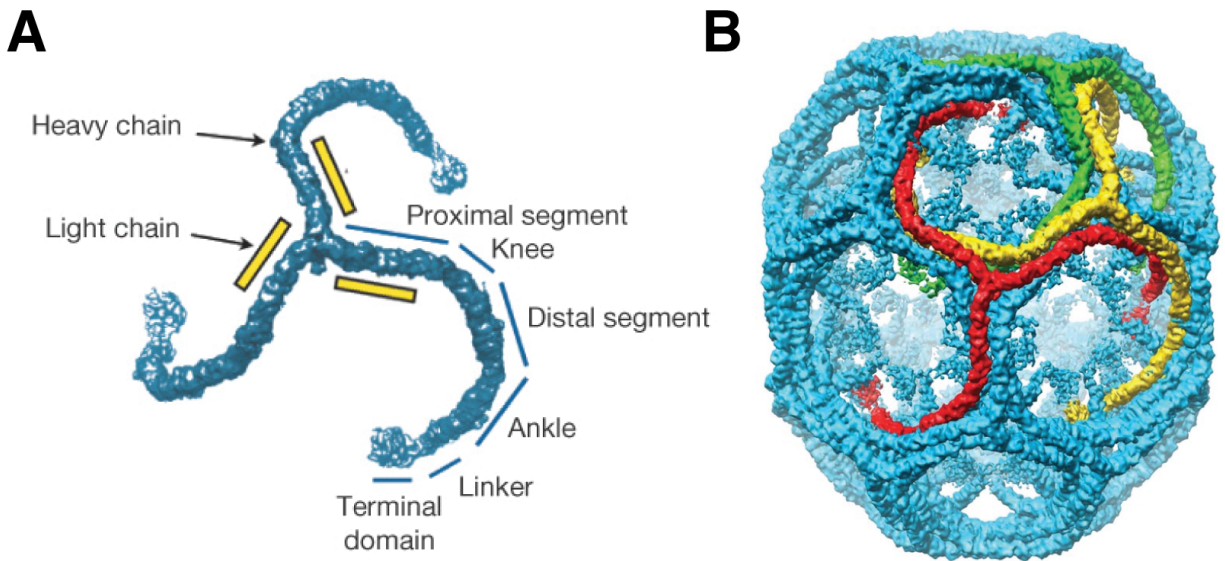


Figure 1-6 Structure of Clathrin

Images of the clathrin triskelion and assembled cage from (Fotin et al., 2004b).

- (A) Clathrin triskelion, labeled with names for the segments of the heavy chain. The terminal domain is the N terminus of the heavy chain, and the vertex is form by the intersection of three C termini. The positions of light chains are diagrammed.
- (B) CryoEM reconstruction of a clathrin hexagonal barrel (heavy chains only) at 7.9 Å resolution. This form of the clathrin cage contains 36 triskelia. The interactions that propogate the cage occur mainly between the α -helical segments of adjacent triskelia.

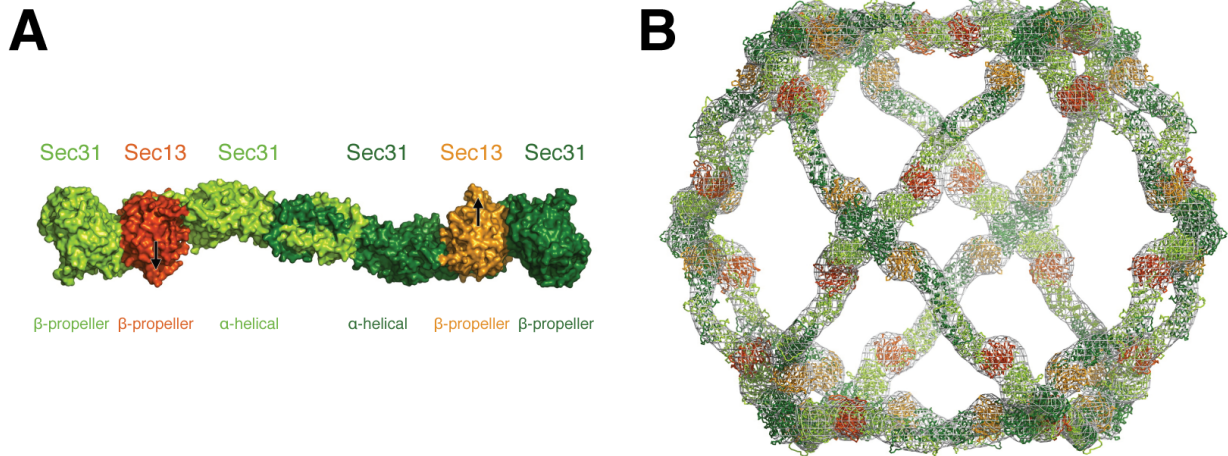


Figure 1-7 COPII Cage or Outer Coat

Images of the COPII cage—the Sec13•Sec31 outer coat—from (Fath et al., 2007).

- (A) Structure of the Sec13•Sec31 assembly unit, a composite of two crystal structures. Sec31 β -propellers and Sec13 β -propellers form the ends of the unit (the “vertex element”). Sec31 threads itself through Sec13 to the α -helical (ACE1) domain. The Sec31 α -helical domains homodimerize to form, with the Sec13 β -propellers, the central part of the unit (the “edge element”).
- (B) Molecular model of the cage formed from 24 copies of the Sec13•Sec31 assembly unit with octahedral symmetry. Crystal structures are fit to the 30 Å cryoEM map from (Stagg et al., 2006). Note that the assembly is propagated by interactions among the β -propeller domains of adjacent vertex elements.

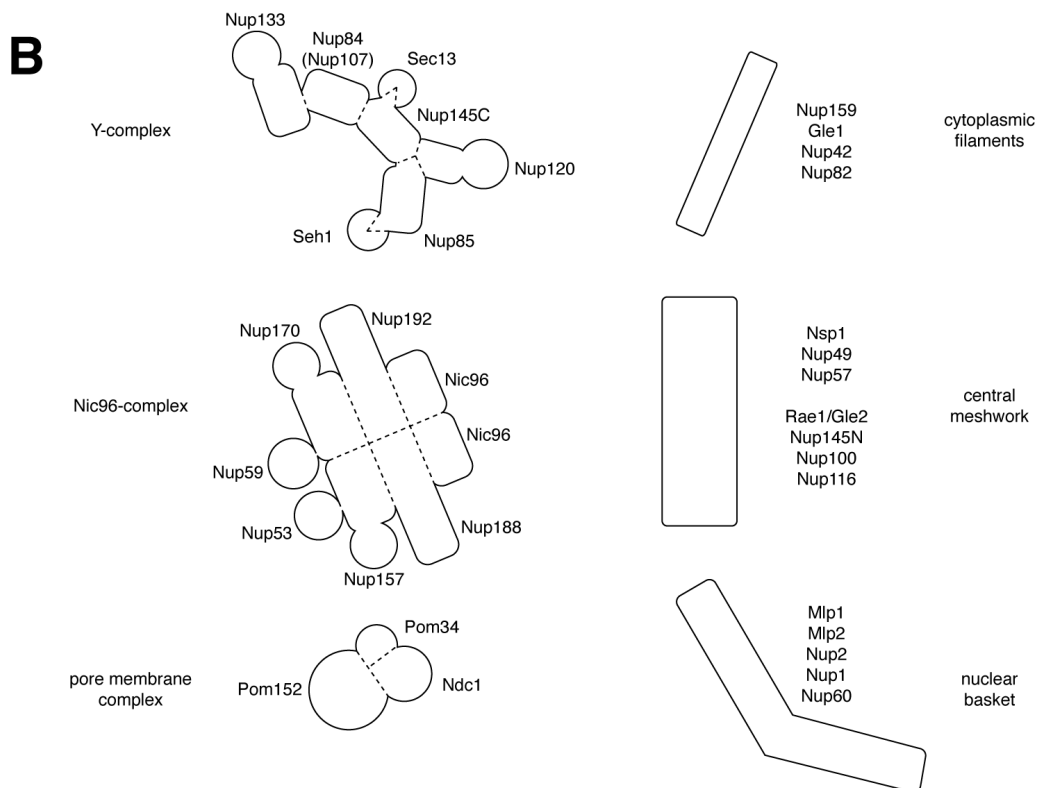
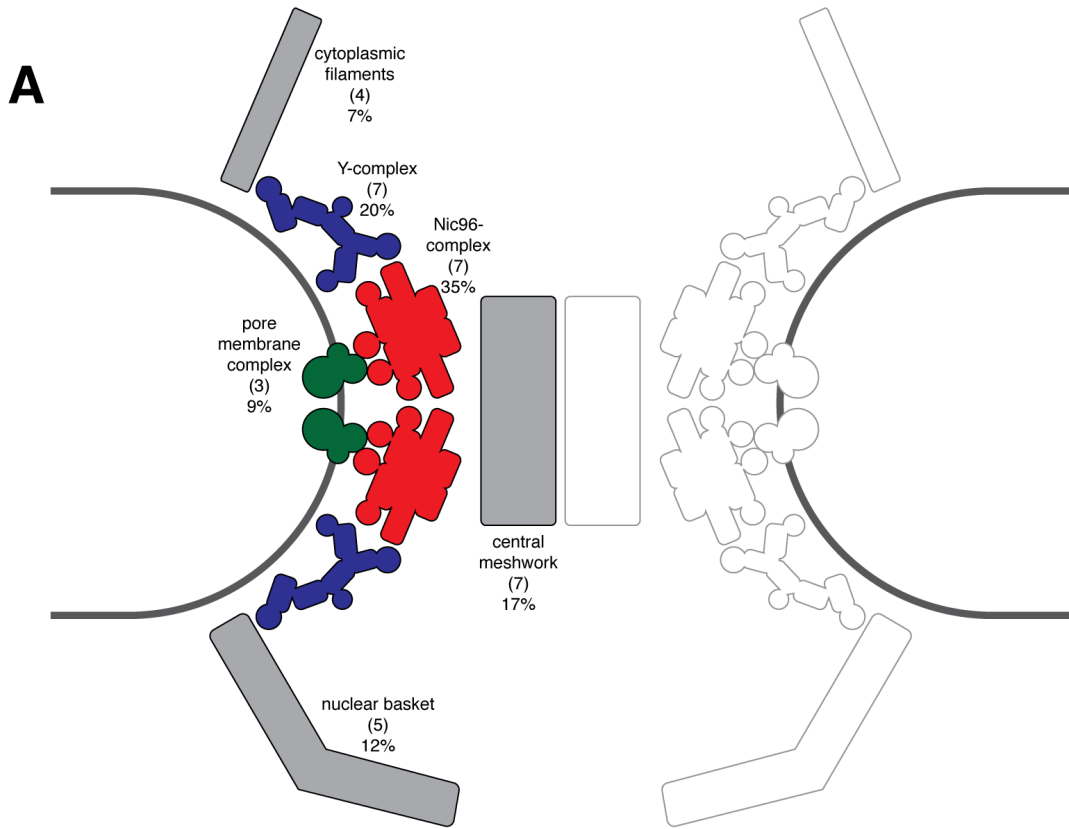


Figure 1-8 Subcomplex Map of the NPC

- (A) The major subcomplexes that make up the NPC are drawn. Curved grey lines represent the membrane of the NE. One of 8 symmetric spokes is drawn in color, and a second in outline. The dimensions of the pore are approximate. Areas of individual components are scaled according to their mass in order to suggest the relative contribution of each subcomplex to the NPC. Each is labeled with the number of nucleoporins in that subcomplex (in parenthesis) and the approximate percentage of mass it contributes to the NPC.
- (B) Composition of individual subcomplexes. Scaffold and pore membrane complexes (left) are enlarged slightly relative to others (right). Dashed lines mark boundaries between proteins. The Y-complex is the best characterized and there the diagram reflects knowledge of binary interactions solved by X-ray crystallography and EM reconstructions. The picture of the Nic96-complex is less precise, and adjacency does not reflect direct interaction. In both, circular shapes represent β -propellers (except Nup53/Nup59 which are not β -propellers) and rectangles represent α -helical domains. In the pore membrane complex, all three nucleoporins are integral membrane proteins and are drawn as circles.

CHAPTER 2 Architectural nucleoporins Nup157/170 and Nup133 are structurally related and descend from a second ancestral element

This chapter has been published as:

Whittle, J.R.R. and T.U. Schwartz. 2009. Architectural Nucleoporins Nup157/170 and Nup133 Are Structurally Related and Descend from a Second Ancestral Element. *Journal of Biological Chemistry*. 284:28442-28452.

Abstract

The nuclear pore complex (NPC) constitutes one of the largest protein assemblies in the eukaryotic cell and forms the exclusive gateway to the nucleus. The stable, ~15-20 MDa scaffold ring of the NPC is built from two multiprotein complexes arranged around a central eight-fold axis. Here we present crystal structures of two large architectural units, yNup170₉₇₉₋₁₅₀₂ and hNup107₆₅₈₋₉₂₅•hNup133₅₁₇₋₁₁₅₆, each a constituent of one of the two multiprotein complexes. Conservation of domain arrangement and of tertiary structure suggests that Nup157/170 and Nup133 derived from a common ancestor. Together with the previously established ancestral coatomer element (ACE1), these two elements constitute the major α -helical building blocks of the NPC scaffold and define its branched, lattice-like architecture, similar to vesicle coats like COPII. We hypothesize that the extant NPC evolved early during eukaryotic evolution from a rudimentary structure composed of several identical copies of a few ancestral elements, later diversified and specified by gene duplication.

Introduction

The membrane-enveloped nucleus is the hallmark of the eukaryotic cell. Physical separation of nucleoplasm and cytoplasm necessitates sites for molecular exchange (D'Angelo and Hetzer, 2008; Tran and Wentz, 2006; Weis, 2003). Nuclear pore complexes (NPCs), plugged into circular openings where inner and outer nuclear membranes fuse, perforate the nuclear envelope and form the sole gateway. The NPC is at ~50 MDa one of the largest protein assemblies in the quiescent cell. It is modular, comprises ~30 different proteins, termed nucleoporins (nups), and forms an eight-fold

symmetric ring embedded in the nuclear envelope (Schwartz, 2005). In accord with the symmetry of the complex, each nucleoporin is present in 8-n copies per NPC.

The architecture of the NPC is roughly conserved among eukaryotes, measuring about 100 nm in outer diameter, with a central transport gate about 40 nm wide (Beck et al., 2004; Beck et al., 2007; Panté and Kann, 2002; Stoffler et al., 2003). The NPC is a highly dynamic assembly. Some nucleoporins are stably attached, but others are more dynamic (Dultz et al., 2008; Rabut et al., 2004a; Rabut et al., 2004b). The main scaffold ring is composed of ~15 architectural nucleoporins that anchor to the inner pore wall. A second set of nucleoporins (FG-nups) is characterized by long, phenylalanine-glycine (FG) rich filamentous extensions. These FG-fibers emanate into the central cavity of the NPC and define the main transport barrier (Frey and Görlich, 2007; Jovanovic-Talisman et al., 2009; Lim et al., 2007). Ions, metabolites, and macromolecules less than 20-40 kDa diffuse, for the most part, freely through the transport gate. Larger molecules pass only when bound to dedicated nuclear transport receptors, termed karyopherins, which directly interact with FG-nups (Chook and Blobel, 2001; Cook et al., 2007; Stewart, 2007). The small GTPase Ran regulates the interaction of protein cargo with import or export karyopherins, conferring directionality to these transport processes. This regulation depends on Ran being GTP-bound in the nucleus and GDP-bound in the cytoplasm, a gradient established by the action of cytoplasmic GTPase-activating protein (RanGAP) and nuclear GTP exchange factor (RanGEF).

To better understand the myriad of functions attributed to the NPC, which go far beyond transporting molecules across the NE (Fahrenkrog et al., 2004; Lim et al., 2008), we are interested in the structural characterization of the NPC, which begins with the stable scaffold structure. The ~15 architectural nucleoporins are organized in two large multiprotein complexes—the well-studied Nup84-complex and the more enigmatic Nic96-complex. The components of each are known (Table 2-1). The

Nup84-complex contains seven universally conserved nucleoporins and adopts a characteristically branched Y-shape (Lutzmann et al., 2002; Siniosoglou et al., 2000; Siniosoglou et al., 1996). In this work, the Nup84-complex is referred to as the Y-complex. Nup120 and Nup85•Seh1 form the two short arms, whereas Nup145C•Sec13, Nup84, and Nup133 build the long, kinked stalk. The Nic96-complex likely contains five distinct nucleoporins, two of them duplicated in yeast (Aitchison et al., 1995; Grandi et al., 1997; Marelli et al., 1998; Miller et al., 2000; Zabel, 1996). It connects to the NE (Weis, 2007) as well as the FG-network (Grandi et al., 1995). These two scaffold complexes likely form ring-like assemblies. Whether these rings are stacked or concentric, or arranged some other way, is controversial (Alber et al., 2007; Brohawn et al., 2008; Brohawn and Schwartz, 2009a; Hsia et al., 2007). This structural framework is important to the assembly and function of the NPC. Severe defects occur when scaffold nucleoporins are deleted or depleted, including failure to recruit other nucleoporins and diminished transport of protein or RNA across the nuclear membrane (Baï et al., 2004; Doye et al., 1994; Gao et al., 2003; Harel et al., 2003; Heath et al., 1995; Li et al., 1995; Shulga et al., 2000; Vasu et al., 2001).

Superficially, the architectural nucleoporins are classified by computational methods as β -propeller domains, α -helical repeat domains, or tandem combinations thereof (Table 2-1) (Devos et al., 2004; Devos et al., 2006; Schwartz, 2005). Experimental structural characterization, however, has revealed that this simplistic description does not adequately reflect the reality. For example, Sec13 and Seh1 are predicted as 6-bladed β -propellers, but turn out to be 7-bladed, with the final blade provided *in trans* by their respective binding partners (Brohawn et al., 2008; Debler et al., 2008; Fath et al., 2007; Hsia et al., 2007). The four ACE1 nucleoporins are built around a ~65 kDa α -helical domain. They are distantly related to one another, and, strikingly, also to Sec31, the main structural component of the outer coat of the COPII vesicle. This ACE1 domain is a tripartite fold-back structure of ~28 α -helices, distinct

from the regular α -solenoid domains found in HEAT-, TPR-, or PPR-repeat proteins (Andrade et al., 2001a; Andrade et al., 2001b), among others. The structural similarity between these ACE1 proteins provided the proof that the NPC and COPII coat derive from a common ancestor (Brohawn et al., 2008), as hypothesized previously (Devos et al., 2004; Devos et al., 2006).

The ACE1 nucleoporin Nup84 binds Nup133. The structure of a fragment of the human Nup84 ortholog, hNup107₆₅₈₋₉₂₅, has been solved in complex with hNup133₉₃₄₋₁₁₅₆ (Boehmer et al., 2008), the C terminus of the protein. This structure showed that the C terminus of Nup133 consists of two α -helical blocks. A rigid block of four α -helices, residues 934-1008, forms an interface bundle that binds Nup84(hNup107). A moderately flexible hinge connects this interface bundle to a second α -helical unit that forms a distinct lobe at the C terminus of the protein. The N terminus of Nup133 is a β -propeller, whose structure is also known (Berke et al., 2004). hNup133₉₃₄₋₁₁₅₆ suggested that Nup133 is not an ACE1 protein.

Here we present crystallographic analysis of two architectural units, yNup170₉₇₉₋₁₅₀₂ and hNup107₆₅₈₋₉₂₅•hNup133₅₁₇₋₁₁₅₆, components of both major scaffold complexes of the NPC. Nup170, its paralog Nup157, and Nup133 each consist of an N-terminal β -propeller followed by an ~80 kDa C-terminal α -helical domain. The structures reveal a common α -helical architecture for Nup157/170 and Nup133 that is distinct from all other known nucleoporins. This α -helical architecture is, with ACE1, another ancestral element of the NPC. We conclude that the basic NPC framework is built from a small set of recognizable structural elements that were already present in multiple copies in the last common ancestor of extant eukaryotes. During the course of evolution, gene duplications occurred and diversified these core elements, generating the complex, multi-functional machine that is the NPC.

Results

Structure of the α -helical domain of Nup170

Nup170 is predicted to contain two structural domains, an N-terminal β -propeller (residues 180-650) and a C-terminal α -helical domain (Figure 2-1A) (Devos et al., 2006; Schwartz, 2005). By expressing a series of N-terminal truncations of the protein and by limited proteolysis, we defined a stable core of the predicted α -helical region, comprising residues 979 to 1502 of Nup170 from *S. cerevisiae* (data not shown). The presumed N-terminal β -propeller domain interacts weakly with the α -helical domain when separated, indicating flexible attachment (Flemming et al., 2009). yNup170₉₇₉₋₁₅₀₂ was expressed recombinantly in *E. coli*, purified to homogeneity, and crystallized. The structure was solved by single-wavelength anomalous dispersion (SAD), using selenomethionine-labeled protein. The asymmetric unit contains one molecule. The experimental SAD electron density allowed for building residues 1020-1460, revealing a continuous, but bipartite stacked α -helical domain (Figure 2-1). Due to the lack of strong crystal contacts, the C-terminal half of the domain is flexibly positioned. Thus, to aid structure determination, this C-terminal 29 kDa subdomain (residues 1253-1502) was separately expressed and crystallized. Data to 2.2 Å resolution were collected and phased by molecular replacement with the relevant portion of the larger protein as initially modeled. The complete, refined model of the C-terminal subdomain ($R_{\text{work}}/R_{\text{free}} = 23.3/27.6\%$) was then used to build the structure of yNup170₉₇₉₋₁₅₀₂ at 3.2 Å resolution ($R_{\text{work}}/R_{\text{free}} = 30.6/32.4\%$). Representative electron density for the 3.2 Å resolution structure is shown in Figure 2-2. Data collection and refinement statistics are summarized in Table 2-2.

yNup170₉₇₉₋₁₅₀₂ adopts an irregular α -helical stack composed of 26 α -helices and overall dimensions of 12 nm x 4 nm x 4 nm (Figure 2-1). We label these helices α 1-26. The domain begins with helices α 1/2, α 3/4 and α 6/7 forming three consecutive pairs of

helices, of various lengths, stacked antiparallel, without superhelical twist. Helix $\alpha 5$ resides in a loop and does not pair to other helices. Helices $\alpha 8-13$ form an extended zig-zag pattern that is rotated by about 90° against the $\alpha 1-7$ stack. This zig-zag can be likened to a stack of three α -helical pairs that has been stretched by pulling on its ends. As a result, helices $\alpha 8-13$ extend over $\sim 38 \text{ \AA}$, reflecting a $\sim 50\%$ stretch compared to a tightly packed 6-helix stack, which would span only $\sim 26 \text{ \AA}$. The hydrophobic core of this extended zig-zag is poorly packed. Few residues are fully buried. Helix $\alpha 14$ is about twice as long as its direct neighbors and connects the two α -helical subdomains. The C-terminal subdomain forms a crescent only loosely definable as a stack. It starts with $\alpha 15$, unexpectedly positioned below, not above, helix $\alpha 14$. This helix abuts end-on-end to $\alpha 12$ of the N-terminal subdomain. The strictly conserved arginine 1232 is sandwiched between the negatively polarized C termini of $\alpha 12$ and $\alpha 15$, presumably for charge-compensation. Nup170 then continues with helices $\alpha 16-26$ forming a compact hydrophobic core, implying rigidity.

To compare the structure of Nup170 with those of other proteins, we performed structure-based searches with VAST and DALI (Holm et al., 2008; Madej et al., 1995). Neither returns significant alignments. No protein aligns to Nup170 over more than 6 consecutive helices. We conclude that Nup170 has only remote structural similarity to known proteins.

Nup133₅₁₇₋₁₁₅₆ adopts a quadripartite domain

Nup133 and Nup170 are predicted to have a similar overall topology. Both comprise an N-terminal β -propeller domain linked to a C-terminal α -helical domain (Figure 2-1A and Figure 2-3A). To compare directly the α -helical domains of Nup133 and Nup170, we solved the structure of the complete α -helical domain of hNup133 in complex with hNup107. hNup107₆₅₈₋₉₂₅ and hNup133₅₁₇₋₁₁₅₆ were co-expressed recombinantly in *E. coli*, purified, and crystallized. The structure was solved by

molecular replacement using the 57 kDa Nup107₆₅₈₋₉₂₅•Nup133₉₃₄₋₁₁₅₆ interaction complex (PDB ID: 3CQC) (Boehmer et al., 2008). The asymmetric unit contains one heterodimer. Crystallographic analysis was challenging, because crystals were small and difficult to grow, suffered severe radiation damage, and diffracted anisotropically. Based on the resulting electron density map, we were able to assign all the helices of Nup133 and unambiguously determine the overall topology. Most connecting loops are also visible in the electron density. The 105 kDa complex was refined to $R_{\text{work}}/R_{\text{free}} = 31.2/37.0\%$ (Table 2-2). The model and electron density for the novel portion is shown in Figure 2-4. hNup133₅₁₇₋₁₁₅₆ forms an elongated structure composed of 28 helices (Figure 2-3). Because the N-terminal β -propeller domain of hNup133 has three helices inserted into it (PDB ID: 1XKS) (Berke et al., 2004), we number hNup133₅₁₇₋₁₁₅₆ beginning at helix α 4. The domain can be described as quadripartite. From the N terminus, it starts with a block of 12 long helices, which form a wide and flat plane. These helices are arranged pairwise and antiparallel, except helices α 9-10, which form an overhand turn. The following six helices (residues 854-944) are all short (2-3 turns) and zig-zag upward, covering a distance of 44 Å. Helices α 21-24 make up the interface with Nup107 and form a α -helical bundle as described previously (Boehmer et al., 2008). Finally, helices α 25-31 fold into a compact C-terminal subdomain.

Comparison to minimal interacting complex

hNup107₆₅₈₋₉₂₅•hNup133₉₃₄₋₁₁₅₆

The Nup107 moiety in the complex solved here is identical to the minimal interaction fragment previously reported. The portion of Nup133 solved here includes the entire helical portion solved previously and the 418 amino acids that connect it to the N-terminal domain. The C-terminal subdomain of Nup133 forms a crystal contact in the current structure. This subdomain is therefore more stable than in the minimal interacting complex. Several loops not modeled previously are apparent. The

metazoan-specific finger helix of Nup107 (labeled $\alpha 6'$ in Figure 2-3B) also forms a crystal contact causing it to bend more than in the previous structure. Otherwise no noteworthy rearrangements occur.

Structural comparison of Nup170 and Nup133

Sequence- and structure-based alignments suggest remote homology between Nup170 and Nup133. Due to the multi-partite nature of the two proteins and the apparent hinges connecting the subdomains, an overall superimposition is not very informative. However, if the separate subdomains are superposed individually, commonalities become apparent (Figure 2-5). The most striking similarity exists between the middle segments of Nup170 and Nup133, where the helices are short and form a characteristically extended zig-zag structure. An elastic network model suggests that both molecules may flex about this central zig-zag. Further, the Nup133 interface bundle and the connection to the C-terminal lobe are particularly conserved. The C-terminal lobe of Nup170 is larger than that of Nup133 (34 kDa versus 27 kDa). N-terminally attached to the zig-zag are helices that form tightly packed bundles, however in Nup133 they form a flat and extended plane, while in Nup170 we observe three tightly stacked α -helical pairs. This remote, but distinctive structural homology is matched by homology observed in the amino acid sequence. A PSI-BLAST search with hNup133₅₁₇₋₁₁₅₆ predominantly returns homologs of Nup133 and Nup170. Detected similarity spans the entire region that is structurally similar (Nup133 residues 830-1120, Nup170 residues 1150-1380). This search result suggests that Nup170 and Nup133 are more closely related to each other than to other proteins.

yNup170₉₇₉₋₁₅₀₂ has two conserved surface features

Nup170 is integrated into the structural framework of the NPC and must interact with other nucleoporins to exert its function, however the direct interaction partners are

not yet firmly established. Interaction sites can often be identified by conservation of neighboring surface-exposed residues. We generated a maximally diverse alignment of Nup170 sequences across all eukaryotes. Surface representation of Nup170 colored by conservation suggests two conserved surfaces (Figure 2-6). Helices α 11-14 contribute to the first surface, which is mildly conserved and negatively charged. According to the structural alignment, Nup170 helices α 11-14 correspond to the Nup133 interface bundle, the group of helices by which Nup133 binds Nup107. The conserved surface on Nup170 corresponds to the Nup133•Nup107 interface. In Nup133, this surface is hydrophobic. The double mutant L973E L976E prevents interaction with Nup107 by placing charged sidechains in the interface (Boehmer et al., 2008). The corresponding residues in Nup170, E1234 and R1238, are charged. If Nup170 binds another protein by this interface, the interaction is not hydrophobic, and likely weaker.

The second surface, built by helices α 16-18, is more strongly conserved and forms a hydrophobic groove. In the sequence alignment (Figure 2-6F), the exposed neighboring residues are conserved: S1305 as serine or threonine, F1308 as phenylalanine or tyrosine, F1325 as a large hydrophobic residue. Therefore, this region has the characteristics of a typical protein-protein interface. Interestingly, in the 2.2 Å crystal structure of the short γ Nup170₁₂₅₃₋₁₅₀₂, the N-terminal helix, α 14, is unwound, and the first 10 residues wrap around the surface of the protein and align in the hydrophobic groove (Figure 2-6C). One may speculate whether this rearrangement and interaction has physiological relevance. With the full α -helical domain present, this motion of helix α 14 would reorient the N-terminal portion dramatically, causing it to extend opposite the direction observed in this structure. Alternatively, we can consider the intramolecular interaction of these 10 residues as a serendipitous crystal artifact, which may mimic the interaction with the natural binding partner. In the later case, this structure would suggest the physical mechanism by which such interaction occurs.

Comparison of Nup170 to Nup157

In *S. cerevisiae*, Nup170 has a paralog, Nup157, not present in metazoa (Aitchison et al., 1995), likely a consequence of the whole genome duplication that occurred in the ancestor of *Saccharomyces* (Wolfe and Shields, 1997). We modeled the homologous α -helical domain of Nup157, which can be done confidently (sequence identity is 41% for the 60 kDa segment in question). We note that the exposed residues at the second conserved surface of Nup170 are identical in Nup157, except residue 1328 is serine instead of alanine. If this hydrophobic groove is a protein interface, we predict Nup170 and Nup157 bind to the same molecule. The most apparent difference between the α -helical domains of Nup170 and Nup157 are three insertions in the very N-terminal portion of the α -helical domain of Nup170, not part of this structure. These Nup170 extensions are predicted as disordered loops. Thus, it is likely that the structures of the two proteins have a very similar topology across the entire α -helical region.

Discussion

The size, complexity and heterogeneity of the NPC make this complex a formidable challenge to structural biology. However, since the NPC is assembled from subcomplexes in modular fashion, the high-resolution structure can be approached by a divide-and-conquer strategy (Schwartz, 2005). Two multiprotein complexes compose the principal scaffold architecture—the Y-complex and the Nic96-complex (Alber et al., 2007). We report here one structure from each: hNup107₆₅₈₋₉₂₅•hNup133₅₁₇₋₁₁₅₆ of the Y-complex and yNup170₉₇₉₋₁₅₀₂ of the Nic96-complex. Structural similarities between Nup133 and Nup170 indicate that these nucleoporins descend from a common ancestor. Since ACE1 proteins are also found in both major structural complexes of the

NPC we conclude that both complexes employ similar structural principles. The extant NPC likely derived from duplication and diversification of a few ancestral genes.

The structure of Nup133 provides a significant portion for a now nearly complete high-resolution model of the heptameric core of the Y-complex, as cartooned in Figure 2-7. This complex has been studied extensively by crystallography and electron microscopy (Berke et al., 2004; Boehmer et al., 2008; Brohawn et al., 2008; Debler et al., 2008; Hsia et al., 2007; Leksa et al., 2009; Lutzmann et al., 2002). A central hub connects two short arms to a long and kinked stalk (Lutzmann et al., 2002; Siniosoglou et al., 2000). The nucleoporins that build this Y connect via binary interactions with strong affinities (Boehmer et al., 2008; Brohawn et al., 2008). Crystal structures of most elements are now known. Seh1•Nup85 and Nup120 form the short arms (Brohawn et al., 2008; Leksa et al., 2009). Sec13•Nup145C is the proximal segment of the kinked stalk (Hsia et al., 2007); Nup84 is the chain-link between Nup145C and the distal Nup133.

Electron micrographs of the Y-complex suggest that some segments can articulate with respect to one another (Kampmann and Blobel, 2009; Lutzmann et al., 2002). Our hNup107₆₅₈₋₉₂₅•hNup133₅₁₇₋₁₁₅₆ reveals one molecular determinant of that flexibility. The extended zig-zig at the center of the Nup133 α -helical domain provides an accordion-like transition that allows the flat, N-terminal α -helical plane of Nup133 to flex against Nup84(hNup107). This motion can be simulated using an elastic network model (Suhre and Sanejouand, 2004). In addition, there is a second hinge between the Nup84(hNup107)-binding interface and the compact, C-terminal, all α -helical domain (Boehmer et al., 2008).

The Nic96-complex is less well studied than the Y-complex. At high resolution, the ACE1 domain of Nic96 is known (Jeudy and Schwartz, 2007; Schrader et al., 2008), as well as the 15 kDa homodimerization domain of Nup53(hNup35) (Handa et al., 2006). Both structures are uncomplexed and the direct interaction partners within the

Nic96-complex are not known with certainty. Nup157/170 is another member of this complex. Here we report the structure of a major portion of the α -helical stack domain of Nup170. Like Nup133, Nup170 contains a flexibly tethered N-terminal β -propeller, followed by a large, ~70 kDa, α -helical domain. The α -helical domains of Nup133 and Nup170 both are divided into rigid segments connected via flexible hinges. Pairwise superposition of these segments accentuates the structural resemblance between the two proteins, particularly in the central zig-zag and in the interface bundle (Figure 2-5).

The Nic96-complex is apparently not as stably associated as the Y-complex. The many different interactions that have been reported for the Nic96-complex indicate that it has a role as a connector. The interaction with the FG-Nup-Nsp1 complex (Grandi et al., 1995) on the one hand and Ndc1 on the other (Hawryluk-Gara et al., 2008) indicates that it spans the width of the NPC scaffold.

The crystal structures solved here solidify the notion that the major scaffold complexes of the NPC are structurally related. On that basis, we suggest that the Nic96-complex adopts a branched structure and that its components are joined through binary interactions. In Nup133, the interaction with Nup84 tethers the protein to the NPC (Boehmer et al., 2008). It is known that, as in Nup133, the α -helical domain of Nup170 is necessary and sufficient to target the protein to the NPC (Flemming et al., 2009). We show here that the surface by which Nup133 binds Nup84 is also conserved in Nup157/170, but is not as hydrophobic, arguing for perhaps a more dynamic interaction.

Weaker interactions and protein-peptide interactions will play auxiliary roles in the assembly of both scaffold complexes, and in their function. For example, the N-terminal 29 residues of the mRNA export factor Gle1 tether it via hNup155(yNup157/170) to the NPC (Rayala et al., 2004). An interaction between Nup120 and Nup157/170 may join the two complexes (Lutzmann et al., 2005).

A comparison of a variety of scaffold nucleoporins is now possible. One class shares the common ACE1 domain (Brohawn et al., 2008), also found in the COPII coat protein Sec31 (Fath et al., 2007). This class includes Nup85, Nup145C, Nic96 and Nup84. ACE1 consists of three α -helical modules, termed crown, trunk and tail. These proteins fold back onto themselves to form a U-turn within the crown module. The trunk is composed of two α -helical units running in opposite directions, capped by the tail module. The tail of Nup84(hNup107) is shown here in complex with Nup133, and the tails of other ACE1 domains also support protein-protein interfaces (Brohawn et al., 2008; Jeudy and Schwartz, 2007). The ACE1 trunk domain, with multiple helices embedded in the hydrophobic core, confers greater rigidity than structures built of stacked α -helical pairs, which are more flexible. For example, all nuclear transport receptors are constructed from repeated α -helical pairs or triples, and the functional significance of flexibility is well documented (Conti et al., 2006). In Nup133 and Nup157/170, the helices do not fold back on one another as in the ACE1 trunk. Instead they typically pair, albeit without a recognizable repeat pattern. Consequently, they are more flexible than ACE1 proteins. Further, Nup133 and Nup157/170 show greater variation than the ACE1—though a central core has much the same accordion-like structure in both, flanking this core there is substantial variation.

As both Nup133 and Nup157/170 have a β -propeller/ α -helical stack tandem arrangement, one can speculate whether this alone indicates a common ancestry. However, Nup120, another nucleoporin with this domain arrangement, resembles neither Nup133 nor Nup170, nor ACE1 (Leksa et al., 2009).

The overall topologies of each class of scaffold nucleoporin are shown in Figure 2-8. The α -helical domains of Nup133 and the ACE1 Nic96 are equally long (Figure 2-8A,B), however the N terminus of the ACE1 is at the middle of the domain rather than at one end. Nup120 has a more convoluted architecture and is shorter (Figure 2-8C). Its α -helical domain is interrupted by a blade of the N-terminal

β -propeller, with which it integrates to form one compact entity. Taken together, these three domain classes are not really structurally related, other than all being α -helical.

The assembly principles of vesicle and nuclear pore membrane coats are related and some of their components evolved from common ancestors. The structural similarity between the ACE1 proteins of the NPC and of the COPII vesicle coat established the common ancestry (Brohawn et al., 2008), as hypothesized previously (Devos et al., 2004; Devos et al., 2006). Both coat assemblies also incorporate the bifunctional protein Sec13. We expect that the scaffold structure of the NPC is as open and lattice-like as the COPII coat and has similar connectivities in parts. However, Nup133 and Nup170 have no known structural homologs outside the NPC and their specific integration into the NPC scaffold needs to be further analyzed. In addition, the NPC core scaffold contains two other large α -helical proteins, Nup188 and Nup192 (Kosova et al., 1999; Nehrbass et al., 1996), whose structures may reveal new surprises.

To build a rudimentary NPC scaffold, one might need only a few different structural building blocks. In an early eukaryote, we speculate, multiple copies of a small number of distinguishable elements formed a complete NPC scaffold. Gene duplications then created families of related nucleoporins. The members of each family evolved divergently into the distinct, non-redundant structural elements of extant NPCs.

This theory for the origin of the NPC explains the perplexing observation that many structural nucleoporins are not essential in yeast. Under stressed conditions, these genes can still partially complement one another. Given that the same structural elements can be detected in the NPCs of all extant eukaryotes, this process of diversification must have occurred in the early eukaryote. No extant eukaryote has a scaffold significantly simpler than the yeast or human NPC (Mans et al., 2004). The NPC likely evolved early in eukaryotic evolution, by multiplication of a few structural

elements. Today, these multiplications are still evident, though the amino acid sequences of these ancestral elements have diverged greatly.

With a growing inventory of nucleoporin structures, the next task will be to determine the higher-order assembly of the NPC. The anatomy of the NPC has been delineated by cryo-electron tomography (Beck et al., 2004; Beck et al., 2007; Stoffler et al., 2003) and a computational analysis produced a draft of the NPC (Alber et al., 2007), but there are still various ways in which these nucleoporins might arrange to form the entire assembly. The lattice-like structure of the NPC provides few spatial restraints, and interactions between complexes are largely still unknown. However, the structures of the architectural nucleoporins—those presented here and those already available—narrow the speculations about the NPC assembly. These structures now allow us to probe the NPC by genetic manipulation of specific structural elements. Some models already can be ruled out. Altogether, from a combination of structural, computational, and cell biology research, the structure of the NPC is fast emerging.

Methods

Protein Expression and Purification

Nup170 from *S. cerevisiae* was cloned into a pET-Duet vector (Novagen) encoding an N-terminal, human rhinovirus 3C (HR3C)-cleavable His₆-tag. N-terminal truncations were generated by PCR methods. Nup133 (residues 517-1156) and Nup107 (residues 658-925) from *H. sapiens* were cloned into a bicistronic pET-Duet vector, modified to encode N-terminal, thrombin-cleavable His₆-tags. Proteins were expressed in *E. coli* strain BL21 (DE3)-RIL (Stratagene) in LB medium, induced with 200 μ M isopropyl- β -D-1-thiogalactopyranoside at 18°C.

Cells expressing yNup170₉₇₉₋₁₅₀₂ or yNup170₁₂₅₃₋₁₅₀₂ were homogenized at 4 °C in 50 mM potassium phosphate pH 8.5, 400 mM NaCl, 40 mM imidazole, 5 mM β -mercaptoethanol (β -ME). The protein was bound to Ni-affinity resin and eluted with 250 mM imidazole, dialyzed against 20 mM Tris-HCl pH 8.5, 150 mM NaCl, 0.5 mM EDTA, 1 mM DTT, and purified, after affinity tags were removed, on a Superdex S75 column (GE Healthcare), equilibrated in 10 mM Tris-HCl pH 8.5, 150 mM NaCl, 0.1 mM EDTA, 1 mM DTT. Selenomethionine-substituted protein was expressed as described (Brohawn et al., 2008).

hNup107₆₅₈₋₉₂₅•hNup133₅₁₇₋₁₁₅₆ were bound to Ni-affinity resin in lysis buffer, 20 mM Tris-HCl, 5 mM potassium phosphate pH 8.5, 250 mM NaCl, 10 mM imidazole, 5 mM β -ME, then eluted with 250 mM imidazole, and purified, after the affinity tags were removed, on a HiTrap FF and then a Superdex 200 column, equilibrated in 5 mM potassium phosphate pH 7, 150 mM NaCl, 0.1 mM EDTA, 1 mM DTT.

Protein Crystallization

yNup170₉₇₉₋₁₅₀₂ was concentrated to 4-8 mg·mL⁻¹. An initial crystallization condition was found by vapor diffusion using commercial screens. Crystallization was greatly improved by addition of tris(2-carboxyethyl)phosphine (TCEP). Crystals were grown at 4 °C, in 2 µl hanging drops over 0.2 M NH₄AcO, 0.1 M Tris-HCl pH 7.9, 5-10 % polyethylene glycol (PEG) 3,350, 5 mM TCEP. Rods, ~80-100 µm x ~80-100 µm x 300-400 µm, with isosceles triangular bases, formed within 3 days. They were flash-frozen in reservoir supplemented with 24% PEG 200, 24% ethylene glycol, or 25 % glycerol.

yNup170₁₂₅₃₋₁₅₀₂ crystallized at 90 mg·mL⁻¹ in 1 µl hanging drops over 0.1 M Tris-HCl pH 8.5, 0.2 M Li₂SO₄, 50 mM NaCl, 22-24% PEG 3,350 within 3-5 days at 18 °C. Plates, 50 µm x 300 µm x 300 µm, were cryoprotected in reservoir solution supplemented with 12% glycerol and flash-frozen.

hNup107₆₅₈₋₉₂₅•hNup133₅₁₇₋₁₁₅₆ was concentrated to 9 mg·mL⁻¹ and 2% PEG 3,350 added. An initial crystallization condition was found using commercial screens. After optimization, crystals were grown in drops of 1 µl protein, supplemented with 2% PEG 3,3350, + 1 µl reservoir of 0.8-1.0 M sodium/potassium phosphate pH 7.8, 15% glycerol at 18 °C, streak-seeded after 12 hours with microcrystals. In most drops, phase separation rather than crystallization was observed. Occasionally, thin needles with dimensions of 30 µm x 30 µm x 150 µm grew within 2 days. Crystals were retrieved on MicroMounts (Mitegen), and flash-frozen in liquid nitrogen.

Data Collection, Structure Solution and Refinement

Data for yNup170₉₇₉₋₁₅₀₂ were collected at 100 K at microfocus beamline 24-IDE at the Advanced Photon Source (Argonne, IL). The crystals that diffracted best, to ~2.5 Å, were perfectly merohedrally twinned. Untwinned data were obtained to 3.2 Å and used for further analysis. Data were collected from selenomethionine-labeled crystals and

processed with the HKL2000 package (Otwinowski and Minor, 1997). Phases were determined by Se-SAD. 9 of 10 possible Se sites were identified with SHELXD (Sheldrick, 2008). Se positions were refined with SHARP (Vonrhein et al., 2007), which also revealed the additional Se site, and experimental phases calculated. The resulting solvent-flattened electron density map was used to build a model with Coot (Emsley and Cowtan, 2004).

To improve model quality and attempt to refine against the twinned data diffracting to higher resolution, the C-terminal subdomain yNup170₁₂₅₃₋₁₅₀₂ was crystallized and 2.2 Å data collected at beamline 24-IDC at the Advanced Photon Source from a large crystal formed from several caked layers. The strongest of the observed diffraction patterns was indexed and integrated. Out of many specimen tested, morphologically indistinguishable, only this crystal diffracted strongly and belonged to space group I222 (Table 2-2). All others belonged to space group P6₃22, diffracted to 3.5 Å, and were not further analyzed. A molecular replacement solution for yNup170₁₂₅₃₋₁₅₀₂ was found using a partial model from the initially obtained 3.2 Å structure of yNup170₉₇₉₋₁₅₀₂. A complete model for yNup170₁₂₅₃₋₁₅₀₂ was built automatically, with minor intervention, using PHENIX (Adams et al., 2002). yNup170₉₇₉₋₁₅₀₂ was rebuilt incorporating this partial model, improving refinement parameters. We note, however, that the model of the yNup170 C-terminal subdomain did not help process the twinned 2.5 Å data (not shown).

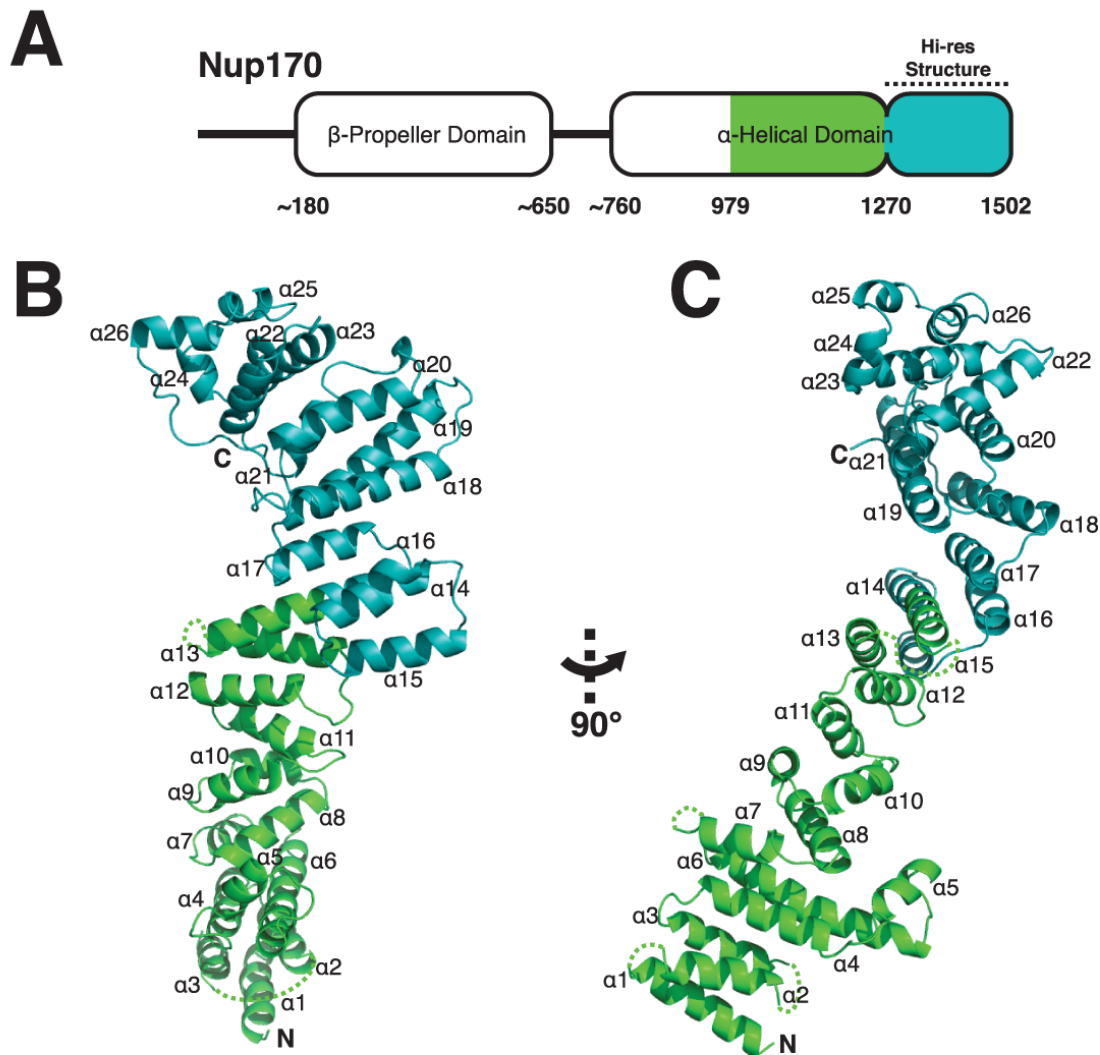
Data for hNup107₆₅₈₋₉₂₅•hNup133₅₁₇₋₁₁₅₆ were collected at 100 K at 24-IDE. Due to significant radiation damage, partial data sets were collected and merged from several crystals grown in the same crystallization drop, each exposed at 3-10 spots. The structure was phased by molecular replacement using the minimal 55 kDa hNup107₆₅₈₋₉₂₅•hNup133₉₃₄₋₁₁₅₆ interaction complex (Boehmer et al., 2008) as a search model in Phaser (McCoy et al., 2007) in the CCP4 suite (Bailey, 1994). The additional 45 kDa domain was built and refined with Coot (Emsley and Cowtan, 2004) and PHENIX

(Adams et al., 2002). Data to 3.5 Å were included, despite low I/σ , as recommended for low-resolution crystallography (Brunger et al., 2009). Anisotropic diffraction was corrected by elliptical resolution truncation and anisotropic B-factor correction using the Diffraction Anisotropy Server (www.doe-mbi.ucla.edu/~sawaya/anisotoc/) (Strong et al., 2006). The obtained electron density maps allowed positioning of the secondary structure elements, which are essentially all α -helical. Connections between helices were mostly visible, allowing tracing of the molecule from N to C terminus. Observed chain topology and variation in the length of helices allowed us to assign each modeled helix unambiguously to the secondary structure as predicted by the PredictProtein server (Rost et al., 2004). In the absence of detailed positional markers, the assigned sequence in the deposited data is approximate, but is likely erroneous only in a few places and shifted by not more than 3-4 residues, i.e. one α -helical turn. Several non-helical loops could be traced confidently, including loops that are disordered in the partial structure hNup107₆₅₈₋₉₂₅•hNup133₉₃₄₋₁₁₅₆ (Boehmer et al., 2008).

Structure Analysis

Nup170 homologs were retrieved from the NCBI website database (<http://www.ncbi.nlm.nih.gov/>) and a multiple sequence alignment calculated by the MUSCLE algorithm (Edgar, 2004). An Average Distance Tree was used to select representative, divergent sequences. Residues were scored for conservation by the AMAS method in JALVIEW (Waterhouse et al., 2009). PDB2PQR (Dolinsky et al., 2004) and APBS (Baker et al., 2001) were used to calculate surface charge, and the PISA server to calculate accessible surface area (Krissinel and Henrick, 2007). MODELLER (Eswar et al., 2007) was used to build a complete model of yNup157₉₀₀₋₁₃₉₁. Pymol (<http://www.pymol.org>) was used to generate figures.

Figures

**Figure 2-1 Nup170₉₇₉₋₁₅₀₂ forms a bipartite, irregular α -helical stack**

- (A) The predicted domain structure of Nup170 is diagrammed, with β -propeller domain, residues 180-650, and α -helical domains, residues 760-1502 drawn as ovals. Indentation at residue 1270 reflects the division into two parts. The portion of the structure solved is colored as in B and C.
- (B) Cartoon representation of the 3.2 Å structure of the α -helical C-terminal domain of Nup170 with its two subdomains shown in green and aquamarine, respectively. Secondary structure elements and termini are labeled. Disordered loops connecting structural elements are drawn as dotted lines. A central, long helix, α 14, spans and connects the two subdomains. The C-terminal subdomain,

helices α 14-26 was also expressed as a separate protein fragment and solved at 2.2 Å resolution.

(C) Structure rotated by 90° compared to B.

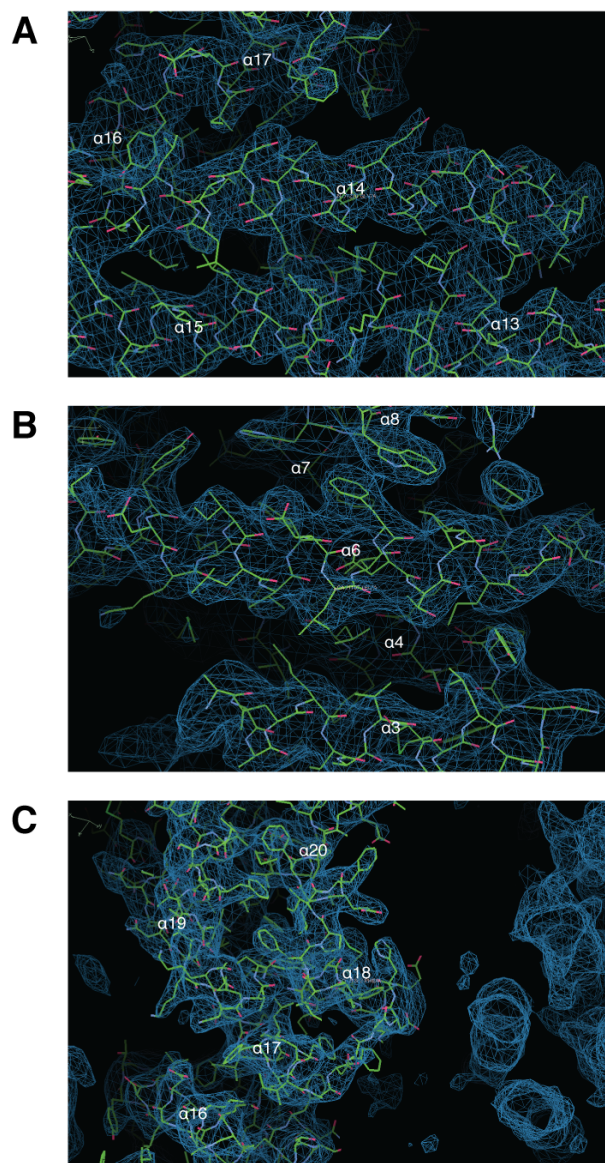


Figure 2-2 Model and Electron Density for Nup170₉₇₉₋₁₅₀₂

Representative sections are shown with 2F_o-F_c map contoured at 1.0 σ .

(A) Helix α 14 bridging the two parts of the helical stack.

(B) The N-terminal helical stack.

(C) End-on view of helices and a connecting loop in the C-terminal helical stack.

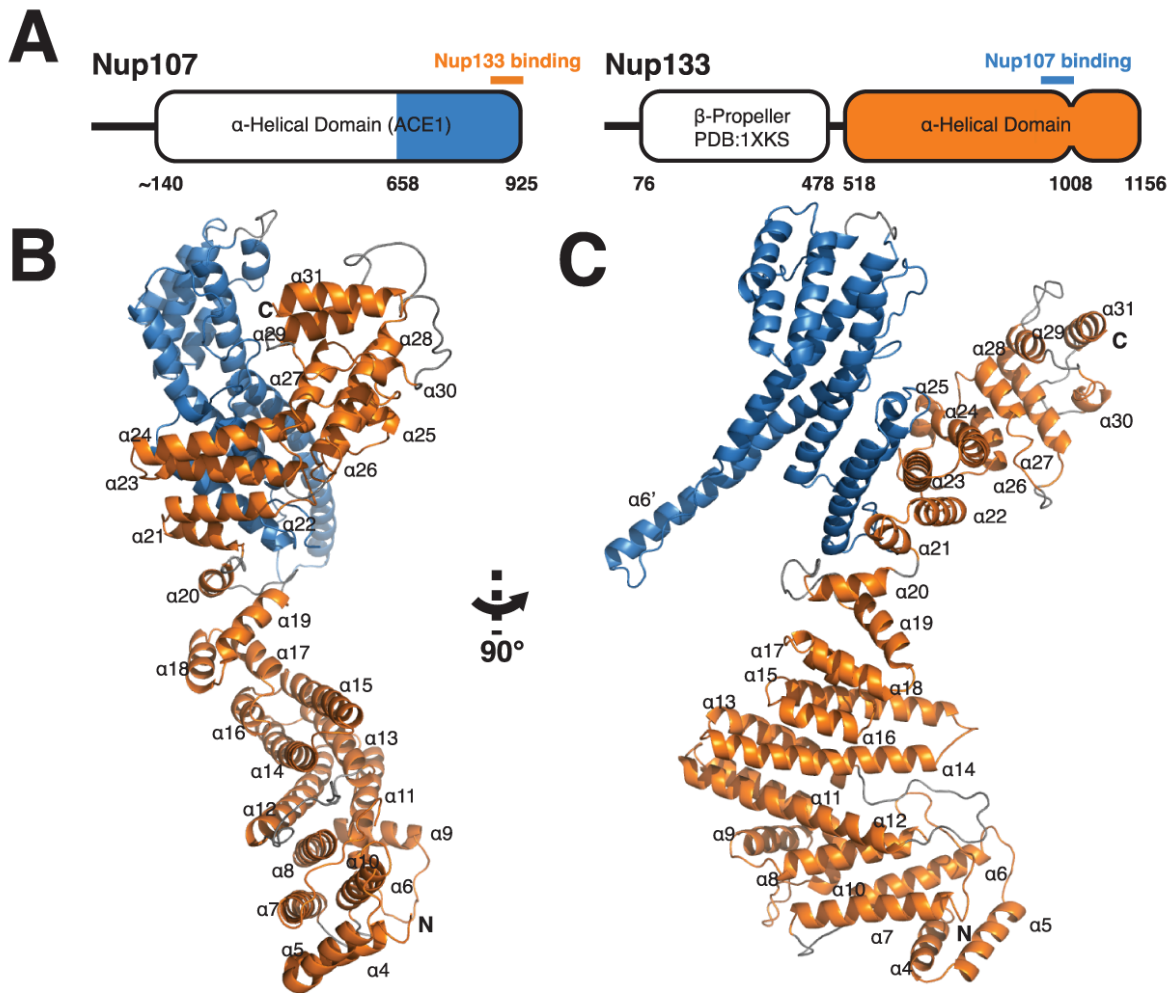


Figure 2-3 Nup133₅₁₇₋₁₁₅₆ in complex with Nup107₆₅₈₋₉₂₅

- (A) The domain structures of Nup107 and Nup133 are diagrammed. Nup107 consists of a single α -helical domain homologous to other ACE1 proteins. Nup133 has a β -propeller domain, residues 76-478, solved previously, and an α -helical domain as shown in B and C. The portions of each molecule solved here are colored. Indentation at residue 1008 of Nup133 reflects the hinge between helices α 24 and α 25.
- (B) The α -helical domain of Nup133 (orange) in complex with Nup107₆₅₈₋₉₂₅ (blue). Loops evident in the electron density, but not modeled for the purpose of refinement, are grey. Secondary structure elements and termini of Nup133 are labeled, beginning at the N terminus of the domain, helix α 4.
- (C) Structure rotated by 90° compared to B. Nup107 helix α 6', a metazoan-specific structural element, is labeled.

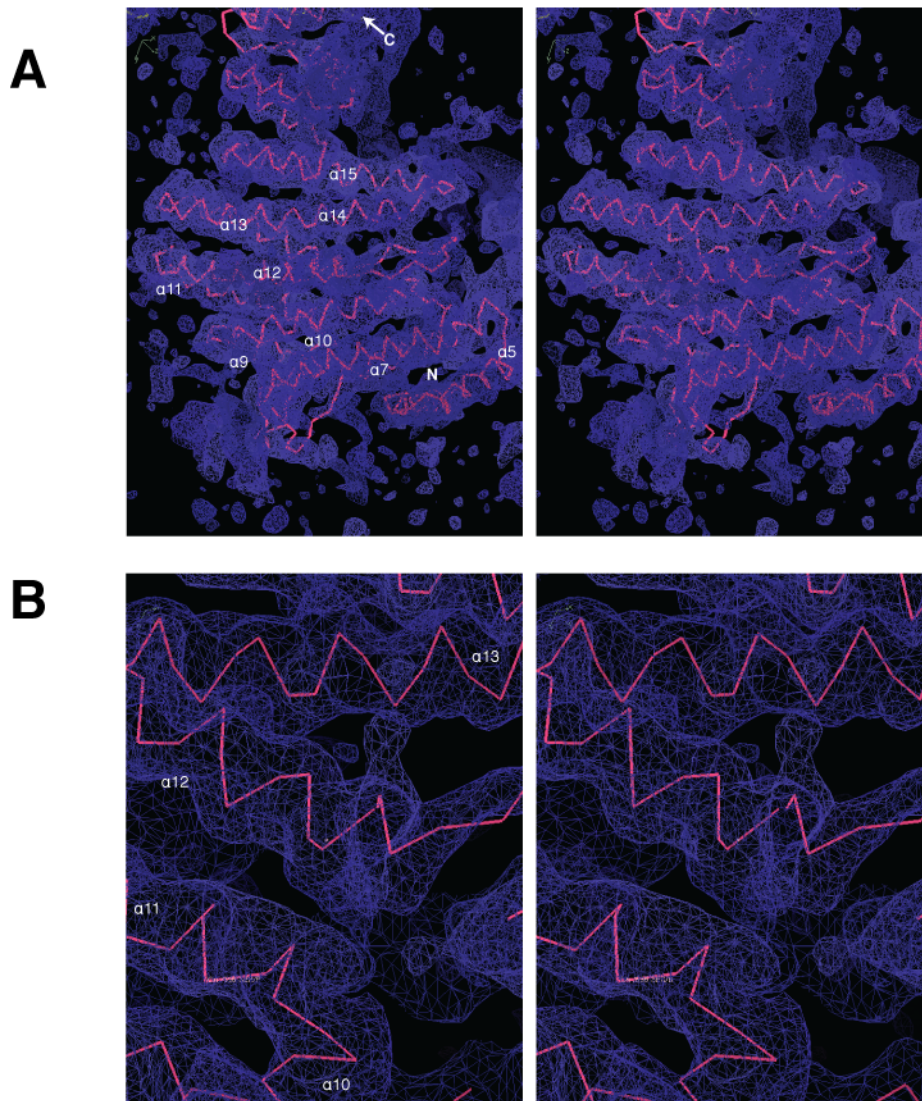


Figure 2-4 Model and Electron Density for Novel Portion of Nup133₅₁₇₋₁₁₅₆

- (A) Overview of residues 517-930, in stereo, $2F_o-F_c$ map contoured at 1.0σ . The sequence is tentatively assigned, however the model in this area is refined as polyserine. The N-terminus of the domain is at the bottom right. The overhand turn connecting helices $\alpha 9$ and $\alpha 10$ is at the lower left. This orientation is similar to that of Figure 2-3B. A small portion of the molecular replacement model is visible at the top.
- (B) Enlargement of the central portion of panel A.

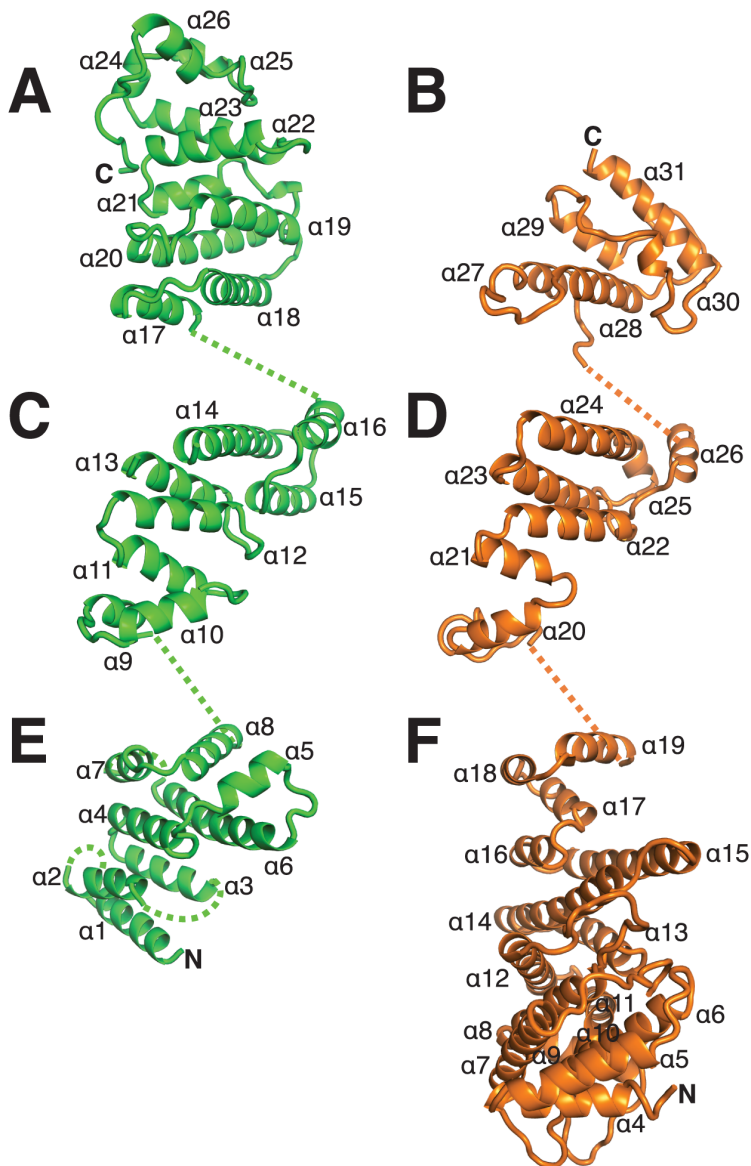


Figure 2-5 Topology of Nup170 and Nup133 α -helical domains is conserved

Nup170 in green and Nup133 in orange were compared by structural alignment of segmental subdomains. Nup170 N-terminal (E), central (C), and C-terminal (A), subdomains were structural aligned to the related segments (F, D, B) in Nup133. Secondary structure elements are labeled. Unmodelled loops and connections between domains are shown as dotted lines. The N-terminal remainder of each molecule not solved here extends where marked N. The C terminus of each molecule is marked C.

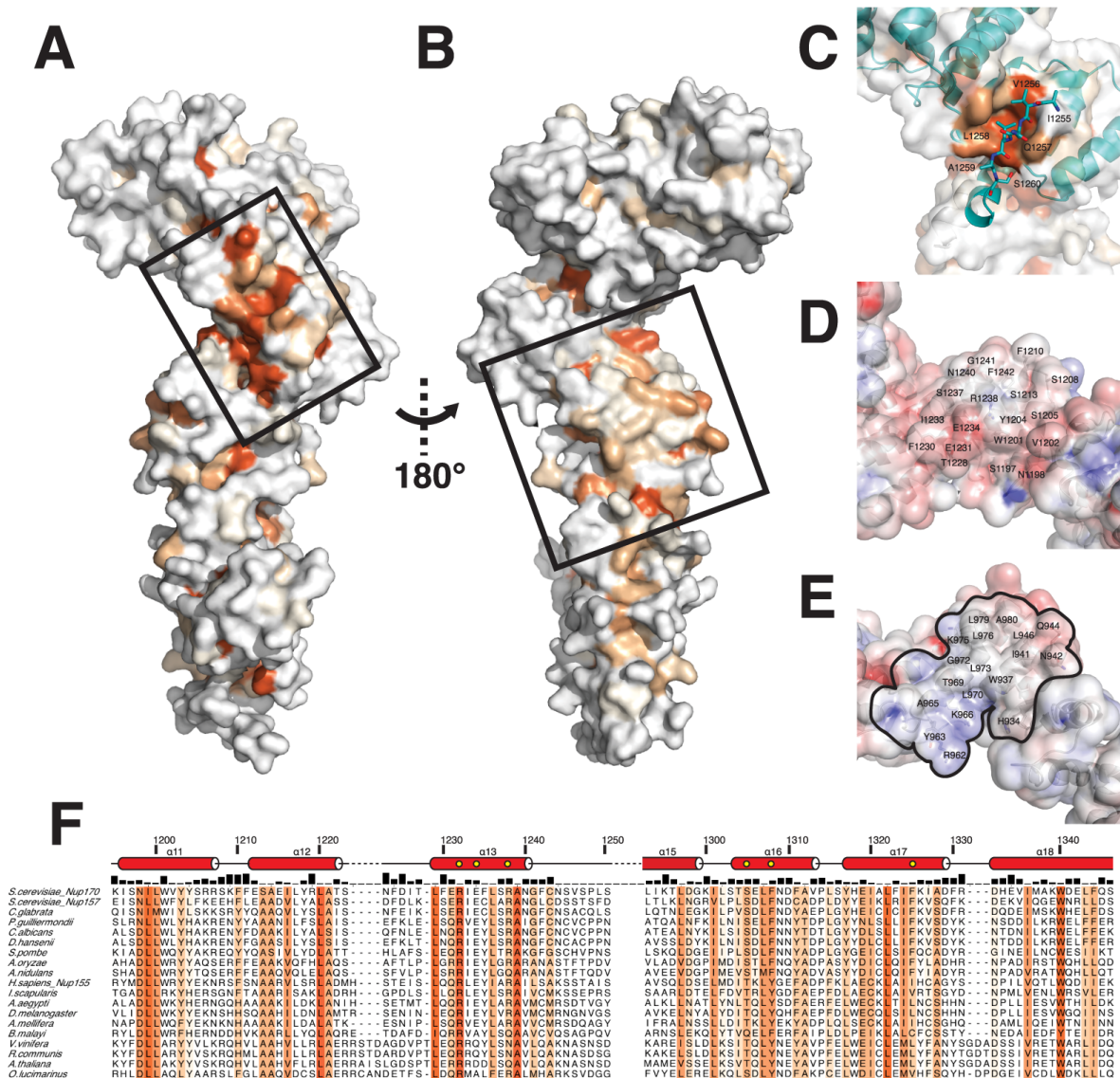


Figure 2-6 Surface conservation of Nup170 suggests two protein-protein interfaces

- (A) Amino acid sequence conservation among Nup170 genes from maximally diverse eukaryotes was mapped on the protein, gradient-colored from white (not conserved) to orange (strongly conserved), orientated as in Figure 2-1B. A conserved groove is boxed.
- (B) Structure rotated 180° compared to A, with conserved surface patch boxed.
- (C) Surface groove boxed in A shown magnified. Structure of C-terminal subdomain at 2.2 Å resolution is superposed and shown in aquamarine as a cartoon. Helix α 14 as white cartoon, extending down and left, in the conformation seen in the full domain, as well as in aquamarine as the well-ordered, extended peptide

seen in the 2.2 Å structure of the isolated C-terminal subdomain. Key residues are labeled.

- (D) Surface patch boxed in B is magnified and shown as a cartoon with exposed residues labeled. Partially transparent surface representation is colored by calculated surface charge, in a gradient from negative (red) to neutral (white) to positive (blue).
- (E) Homologous section of Nup133 colored and labeled as in D with extent of interface to Nup107 delimited by a solid black line.
- (F) Sequence alignment of maximally diverse selection of eukaryotic Nup170 sequences, colored by conservation as in A, B, and C. Helical segments are shown as red cylinders and labeled. Bar graph shows accessible surface area for each residue. Yellow circles mark: conserved, buried arginine 1232; two hydrophilic surface residues, glutamine 1234 and arginine 1238, that would be buried were this surface, shown in D, indeed a protein-protein interface, as in Nup133, shown in E; and residues serine 1305, phenylalanine 1308 and phenylalanine 1325, lining the groove shown in C.

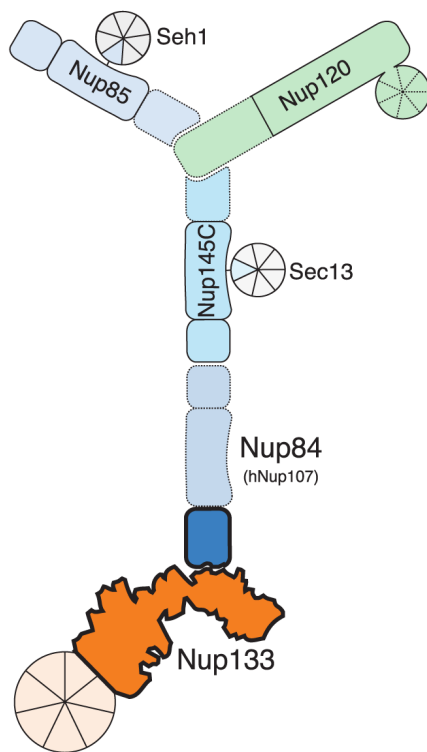


Figure 2-7 Schematic Representation of the Heptameric Nup84-complex, or Y-complex

The Nup84 subcomplex is composed of three ACE1 proteins (blues), Nup133 (orange), Nup120 (green), and β -propeller proteins Seh1 and Sec13 (grey). Nup85 and Nup145C each contribute *in trans* one blade of the Seh1 and Sec13 β -propellers. The portions of Nup133 and Nup107 solved here, as shown in Figure 2-3, are outlined in bold. The

N-terminal β -propeller of Nup133 and all portions of the Y outlined by solid lines have been solved at atomic resolution previously. Dashed lines denote portions of the Nup84 subcomplex for which no atomic resolution structures have yet been published.

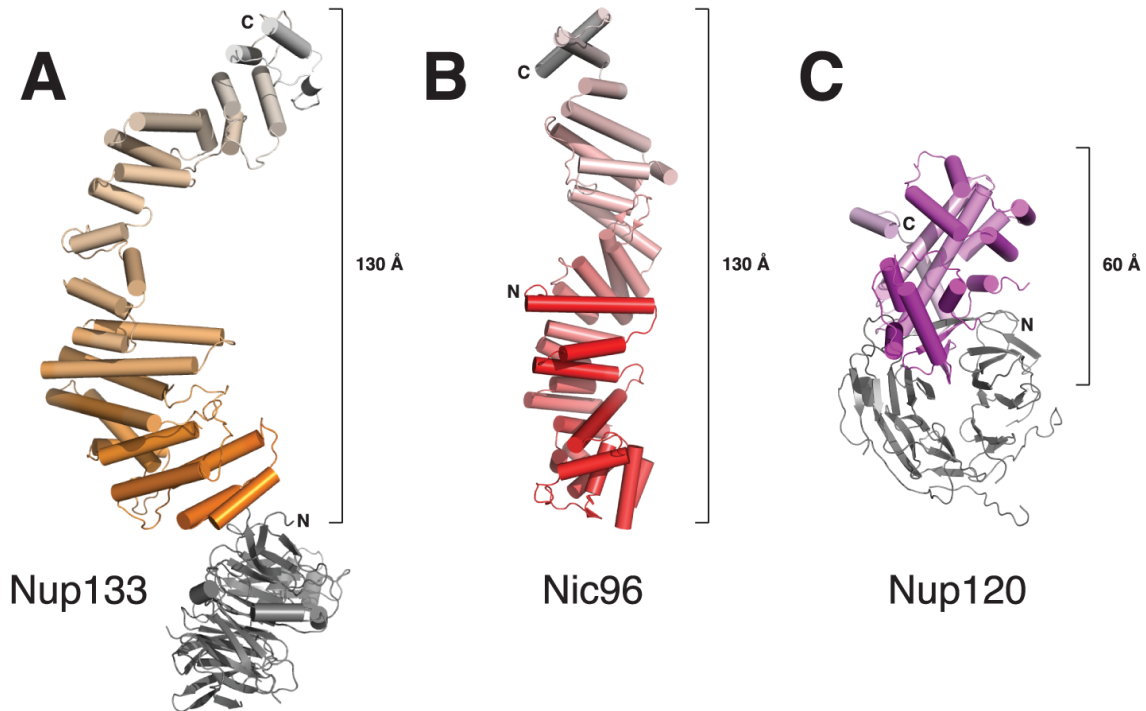














Figure 2-8 Representative Nucleoporin α -Helical Stack Domains

- (A) The overall topology of human Nup133 (residues 75-1156) is shown. The structure is gradient-colored from orange to white from the N terminus of the helical domain to the C terminus. The β -propeller domain is colored grey.
- (B) The overall topology of yeast Nic96 (residues 200-835), an ACE1, is shown. The structure is gradient colored from red to white from N to C terminus.
- (C) The overall topology of yeast Nup120 (residues 1-730 of 1037) is shown. The α -helical domain is gradient-colored from magenta to white from N to C terminus. Residue 1-381 are colored grey and form β -propeller blades β 1- β 6 and strand β 7D. Note that strands A-C of blade β 7 are contributed by the portion of the α -helical domain that links helix α 4 to helix α 5.

Gene Name		PDB codes	Domain Architecture
<i>S. cerevisiae</i>	<i>H. sapiens</i>		
<u>Nic96</u>	Nup93	2QX5, 2RFO	
<u>Nup170</u>	Nup155	3I5P, 3I5Q	
Nup157	Nup155		
Nup192	Nup205		
Nup188	Nup188		
Nup53	<u>Nup35</u>	1WWH	
Nup59			
<hr/>			
Nup84	<u>Nup107</u>	3CQC, 3I4R	
Nup133	<u>Nup133</u>	1XKS, 3CQC, 3I4R	
<u>Nup120</u>	Nup160	3HXR	
<u>Nup85</u>	Nup85	3EWE, 3F3F	
<u>Seh1</u>	Seh1	3EWE, 3F3F	
<u>Nup145C</u>	Nup96	3BG1	
<u>Sec13</u>	<u>Sec13</u>	3BG1	








 α -helical domain
 α -helical domain (ACE1)
 β -propeller domain
 β -propeller insertion blade
 coiled-coil
 α/β domain
 loop

Table 2-1 Proteins of the NPC Core Structural Scaffold

Structures of the underlined proteins have been published. Gene names and PDB codes from this work are in bold.

	hNup107 ₆₅₈₋₉₂₅ • hNup133 ₅₁₇₋₁₁₅₆	yNup170 ₉₇₉₋₁₅₀₂	yNup170 ₁₂₅₃₋₁₅₀₂
		SeMet	Native
PDB Code	3I4R		3I5P
Data Collection			3I5Q
Spacegroup	P2 ₁ 2 ₁ 2 ₁	H32	H32
Cell Dimensions			I222
a, b, c (Å)	115.6, 133.0, 176.3	121.4, 121.4, 258.1	121.4, 121.4, 256.7
α, β, γ (°)	90, 90, 90	90, 90, 120	90, 90, 120
Resolution range (Å)	37.6-3.5 (3.63-3.5)	30-3.5 (3.63-3.5)	30-3.2 (3.31-3.2)
No. of unique reflections	29866	9123	12125
Completeness (%)	85.7 (40)	96.8 (96.4)	98.6 (90.0)
Redundancy	5.4 (2.6)	7.9 (7.2)	3.4 (3.1)
R _{sym} (I) (%)	15.7 (-)	9.8 (37.5)	5.6 (25.4)
I/σI	11.6 (0.59)	26.7 (4.5)	25.9 (2.6)
Elliptical Truncation Radii (Å)	4.3, 3.5, 4.2		
Anisotropic Scale Factors (Å ²)	39.9, 8.50, -48.4		
No. of unique reflection remaining	23455		
Refinement			
Resolution range (Å)	37.6-3.5		30-3.2
R _{work} (%)	31.2		30.6
R _{free} (%)	37		32.4
Number of reflections	23455		11975
Number of atoms			32541
Total	5485		3552
Waters	0		0
Average B-factor (Å ²)	185		148
Ramachandran analysis (%)			
Favored	90.9		90.4
Allowed	7.9		8.9
Disallowed	1.2		0.7

Table 2-2 Data Collection and Refinement Statistics

The highest resolution shell is shown in parentheses.

CHAPTER 3 Structure of the Sec13•Sec16 edge element, a template for assembly of the COPII vesicle coat

This chapter has been submitted for publication at the *Journal of Cell Biology*.

Abstract

Ancestral coatomer element 1 (ACE1) proteins assemble latticework coats for COPII vesicles and the nuclear pore complex. The ACE1 protein Sec31 and Sec13 make a 2:2 tetramer that forms the edge element of the COPII outer coat. Here we report that the COPII accessory protein Sec16 also contains an ACE1. The 165 kDa crystal structure of the central domain of Sec16 in complex with Sec13 was solved at 2.7 Å resolution. Sec16 and Sec13 also make a 2:2 tetramer, another edge element for the COPII system. Domain-swapping at the ACE1•ACE1 interface is observed both in the prior structure of Sec13•Sec31 and in Sec13•Sec16. A Sec31 mutant in which domain-swapping is prevented adopts an unprecedented laminated structure, solved at 2.8 Å resolution. Our *in vivo* data suggest that the ACE1 element of Sec31 can functionally replace the ACE1 element of Sec16. Our data support Sec16 as a scaffold for the COPII system and a template for the Sec13•Sec31 coat.

Introduction

The COPII coat complex mediates formation of transport vesicles that bud from the endoplasmic reticulum (ER) and traffic secretory proteins to other organelles (Antonny and Schekman, 2001; Bonifacino and Glick, 2004; Hughes and Stephens, 2008; Tang et al., 2005). COPII consists of an inner coat composed of the Sec23•Sec24 dimer and the small GTPase Sar1, and an outer coat composed of Sec31 and Sec13 (Stagg et al., 2007). Sec13 is a β -propeller protein and has a dual role, as it also is present in the nuclear pore complex (NPC) (Siniosoglou et al., 1996). The ER and nuclear envelope (NE) form a contiguous lipid bilayer. The NPC coats the NE at nuclear pores, establishes the selective permeability barrier of the NE, and

serves as the sole conduit for transport across the NE (Brohawn et al., 2009). It is composed of ~30 proteins, termed nucleoporins, each present in 8-n copies, which are organized into subcomplexes symmetrically arranged about a central axis. A subset of architectural nucleoporins comprises the core structural scaffold of the NPC.

Crystallographic studies have demonstrated that the central α -helical unit of Sec31 is structurally similar to four large architectural nucleoporins, one of which binds Sec13. This α -helical unit, common to COPII and the NPC, is therefore termed the ancestral coatomer element 1 (ACE1) (Brohawn et al., 2008).

The ACE1 has a unique, irregular (not α -solenoidal) structure. It folds back on itself to form a J-shape, divided into three modules (Figure 3-1). The N-terminal and middle subdomains of the ACE1 fold together to constitute the “trunk.” The U-turn between these subdomains is the “crown.” The ACE1 of nucleoporins has an additional module at the C-terminus, the “tail.” Sequence similarity among the five known ACE1 proteins is weak—they have tolerated considerable mutation without compromising the overall structure. Their common ancestry was thus noted only after crystal structures were solved (Brohawn et al., 2008). Sec31 and Nup145C each bind Sec13 using the same mechanism, insertion of a single β -blade to close the open, six-bladed propeller of Sec13 *in trans* (Fath et al., 2007; Hsia et al., 2007). The common ancestry of coat protein and nucleoporin ACE1s provides strong evidence for the protocoatomer hypothesis, that various coat and coat-like protein complexes evolved from a small set of more versatile complexes (Dacks and Field, 2007; Devos et al., 2004; Field and Dacks, 2009). ACE1 is evidence that the NPC and the COPII coat derive from a common membrane-coating protein complex, already present in a primitive eukaryotic progenitor (Brohawn et al., 2008).

The COPII system is among the best-studied intracellular transport systems (Bonifacino and Glick, 2004; Fromme and Schekman, 2005; Hughes and Stephens, 2008; Mancias and Goldberg, 2005). Its components were identified genetically (Kaiser

and Schekman, 1990), and can be reconstituted into a functional system *in vitro* (Barlowe et al., 1994; Matsuoka, 1998; Salama et al., 1993; Sato and Nakano, 2004; Shaywitz et al., 1997). The COPII outer coat, Sec31 and Sec13, can assemble into polyhedral cages without membrane or other proteins (Antonny et al., 2003; Stagg et al., 2006). The structure of this cage has been determined by cryo-EM (Stagg et al., 2008; Stagg et al., 2006) and by X-ray crystallography (Fath et al., 2007). Sec31 homodimerizes via a crown-to-crown interface of its ACE1. This homodimer forms the central rod of a Sec13•Sec31₂•Sec13 tetramer, which self-assembles in multiple copies to form the complete cage. In addition to Sec13, Sec31, and three proteins of the inner coat, COPII transport also employs the essential accessory protein Sec16 (Kaiser and Schekman, 1990). Sec16 is, however, much more poorly understood.

Sec16 interacts genetically and physically with components of COPII (Espenshade et al., 1995; Gimeno et al., 1996; Gimeno et al., 1995; Kaiser and Schekman, 1990; Shaywitz et al., 1997). In particular, temperature-sensitive alleles of Sec13 and Sec16 are synthetic lethal. Sec13 and Sec16 interact weakly by yeast-two-hybrid (Shaywitz, 1997). A sequential mechanism for assembly of the COPII coat complex has been delineated, and Sec16 is implicated in early steps of this assembly process, but absence of structural data on Sec16 has impeded a full understanding of its function. At 242 kDa in *S. cerevisiae*, Sec16 is notoriously difficult to work with *in vitro*.

Here we show that Sec16 contains a central 40 kDa domain of the ACE1 type. We report the 165 kDa heterotetrameric crystal structure of Sec16₉₈₄₋₁₄₂₁ in complex with Sec13 and compare the related Sec13•Sec31 edge element to this novel Sec13•Sec16 edge element. Intriguingly, both Sec16 and Sec31 are shown to homodimerize by domain-swapping. Furthermore, we report the crystal structure of a Sec13•Sec31 mutant with a compromised domain-swap, showing it still forms an edge, however with a drastically different and unexpected topology. Mutants of Sec16 or Sec31 that

compromise the domain-swap, that exchange the ACE1 units of these proteins, or affect other aspects of their structures were created and tested *in vivo*. Together structural and *in vivo* results suggest that Sec16 templates assembly of the COPII outer coat.

Results

Structure of the Sec13•Sec16 tetramer

Sec16 is proposed to scaffold COPII assembly, but its precise function is ill defined. It has never been purified in high yield as a full-length protein. A central conserved domain (CCD), ~400 amino acids, is well conserved among Sec16 homologs in various organisms (Connerly et al., 2005). A sequence alignment for the CCD is shown (Figure 3-2). Secondary structure prediction suggested that the CCD of Sec16 is largely α -helical, and flanked by unstructured regions. Noting that it shares sequence similarity with the ACE1 of Sec31, (16% identity, 34% similarity over 391 residues), we inferred that the CCD of Sec16 might comprise two structural elements: a single N-terminal β -blade, which would bind the open Sec13 β -propeller by insertion, followed by an α -helical ACE1. (While this thesis was in preparation, it was reported that the CCD of human Sec16A interacts with Sec13 by yeast-two-hybrid (Hughes et al., 2009).) The CCD of Sec16 (residues 984-1421) and full-length Sec13, from *S. cerevisiae*, were co-expressed in *E. coli* from a bicistronic plasmid, and purified to homogeneity. Soluble and highly expressed (~40 mg pure protein per liter culture, final yield), Sec16₉₈₄₋₁₄₂₁ and Sec13 formed a stable, equimolar complex that eluted at 11.6 mL on a Superdex 200 10/300 column, indicating an apparent molecular mass of ~375 kDa, when compared to globular protein standards (Figure 3-3A). Gel filtration systematically overestimates the molecular weight of elongated macromolecules, because an elongated molecule passes through the column in less volume than a

globular protein of the same molecular weight (Siegel and Monty, 1966). To determine the oligomeric state of the complex more accurately, sedimentation velocity ultracentrifugation was performed and indicated this species was tetrameric and homogenous ($s = 6.5$, $M_f = 177$ kDa, Figure 3-3B). Taken together, these experiments indicated that Sec16 and Sec13 form a 2:2 tetramer of 165 kDa, whose shape is elongated, not globular.

Crystals of Sec16 in complex with Sec13 grew in the orthorhombic spacegroup $P2_12_12_1$, or its monoclinic subgroup $P2_1$, and diffracted to 2.7 Å resolution. The structure was solved by single-wavelength anomalous dispersion, using selenomethionine-substituted protein (Se-SAD). The asymmetric unit in $P2_12_12_1$ contains one Sec13•Sec16₂•13 tetramer. For simplicity, we refer to this complex as the Sec13•Sec16 tetramer. Two Sec13 molecules were placed by phased molecular replacement. Two Sec16 molecules were built using the experimental map. The model was refined to $R_{\text{work}}/R_{\text{free}} = 19.4\%/25.0\%$ (Table 3-1). The Sec13•Sec16 tetramer is arranged such that Sec13 forms the two ends of the elongated structure, while the two Sec16 molecules homodimerize in the center. The tetramer has overall dimensions of 165 Å x 70 Å x 50 Å (Figure 3-4B). The N terminus of Sec16₉₈₄₋₁₄₂₁ is a β-blade that completes the open, 6-bladed β-propeller of Sec13 *in trans*, creating a 2820 Å² interface. Sec16 provides three β-strands of this seventh β-blade, while residues 1-6 of Sec13 donate the outermost β-strand, forming a velcro closure, as seen in many β-propeller structures (Chaudhuri et al., 2008). The remainder of Sec16 forms an α-helical block, with dimensions ~ 70 Å x 30 Å x 30 Å. Two Sec16 molecules form a homodimer centered on the 2-fold axis of the tetramer. The dimer interface is composed of identical residues from each Sec16 molecule, measuring 2960 Å² in size.

The β-blade connects through helix α0 to helices α1-α3, which form an antiparallel stack (Figure 3-4B). Helix α4 and a 14-residue loop extend out and around the other Sec16 molecule and connect to helix α5. Helices α5-α9 form a second antiparallel

stack that returns towards the N terminus, forming a hydrophobic interface with helices $\alpha 5'$ - $\alpha 9'$ in the other Sec16 molecule. The stack continues with helix $\alpha 10$. To be consistent with the ACE1 helix nomenclature (Brohawn et al., 2009), the next helix is labeled $\alpha 10a$. Helix $\alpha 10a$ lies outside the stack, perpendicular to $\alpha 10$ and $\alpha 11$. Helices $\alpha 11$ - $\alpha 15$ bind helices $\alpha 1$ - $\alpha 3$, placing the C terminus near the N terminus. Helix $\alpha 14$ of a canonical ACE1 is absent. In place of helix $\alpha 14$, a structured but non-helical stretch of 20 residues winds out, is exposed on the convex surface of the tetramer, traverses the stack, and connects back to the next helix, labeled $\alpha 15$. A final helical bundle, $\alpha 16$ - $\alpha 18$, completes the stack and braces against Sec13. At the C terminus, residues 1391-1421 are not structured.

In crystallography, the quality of electron density and the temperature (B) factors for a portion of a model indicate how rigidly that portion of the model is held in place (Wlodawer et al., 2008). We observed much poorer electron density and two-fold higher B factors for one copy of Sec13 than the other (Table 1). The better-ordered copy of Sec13 is positioned near a crystallographic 2_1 -axis, stabilized by 1420 \AA^2 of crystal contacts. The poorly-ordered Sec13 molecule, however, is barely constrained by crystal packing interactions. Since the remainder of the model is rather well-ordered, this observation suggests that Sec13 may pivot relative to Sec16 *in vivo*, when not constrained by crystal packing.

As anticipated from its sequence, the α -helical portion of the Sec16 CCD is an ACE1. The CCD as defined by Glick and colleagues is residues 992-1420 in *S. cerevisiae* (Connerly et al., 2005), nearly the same fragment as the crystallization construct. The CCD contains two structural elements: the β -blade that binds Sec13 and the α -helical ACE1. As in other ACE1s, helices $\alpha 1$ - $\alpha 3$ and $\alpha 13$ - $\alpha 18$ form the trunk, while helices $\alpha 5$ - $\alpha 11$ form the crown. The crown creates a U-turn that caps the α -helical block and binds the second Sec16 molecule. Each α -helix corresponds to an α -helix in the canonical ACE1, except $\alpha 10a$, which is added, and $\alpha 14$ which is replaced

by non-helical structure. There is very low sequence homology to ACE1 members other than Sec31. As is true of the entire ACE1 class, individual modules (i.e. crown, trunk, and tail) superimpose well, but their orientations vary. Specific structural differences, such as insertion of α 10a or unwinding of α 14, dictate placement of each module.

We mapped the amino acid substitutions that cause known temperature sensitive alleles of Sec16 onto the structure (Figure 3-5). The *dot1* mutation from *P. pastoris* substitutes a proline with leucine in the connection between insertion blade and ACE1 (Connerly et al., 2005). Proline (as a cyclic secondary amino acid) is particularly suited to create a sharp turn in the polypeptide backbone, and the mutation occurs in the turn created by the motif FPGPL, which is strongly conserved among Sec16 orthologs. The five known temperature sensitive alleles in *S. cerevisiae* are caused by four distinct point mutations (Espenshade et al., 1995). (*sec16-2* and *sec16-5* are the same.) Although these are dispersed in the sequence, they cluster together in the structure. All replace hydrophobic residues in the core of the interaction between the N- and C-terminal halves of the trunk, undoubtedly hindering the ACE1 from folding into its proper shape.

Structural comparison of ACE1 edge elements

The Sec13•Sec16 tetramer is similar to the previously reported structure of the Sec13•Sec31 tetramer (Figure 3-4C,D) (Fath et al., 2007). Unlike Sec16, Sec31 has a structured N-terminal domain, a β -propeller, immediately preceding the Sec13 interaction site (Figure 3-4C). In the *in vitro* assembled Sec13•Sec31 cage, the N-terminal β -propeller forms the major vertex interactions that propagate the cage. Sec13 and the ACE1 of Sec31 form the edges of this cage, which was termed the Sec13•Sec31 edge element (Figure 3-4D) (Fath et al., 2007). The Nup84•Nup145C•Sec13 trimer is an analogous edge element for the NPC (Brohawn

and Schwartz, 2009b). The crystal structure reported here shows that the Sec13•Sec16 tetramer is another edge element for the COPII system. In all three edge elements, ACE1 units form a central dimer by interaction of their crowns. However, the crown-to-crown interactions in Sec16, Sec31, and Nup84•Nup145C, have important differences detailed below.

Central Angle of the Edge Element

The dimerized ACE1 units in the edge elements of COPII and the NPC create varying angles: 90° at the Sec16•Sec16 interface, 120° at the Nup84•Nup145C interface, and 165° at the Sec31•Sec31 interface (Brohawn and Schwartz, 2009b; Fath et al., 2007). In the assembled Sec13•Sec31 cage, the angle of Sec31 is more acute than in the crystal structure, 135° (Stagg et al., 2008; Stagg et al., 2006). It is striking that in its crystal structure the crown-to-crown interface of Sec16 is more bent than Sec31 in either the crystal structure (Fath et al., 2007) or the assembled cage (Stagg et al., 2008; Stagg et al., 2006). We asked whether the Sec13•Sec16 tetramer is indeed more bent than the Sec13•Sec31 tetramer in solution, or whether crystal packing alone accounts for the discrepancy between Sec16 and Sec31. The hydrodynamic radius of each edge element was calculated from its crystal structure, using HYDROPRO (García De La Torre et al., 2000). The calculated hydrodynamic radii are 5.3 nm for Sec13•Sec16, and 5.5 nm for Sec13•Sec31. The smaller radius for Sec13•Sec16 reflects its more compact structure, even though it is 10% greater in mass than Sec13•Sec31, 165 kDa vs. 150 kDa. Sec13•Sec16 and Sec13•Sec31 edge elements were compared by size exclusion chromatography (Figure 3-3A). Consistent with its smaller calculated hydrodynamic radius, Sec13•Sec16 elutes after Sec13•Sec31. We conclude that the crystal structures reflect a true difference between Sec13•Sec16 and Sec13•Sec31. The central angle of the Sec13•Sec16 edge element is more bent than the Sec13•Sec31 edge element in solution.

Domain-swapping of the Edge Element

When the structure of Sec31 was first reported (Fath et al., 2007), no closely related structures were known. We compared Sec16 and Sec31 to the ACE1 structures solved in the interim. This showed that Sec16 and Sec31 are domain-swapped dimers, that is, they interact by exchange of identical subunits (Bennett et al., 1995; Liu and Eisenberg, 2002; Rousseau et al., 2003). Strictly speaking, domain-swapping is said to occur only when a closed, monomeric form of the protein also exists (Gronenborn, 2009). Comparison to the closed form of a homolog can also be used. To define the closed form, we refer to the unswapped ACE1s, Nup85, Nic96, and Nup145C (Figure 3-6). In the crowns of Nic96 and Nup85, helices $\alpha 5$ - $\alpha 7$ pack against the trunk, forming a compact α -helical block (Brohawn et al., 2008; Debler et al., 2008; Jeudy and Schwartz, 2007; Schrader et al., 2008). Similarly, Nup145C adopts a closed form, whether or not bound to Nup84 (Brohawn and Schwartz, 2009b; Hsia et al., 2007). In the Nup84•Nup145C•Sec13 trimer, Nup145C adopts a structure very similar to that in a Nup145C•Sec13 dimer (1.4 Å rmsd over 420 C α positions). By contrast, in Sec16 (this work) and Sec31 (Fath et al., 2007), helices $\alpha 5$ - $\alpha 7$ exchange with the corresponding helices $\alpha 5'$ - $\alpha 7'$ in the binding partner. We call helices $\alpha 5$ - $\alpha 7$ the swap domain.

Among known examples of domain-swapping, rarely is the swap domain a central element (Gronenborn, 2009; Schwartz et al., 2006). More commonly, the N or C terminus of the protein is exchanged. To swap a central element, typically at least one of the two linkers to the remainder of the protein needs to be flexible to allow the rearrangement. In Sec16 and Sec31, a swap loop connects helices $\alpha 1$ - $\alpha 4$ to the swap domain. This loop must be long enough to reach out and around the other molecule. In closed monomers, no such loop is needed, because helix $\alpha 4$ already lies near helix $\alpha 5$. Nevertheless, all ACE1s except Nup145C have some insertion between $\alpha 4$ and $\alpha 5$. Nic96, Nup84, and Nup85 each have inserted α -helical segments. These may be

capable of unfolding and extending. At its opposite end, the swap domain is connected to helices $\alpha 8$ - $\alpha 18$ by a swap hinge. This hinge rotates out from its position in “closed” monomers—that is, monomers in which the swap domain is tucked against the rest of the α -helical stack. It is a tight turn in all ACE1s, except Nup84. Nup84 has three short α -helical segments inserted between $\alpha 7$ and $\alpha 8$; (these segments interact directly with Nup145C).

Domain-swapping substantially increases interface areas. We computed interface surfaces in swapped or hypothetical un-swapped conformations for Sec16 and Sec31. The swap loop and swap hinge were excluded from calculations, because it is not possible to know their position in the un-swapped conformation. In swapped Sec16, the interface is $\sim 2500 \text{ \AA}^2$, compared to $\sim 800 \text{ \AA}^2$ in un-swapped Sec16. Similarly, in swapped Sec31, the interface is $\sim 3000 \text{ \AA}^2$, compared to $\sim 1000 \text{ \AA}^2$ in un-swapped Sec31. Domain-swapping triples the interface area in the Sec16 and Sec31 crown-to-crown interfaces. Nup84•Nup145C, though un-swapped, has an interface surface area of $\sim 2000 \text{ \AA}^2$, because addition sites in conserved loops frame the primary interaction surface.

Interlocking of the Edge Element

Although Sec16 and Sec31 both dimerize by domain-swapping, the path taken by the swap loop causes a key difference. The Sec31 dimer is interlocked, while the Sec16 dimer is not. In Sec31, the swap loops extend around and over the binding partner to connect back to the swap domain (Fath et al., 2007). 23 residues of the swap loop are disordered and not visible in the crystal structure. The gap left by these unmodeled 23 residues is 25 \AA . In comparison, an adjacent segment of the swap loop spans 25 \AA in only 9 residues. If we accept that the unstructured segment does indeed connect the two ends of the swap loop across this gap, then the crystal structure shows that the Sec31 dimer is interlocked. In contrast, in Sec16, symmetric swap

loops extend over the top of the crown, touch in the middle, and then turn back to connect to their respective swap domains (Figure 3-6). This swap loop is entirely ordered and modeled in the final structure. To confirm the path of this loop, a simulated annealing omit map for the loop was calculated, unequivocally showing the complete amino acid trace (Figure 3-7). The path of the swap loop leaves the two Sec16 copies not interlocked, i.e. if pulled by the ends, the Sec16 dimer would break apart. Because the Sec31 dimer is interlocked, if pulled by the ends, the Sec31 dimer would remain entangled with itself. Thus, the Sec31 dimer can only be formed or broken by disrupting the interaction between N- and C-terminal halves of the trunk. This suggests that creation of the Sec31 dimer is coordinated with folding of the ACE1 unit.

Structure-based mutants of Sec31

The structures of the Sec13•Sec16 edge element, reported here, and that of the Sec13•Sec31 edge element (Fath et al., 2007), were used as a basis to design specific mutations to probe functional and structural integrity of these related complexes.

Solution behavior of Sec31 mutants Sec31EE and Sec31 Δ L

The difference between the un-swapped ACE1s found in the NPC and the domain-swapped dimers observed in Sec16 and Sec31 is intriguing. In order to investigate whether domain-swapping is physiologically relevant, we designed a mutation to prevent domain-swapping of Sec31 in the Sec13•Sec31 edge. The swap loop of Sec31 was deleted, to form Sec31 Δ L. This deletion prevents helix α 5 from swinging out from helix α 4, otherwise a strict requirement for domain-swapping to occur. We also designed a mutation to prevent Sec31 dimerization. In previous work on the Nup84•Nup145C edge element, it was shown that charged residues introduced into helix α 7 of either protein prevent dimerization, when these are chosen to replace

conserved hydrophobic residues crucial to high-affinity binding (Brohawn et al., 2008; Brohawn and Schwartz, 2009b). A similar mutant of Sec31 was designed. Two residues, methionine 540 and leucine 544 in helix $\alpha 7$, were mutated to a charged residue, glutamic acid (E), to generate Sec31EE.

The Sec13•Sec31 edge element was expressed and purified in three forms: wild-type, Sec31 Δ L, or Sec31EE. The purified complexes were compared by size exclusion chromatography on a Superdex 200 10/300 column (Figure 3-8A). Sec31 Δ L is 4 kDa (9%) smaller than Sec31 and therefore migrates slightly faster on SDS-PAGE. Despite its reduced mass, Sec13•Sec31 Δ L forms a tetramer with the same hydrodynamic radius as wild-type Sec13•Sec31. The interface mutant Sec13•Sec31EE elutes from the column later indicating that, indeed, the double point mutation from Sec31 to Sec31EE is sufficient to disrupt tetramer formation. Sec13•Sec31EE instead forms a 1:1 heterodimer.

Crystal structure of Sec13•Sec31 Δ L

To determine definitively whether deletion of the swap loop prevents domain-swapping, we solved the crystal structure of Sec13•Sec31 Δ L, by molecular replacement, in spacegroup P2₁ at 2.8 Å resolution (Table 3-1). The structure of wild-type Sec13•Sec31 was used as a search model. To obtain an unbiased electron density map of the mutated swap loop (connecting helices $\alpha 4/5$) and the swap hinge (connecting helices $\alpha 7/8$), these were deleted from the search model. Further, the model was split into two parts—the ACE1 of Sec31, and the completed β -propeller, (6-bladed Sec13 and the insertion β -blade of Sec31). The asymmetric unit contains two copies of a Sec13•Sec31 Δ L tetramer. The crystal lattice of Sec13•Sec31 Δ L is different from that of wild-type Sec13•Sec31. Yet, compared to wild-type Sec13•Sec31 (Fath et al., 2007), the shape of the tetramer changes only slightly. The angle of the edge, 165°, is the same in both structures. The C-terminal 3-helix bundle of the ACE1 and the

Sec13 β -propeller are displaced ~ 15 Å with respect to the central rod, in the plane parallel to a face of a Sec13•Sec31 cage.

The structure of Sec13•Sec31 Δ L at the crown-to-crown interface revealed an unexpected result. In re-building the structure, strong difference density at the swap hinge was apparent (Figure 3-9). Because deletion of the swap loop prevents domain-swapping, we expected the swap hinge to rotate inward to accommodate an un-swapped conformation. Surprisingly, we find the swap hinge in the same place as in wild-type Sec13•Sec31. In consequence, deletion of the swap loop does prevent domain-swapping, but in an unexpected manner. To have helix $\alpha 5$ adjacent to $\alpha 4$, as it is dictated by the truncated swap loop, and to retain the swap hinge still in the same conformation, Sec31 Δ L laminates with its binding partner across its entire length (Figure 3-8B). Instead of folding back into a J-shape as in wild-type Sec31, the two copies of Sec31 Δ L extend completely and lie flat against one another. Because the entire transverse section of the dimer is an interface between two molecules, the interface surface area of Sec31 Δ L is 6260 Å². The final model was refined to $R_{\text{work}}/R_{\text{free}} = 26.7\%/30.0\%$ (Table 3-1).

The structure of Sec13•Sec31 Δ L suggests that there is a large energetic penalty for rotating the swap domain into the closed conformation. The laminated structure of Sec13•Sec31 Δ L is therefore indirect evidence that the domain-swapped conformation of Sec31 is favored over the closed conformation, and hence that the crystal structure of Goldberg and colleagues (Fath et al., 2007) is the physiological structure.

Complementation of sec16 Δ or sec31 Δ by structure-based mutants

SEC16 and *SEC31* are both essential genes. In order to assess the physiological relevance of structural characteristics of COPII edge elements, we tested in a plasmid shuffle assay whether several designed mutants complement null alleles of *SEC16* or *SEC31* (Figure 3-10). Haploid strains *sec16* Δ x pRS316[*SEC16*] or *sec31* Δ x

pRS316[*SEC31*] were isolated, transformed with plasmids containing designed mutants of *SEC16* or *SEC31*, and tested for growth on media containing 5-fluoroorotic acid, which selects against pRS316, causing the strain to lose the wild-type gene. This experiment shows that the ACE1 is required for the essential function of *SEC31* (Figure 3-10A). Furthermore, failure of Sec31EE to rescue *sec31Δ* proves that Sec31 must form a proper edge element. Deletion of the insertion blade that binds Sec13 also disables the gene. In contrast, domain-swapping is not required for the essential function of *SEC31*. Sec31ΔL complements the null at all temperatures tested. Evidently, the radical rearrangement observed in laminated Sec31ΔL does not prevent Sec31 from assembling a functional edge element for the COPII cage.

The corresponding mutations were also generated for *SEC16* (Figure 3-10B). Expectedly, purified Sec16ΔL•Sec13 behaves as a tetramer in solution, and Sec16EE•Sec13 forms a dimer, as determined by size exclusion chromatography (data not shown). We find that *SEC16* is more robust to mutation than *SEC31*. A strain in which the ACE1 of Sec16 is deleted is able to grow normally at 30°C, but grows very slowly at 37°C. Deletion of the swap loop to prevent domain-swapping, deletion of the β-blade to prevent binding of Sec13, or the EE mutation to prevent dimerization, each likewise is tolerated at 30°C, but not at 37°C.

Because Sec16 and Sec31 form similar edge elements, we asked whether the ACE1 units of these two proteins are interchangeable. To test this, chimeric genes were designed that place the ACE1 of each gene into the middle of the other. Sec31[Sec16 ACE1] and Sec16[Sec31 ACE1] were tested in the plasmid shuffle assay (Figure 3-10). *sec31Δ* is not complemented by Sec31[Sec16 ACE1]. We found, though, that *sec16Δ* is complemented at all temperatures tested by Sec16[Sec31 ACE1]. Unlike the other Sec16 mutants, Sec16[Sec31 ACE1] exhibits no temperature sensitivity. Remarkably, despite only 34% sequence similarity, the ACE1 of Sec31 can substitute for the ACE1 of Sec16.

Discussion

Our studies of the ancestral coatomer element 1 (ACE1) have revealed that the central conserved domain of Sec16 comprises a β -blade and 19 α -helices that closely resemble the core of the COPII vesicle coat protein Sec31. Sec16 is considered a scaffold for the COPII system, because it localizes to the cytoplasmic surface of the ER, binds the major components of the COPII system, and promotes vesicle coating (Espenshade et al., 1995; Gimeno et al., 1996; Shaywitz et al., 1997; Supek et al., 2002). These studies have shown that Sec16 binds the cargo adaptor Sec24, the GTPase activating protein Sec23, and the GTPase Sar1, and additionally that it binds Sec31 and possibly Sec13. Additional studies on Sec16 in yeast, fly and mammalian systems have substantiated its role in COPII transport (Bhattacharyya and Glick, 2007; Connerly et al., 2005; Hughes et al., 2009; Ivan et al., 2008; Watson et al., 2006).

We show that Sec16 and Sec13 form a stable, tetrameric complex. The crystal structure of Sec16₉₈₄₋₁₄₂₁ in complex with Sec13 reveals that Sec16 forms a Sec13•Sec16₂•Sec13 tetramer. This tetramer is similar to the Sec13•Sec31₂•Sec13 edge element, which assembles into the COPII outer coat (Fath et al., 2007; Stagg et al., 2008; Stagg et al., 2006). It is also analogous to the Nup84•Nup145C•Sec13 edge element of the NPC (Brohawn and Schwartz, 2009b). Since Sec16, and Sec31, (as well as Nup145C), occupy the same binding interface on Sec13, their interactions with Sec13 are mutually exclusive. It is likely that these proteins bind distinct pools of Sec13. This explains the observation that Sec16 is present at the transitional ER in lower abundance than Sec13 (Connerly et al., 2005).

The discovery that Sec16 and Sec31 are related proteins provides novel insight into the function of Sec16 in the COPII system. Sec16 and Sec31 form with Sec13 analogous heterotetrameric edge elements. Unlike Sec31, secondary structure prediction shows that Sec16 does not have an N-terminal β -propeller domain. In the

COPII cage, the Sec13•Sec31 tetramers self-assemble through contacts primarily mediated by the N-terminal β -propeller domains of adjacent Sec31 molecules (Fath et al., 2007; Stagg et al., 2008; Stagg et al., 2006). It is important to note that without such a β -propeller, Sec16 lacks a vertex element, and thus is unlikely to form a cage in a similar manner.

One unresolved question about the Sec13•Sec31 edge element has been the nature of the central angle of the Sec31 homodimer (Fath et al., 2007; Stagg et al., 2008; Stagg et al., 2006). This angle is more acute in the cryo-EM structure of the assembled Sec13•Sec31 cage than in the crystal structure of the edge element. Several reasons to explain this difference have been proposed (Fath et al., 2007; Stagg et al., 2008): (1) flexing this angle allows the Sec13•Sec31 cage to accommodate cargos of different size; (2) a conformational change occurs upon cage assembly making the angle more acute; (3) the edge element in the crystal structure is distorted from its native conformation by crystal packing; (4) the yeast protein in the crystal structure differs from the human protein used for cage assembly; (5) the C-terminal half of Sec31, which is not included in the crystal structure, influences the angle. Stagg et al. show that the angle of Sec31 stays the same whether the cage formed is a cuboctahedron 60 nm in diameter, or an icosidodecahedron 100 nm in diameter (Stagg et al., 2008). In other words, the adjustments that change the shape of the cage occur primarily at the interfaces between vertex elements, rather than within the ACE1 blocks, arguing against the first explanation, that variation in this angle is used to form cages of different sizes.

In the structure of Sec13•Sec16₂•Sec13, the Sec16 homodimer forms the analogous central angle. We noted with interest that this angle is 90°, much more bent than in Sec13•Sec31. Since one end of the Sec13•Sec16 edge element is not held by significant crystal contacts, we believe the conformation of Sec13•Sec16 in the crystal structure is near to the native conformation in solution. Our data show that, consistent

with the crystal structures, in solution the Sec13•Sec16 tetramer is more bent than the Sec13•Sec31 edge element. Additionally, our crystal structure of Sec13•Sec31 Δ L reveals that this mutant has the same angle at the Sec31•Sec31 interface, 165°, as wild-type Sec13•Sec31.

A striking feature of the COPII edge elements is domain-swapping, which is rarely observed in the middle of a polypeptide chain. In reporting the crystal structure of Sec13•Sec31, Goldberg and colleagues noted that the two molecules of Sec31 interlock (Fath et al., 2007). It becomes apparent that domain-swapping occurs in Sec31, when this structure is compared to those of ACE1 nucleoporins, which were solved later and which form compact J-shaped helical units. Prior to solving the structure of Sec16, it remained unclear whether domain-swapping in Sec31 is due to crystallization alone or is physiologically relevant. The crystal structure of Sec13•Sec16 shows that like Sec31, Sec16 homodimerizes by domain-swapping. This is strong evidence that domain-swapping in Sec31 is physiologically relevant. It is unlikely to be coincidence that domain-swapping occurs in two different ACE1 proteins, in unrelated crystal lattices.

Domain-swapping triples the interface surface area of this crown-to-crown interaction to $\sim 3000 \text{ \AA}^2$, suggesting that the domain-swapped interaction is very strong. Indeed, each of the COPII edges is observed to remain stably associated in solution. Sec13•Sec16 and Sec13•Sec31 edge elements are likely similarly stable *in vivo*. Their structures support the notion that cage assembly and disassembly is mediated at the vertices of the cage, not by making and breaking the edge itself.

In attempting to prevent domain-swapping in Sec16 and Sec31, we generated and solved the crystal structure of a variant of the Sec13•Sec31 edge element that laminates across its entire length, rather than forming two J-shaped molecules. This laminated variant provided a means to test the physiological importance of domain-swapping. We find that the laminated Sec31 variant, Sec31 Δ L, is able to

complement deletion of Sec31, but a mutant designed to prevent dimerization, Sec31EE, fails to complement this null. We further show with the chimeric gene Sec16[Sec31 ACE1] that the ACE1 of Sec31 can functionally replace the ACE1 of Sec16. This result suggests that its architectural role—forming an edge element—is the most important function of the ACE1 of Sec16.

Sec16 as a template for the COPII coat

Sec16 has been called a scaffold for the COPII coat. The term scaffold refers to a protein that binds several factors in order to bring them together in the cell. It is clear that by binding many components of the COPII system, Sec16 performs this function. In other contexts, the term scaffold also refers to proteins that organize a system into a pre-determined structure. For example, in viral assembly, scaffolding proteins recruit elements of the naïve viral capsid, organize them, and establish the desired size and shape of the capsid. Such viral scaffolding proteins also act as chaperones for capsid proteins and exclude host proteins from the capsid. Scaffolding proteins are then left out of the mature viral capsid (Fane and Prevelige, 2003; Thuman-Commike et al., 1998). Sec16 is similarly thought to assist in organizing and shaping the assembly of the COPII coat, and to be excluded from the final coat, because it is present substoichiometrically and is not required for assembly of the coat *in vitro* (Connerly et al., 2005; Matsuoka, 1998).

The structure of Sec16 in complex with Sec13 now allows us to make this model more specific. Sec13•Sec16 is shown to form an alternative edge element for the COPII system. It dimerizes, allowing it to concentrate twice the number of COPII components in its vicinity. Furthermore, it mimics the Sec13•Sec31 edge element, which should allow it to position precisely COPII components with respect to the Sec13•Sec31 outer coat. For this reason, it could be termed a template for the COPII coat. Because the similarity between Sec16 and Sec31 was not previously known, this

is a new interpretation of Sec16's role in the COPII system, but one that is consistent with prior experiments. It suggests a few further directions for studying Sec16. Because Sec16 lacks a vertex element like the β -propeller domain of Sec31, it still is not clear whether or not Sec16 can form cage-like structures. It may form a precursor coat for the COPII system over which the Sec13•Sec31 cage is laid. Or, it may co-assemble with Sec13•Sec31 at an early stage of COPII assembly, before being replaced. We hypothesize that Sec13 bound to Sec16 may form weak homotypic interactions with other copies Sec13 or with the β -propeller of Sec31, organizing Sec13•Sec16 tetramers with respect to one another and with respect to Sec13•Sec31.

It has been noted that COPII coat assembly is delicately balanced between forces that drive assembly in the presence of Sar1•GTP and forces that promote disassembly once Sar1•GTP converts to Sar1•GDP (Supek et al., 2002). Because Sec31 promotes hydrolysis of GTP by Sar1, *in vitro* assembly of Sec13•Sec31 (counter-intuitively) rapidly triggers its own disassembly (Antonny et al., 2001). It thus remains to be explained how Sec13•Sec31 is able to assemble a full coat without prematurely falling apart. By establishing an organized template, Sec16 may help tip the balance towards assembly in the early moments following Sec13•Sec31 recruitment.

Model for the function of Sec16 in the COPII coat

We propose the following model for COPII assembly (Figure 3-11), based largely on experimental evidence and models proposed previously (Bonifacino and Glick, 2004; Fromme and Schekman, 2005; Gürkan et al., 2006; Mancias and Goldberg, 2005). The Sec13•Sec16 tetramer binds to the ER membrane through charged segments of the N-terminal unstructured region and by interaction with Sed4 (or Sec12) through its C-terminal helical domain. Sar1 is recruited when it is converted from GDP- to GTP-bound state. Insertion of the N-terminal amphipathic α -helix of Sar1 into the membrane induces curvature of the ER membrane, assisted by

Sec16-mediated clustering. The Sec23•Sec24 dimer binds both Sec16 and Sar1, joining them together. Since the Sec23•Sec24 dimer forms two independent interactions with Sec16, the Sec23•Sec24 dimer may help cross-link adjacent Sec13•Sec16 tetramers into higher-order oligomers. Cargo is concurrently recruited via interactions with Sec24. Once this pre-coat is formed, Sec13•Sec31 begins to assemble. Interactions of Sec31 with Sec23•Sec24 and Sar1 facilitate this assembly, as do direct interactions between Sec31 and Sec16, and, perhaps, homotypic interactions between Sec13 molecules on different edges. Sec13•Sec16 is similar in size and shape to Sec13•Sec31 and places all Sec31's partners close at hand. Sec16 acts against Sec31-promoted hydrolysis of GTP by Sar1, either directly or by holding Sed4 (or Sec12) nearby to recycle Sar1•GDP to Sar1•GTP. Sec13•Sec16 is gradually displaced. It is included substoichiometrically, or not at all, in the final COPII coat, which then severs from the ER.

The crystal structure of the Sec13•Sec16 tetramer, the structure of a laminated Sec13•Sec31 mutant and supporting functional data, support a new interpretation of Sec16's role in assembly of the COPII coat. This hitherto mysterious protein contains an ACE1, structurally related to both nucleoporins and the COPII coat protein Sec31. The central domain of Sec16 allows the Sec13•Sec16 tetramer to act as an alternative edge element for COPII. The structure of the Sec13•Sec16 edge element may allow it to precisely template assembly of the COPII vesicle coat.

Methods

Sequence Analysis

PSI-BLAST was performed using the NCBI server (<http://blast.ncbi.nlm.nih.gov>). Secondary structure prediction was performed with the PredictProtein server (<http://www.predictprotein.org/>). Alignments were generated using the MAFFT algorithm in JalView (Waterhouse et al., 2009), and a figure prepared in ALINE (Bond and Schüttelkopf, 2009).

Protein Expression Constructs

Sec16 (residues 984-1421) and Sec13 were cloned into a bicistronic pET-Duet vector (Novagen), engineered to encode a human rhinovirus 3C (HR3C)-cleavable His6-tag at the N terminus of Sec16. The construct was modified by PCR methods to create Sec16 Δ L (deletion of residues 1115-1128) or Sec16EE (mutations A1159E and L1162E). Sec31 (residues 370-746) and Sec13 were cloned likewise, with Sec31 tagged at the N terminus, and modified to create Sec31 Δ L (deletion of residues 474-507) or Sec31EE (mutations M540E and L544E).

Protein Preparation and Crystallization

The proteins were expressed in *E. coli* strain BL21 (DE3)-RIL (Stratagene) in LB medium, induced with 200 μ M isopropyl- β -D-1-thiogalactopyranoside at 18°C. Harvested cells were homogenized at 4 °C in 50 mM potassium phosphate pH 8.5, 400 mM NaCl, 40 mM imidazole, 5 mM β -mercaptoethanol. The Sec13•Sec16 complex, Sec13•Sec31 complex, or each mutant complex was purified by Ni-affinity chromatography, then dialyzed against 10 mM Tris-HCl pH 8.5, 250 mM NaCl, 0.5 mM EDTA, 1 mM DTT. After removing the His6-tag, each complex was further purified on a

Superdex 200 26/60 column (GE Healthcare), equilibrated in 5 mM Hepes pH 7.5, 100 mM NaCl, 0.1 mM EDTA, 1mM DTT. Selenomethionine-substituted protein was expressed as described (Brohawn et al., 2008).

Sec13•Sec16 was concentrated to 70 mg·mL⁻¹. An initial crystallization condition was found by vapor diffusion using commercial screens. Crystals grew as bundles of rods each 50 μm x 100 μm x 200-400 μm, within days, at 16°C in 2 μl hanging drops, over 0.1 mM bis-Tris propane pH 6.5, 0.2 M NaBr, 12% polyethylene glycol (PEG) 3,350. Selenomethionine-substituted protein crystallized subsequent to streak-seeding with microcrystals of the native protein. Crystals were cryoprotected by serial transfer through reservoir solution supplemented by increasing amounts of PEG 200, 16% final concentration, then flash-frozen in liquid nitrogen.

Sec13•Sec31ΔL was concentrated to 70 mg·mL⁻¹, and an initial crystallization condition found likewise. Crystals grew as rods, 100 μm x 100 μm x 200-400 μm, within days, at 16°C in 2 μl hanging drops, over 0.1 mM bis-Tris propane pH 6.9, 0.2 M sodium citrate, 16% PEG 3,350. Crystals were cryoprotected by serial transfer through reservoir solution supplemented by increasing amounts of PEG 200, 18% final concentration, then flash-frozen in liquid nitrogen.

Data Collection and Structure Solution

For Sec13•Sec16, diffraction data to 2.7 Å resolution were collected at 100 K at beamline 24-IDC at the Advanced Photon Source (Argonne, IL) and processed with the HKL2000 package (Otwinowski and Minor, 1997). Merging factors $R_{r.i.m.}$ and $R_{p.i.m.}$ were calculated with RMERGE (Weiss, 2001). The majority of crystals were orthorhombic, belonging to spacegroup P2₁2₁2₁. The selenomethionine crystal that diffracted best belonged to the monoclinic subgroup P2₁. Phases were determined by Se-SAD. In the P2₁ crystals, the asymmetric unit contains two Sec13•Sec16₂•Sec13 heterotetramers. 50 of (4×13=) 52 possible Se sites were identified by PHENIX AutoSol (Adams et al.,

2002). Density-modified maps were used to build and assign the structure of the four Sec16 monomers. Phased molecular replacement, as implemented in MolRep (Vagin and Isupov, 2001), was used to position two of four Sec13 monomers (PDB ID: 2PM6). The other two Sec13 monomers are poorly ordered in the crystal. The symmetry relating the Sec16 monomers was used to infer the location of these Sec13 monomers, for which the observed electron density is weak, as explained in the Results. For refinement, the native dataset in spacegroup $P2_12_12_1$ was used. The two crystal forms are nearly the same: the non-crystallographic symmetry operator relating two heterotetramers in spacegroup $P2_1$ becomes a crystallographic symmetry operator in $P2_12_12_1$, and consequently, the asymmetric unit of the native crystal contains only one heterotetramer. In Sec16, the C terminus (residues 1391-1421) and one loop (residues 1185-1192) are not structured and were not modeled. The structure was refined against the native data with PHENIX (Adams et al., 2002), using NCS-restraints and TLS refinement ($R_{\text{work}}/R_{\text{free}} = 19.4\%/25.0\%$).

For Sec13•Sec31 Δ L, diffraction data to 2.8 Å resolution were collected and processed with XDS and XSCALE (Kabsch, 2010). The structure was solved by molecular replacement using Phaser (McCoy et al., 2007), and refined in Refmac (Bailey, 1994; Murshudov et al., 1997), using keyword TWIN to account for partial merohedral twinning of the data, (twin fraction = 0.23; $R_{\text{work}}/R_{\text{free}} = 26.7\%/30.0\%$). Data Collection and refinement statistics are summarized in Table 3-1. Figures were created in PyMOL (<http://www.pymol.org/>).

Analytical Ultracentrifugation and Size Exclusion Chromatography

Sedimentation Velocity (SV) ultracentrifugation was performed on a Beckman Coulter XL-I, at 42 krpm, 20°C, using interference optics, in 50 mM potassium phosphate pH 7.0, 150 mM NaCl, 0.1 mM EDTA, 1 mM DTT, using Sec13•Sec16 at 0.25 mg·mL⁻¹. Data were collected every 1.5 minutes and fit to a single species model

by SEDFIT. No significant residuals were observed, confirming a single, pure species. Size exclusion chromatography was performed on a 10/300 Superdex 200 column in 10 mM Hepes pH 7.0, 150 mM NaCl, 0.1 mM EDTA, 1 mM DTT, using 100 μ L of sample at 0.25 A_{280} .

Complementation Assay

SEC16 or *SEC31*, with flanking sequence -1500 base pairs and +500 base pairs, were cloned into pRS315 and pRS316 (Sikorski and Hieter, 1989). Diploid strains, *SEC16/sec16 Δ* and *SEC31/sec31 Δ* , from the Euroscarf deletion collection were transform using the lithium acetate/polyethylene glycol method with pRS316[*SEC16*] or pRS316[*SEC31*]. Cells grown on media lacking uracil were sporulated for one week in 0.02% raffinose and dissected for tetrads. Haploid null strains were selected by G418 resistance. Mutations were introduced to pRS315[*SEC16*] or pRS315[*SEC31*] by PCR methods, transformed into the respective null strains, and selected on media lacking leucine. Complementation was tested on media supplemented with 5-fluoroorotic acid, to select against pRS316[*SEC16*] or pRS316[*SEC31*].

Figures

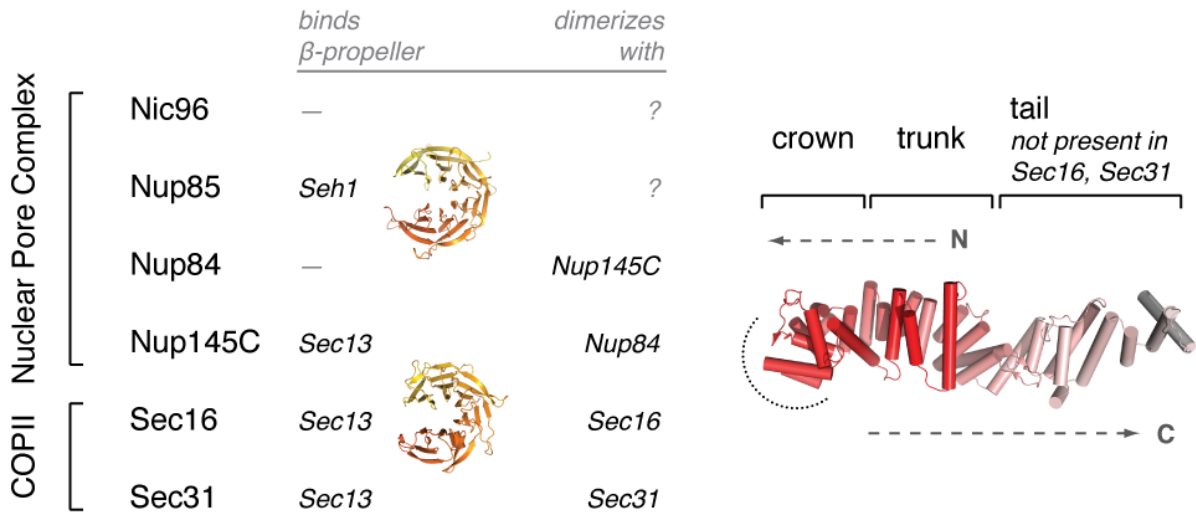
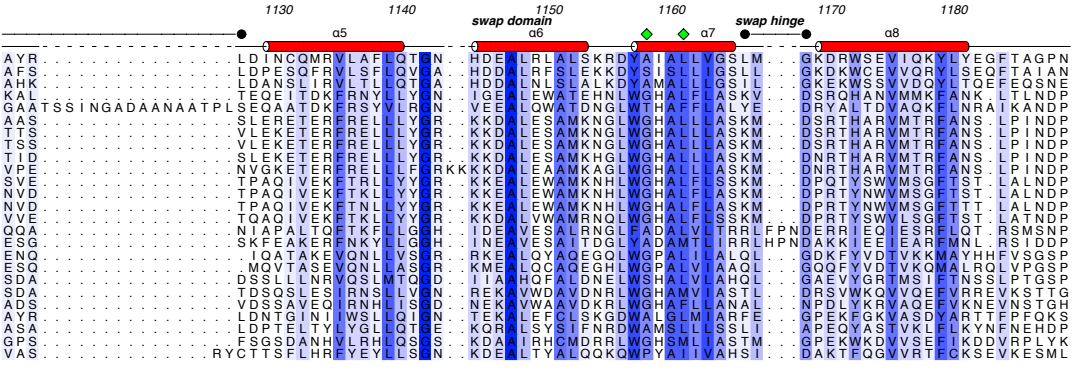
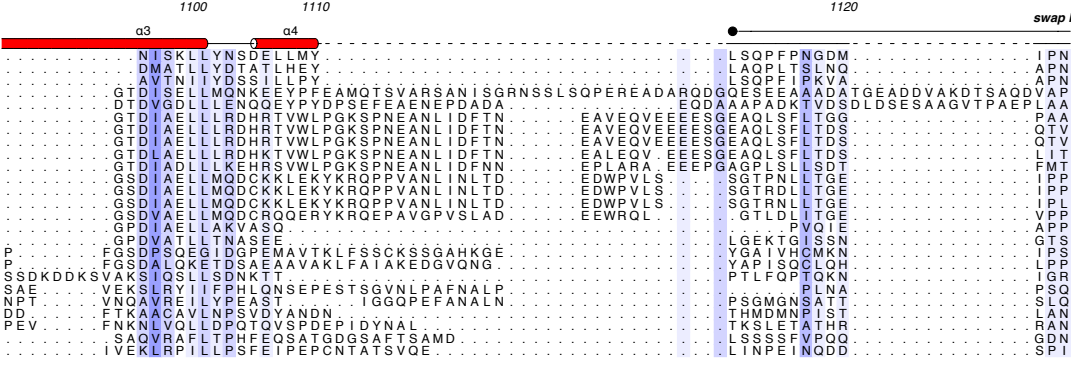
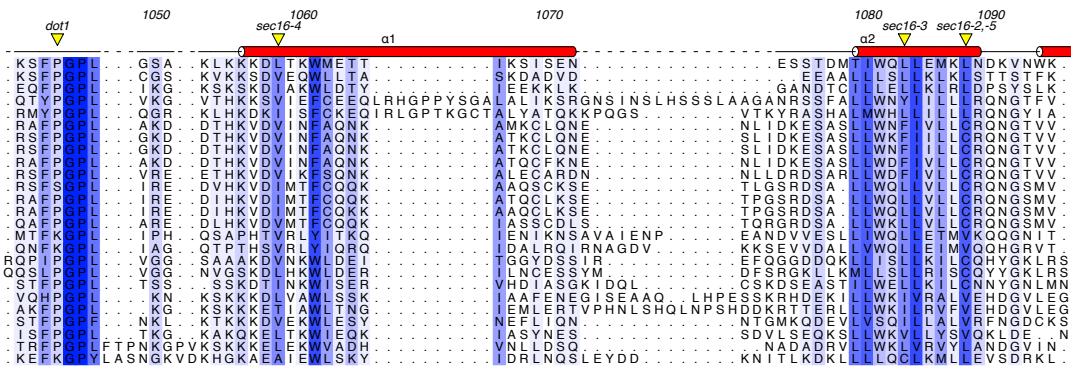
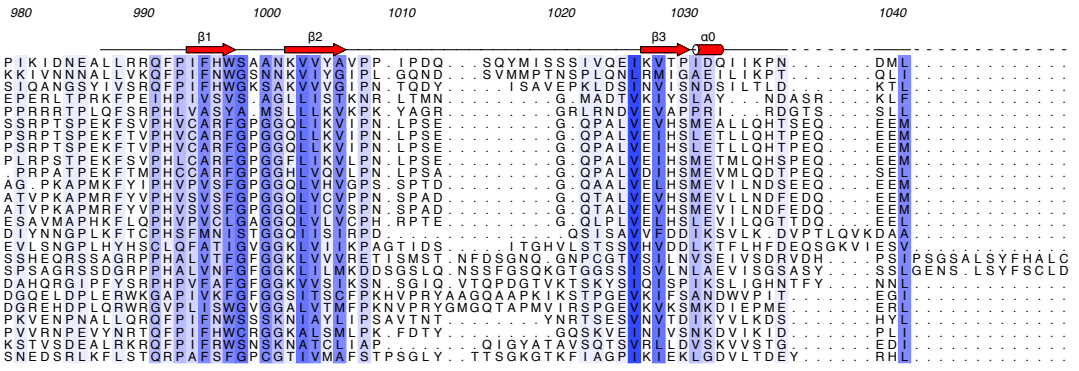


Figure 3-1 Summary of Ancestral Coatomer Element 1 (ACE1) Proteins

ACE1 was originally identified based on structural homology between Nup85, Nic96, Nup84, Nup145C, and Sec31. Sec16 is shown to contain an ACE1 in this study. Three ACE1 proteins bind Sec13, mutually exclusively; Nup85 binds its homolog Seh1. Nup84 and Nup145C form a heterodimer, and Sec16 and Sec31 form homodimers. The structure of Nic96 is shown to illustrate the three modules that compose the ACE1—crown, trunk, and tail. The COPII ACE1 domains might lack the tail module. The structure is colored red to white from N to C terminus, as labeled. Dashed arrows show how the ACE1 forms a J-shape. A dotted arc encircles the surface by which ACE1 dimerization occurs.

Structural Studies of Nucleoporins and Coat Proteins



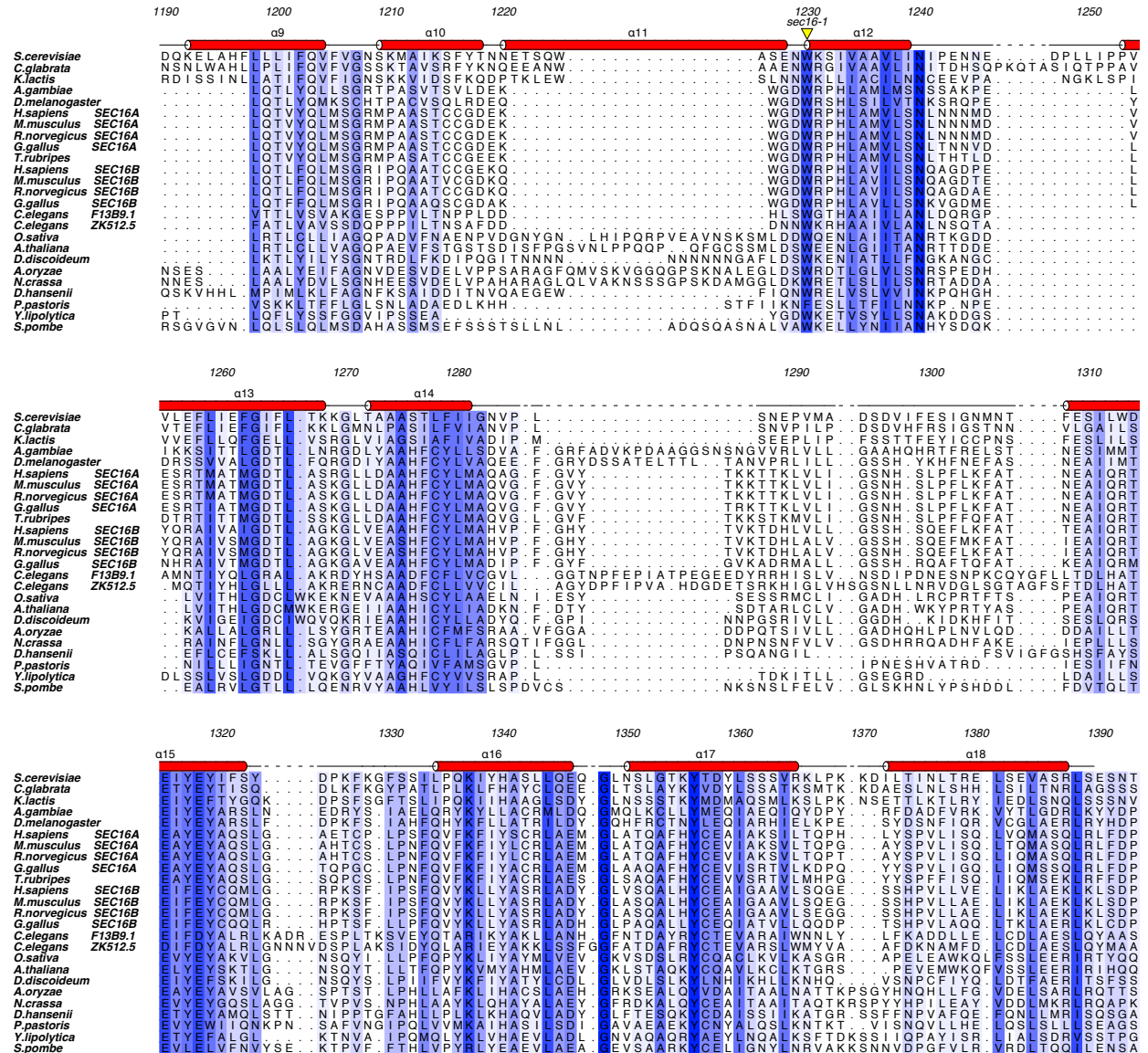


Figure 3-2 Multiple Sequence Alignment of the CCD of Sec16 Homologs

Sequences were retrieved by PSI-BLAST, trimmed to contain only the CCD, and aligned by MAFFT. Columns are colored by sequence similarity. β -strands β_1 -3 and α -helices α_0 -18 are diagrammed. The causative mutations for known temperature-sensitive alleles in *S. cerevisiae* (*sec16-1*, *-2*, *-3*, *-4*/*-5*) or *P. pastoris* (*dot1*) are marked with yellow triangles. Green diamonds mark alanine 1159 and leucine 1162, which were mutated to glutamic acid to generate the mutant Sec16EE. The swap domain, α -helices α_5 -7, is labeled, as are swap loop and swap hinge. Numbering is according to the sequence in *S. cerevisiae*.

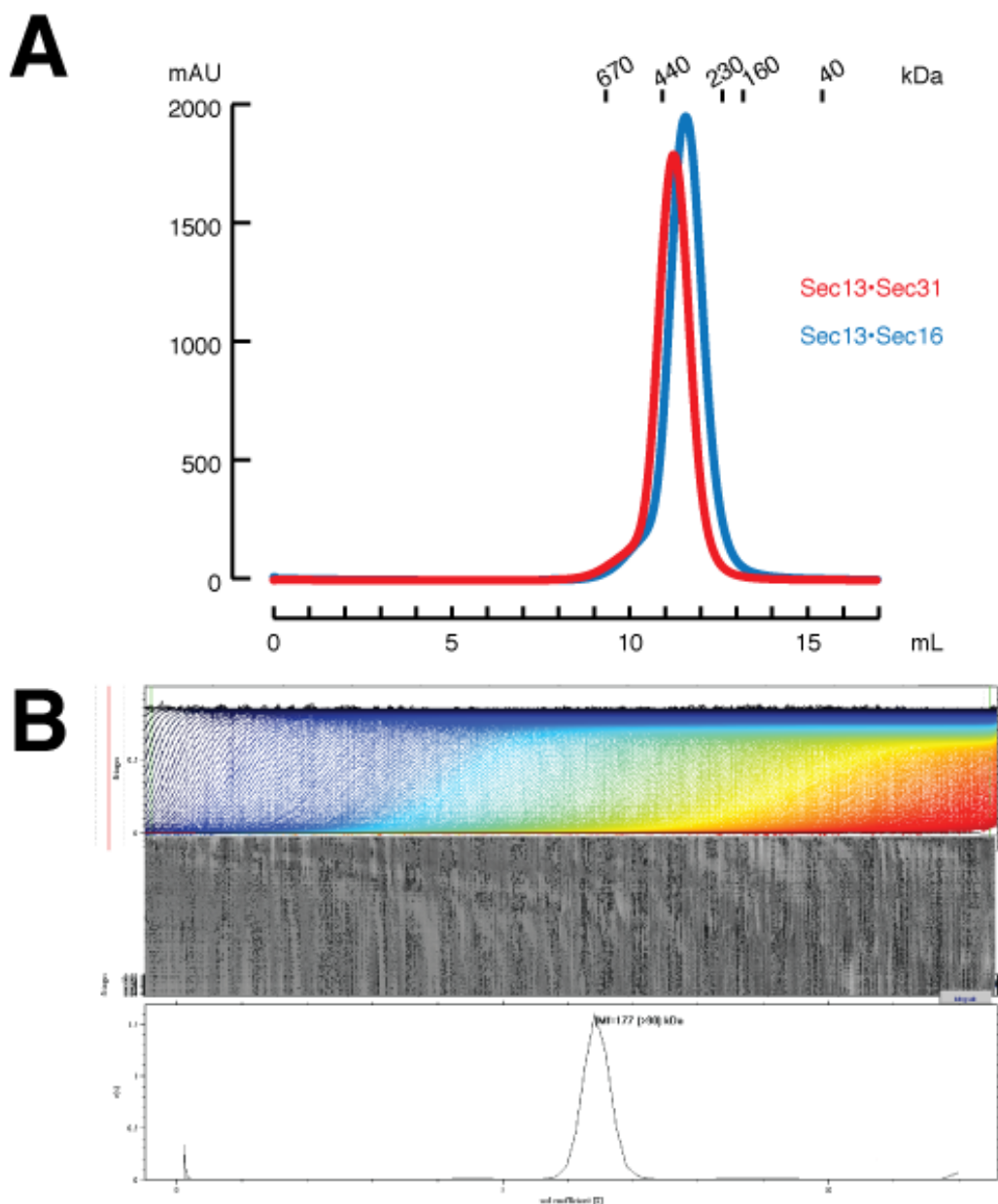


Figure 3-3 Hydodynamic Characterization of Sec13•Sec16

- (A) Size exclusion chromatography of Sec13•Sec16 compared to Sec13•Sec31 on a Superdex 200 10/300 column. Absorption at $\lambda = 280$ nm is plotted against elution volume for each sample.
- (B) Sedimentation velocity analytical ultracentrifugation of Sec13•Sec16. Data collected in interference mode were analyzed with SEDFIT using the continuous sedimentation coefficient distribution, $c(s)$, and an estimated molecular mass, M_r , calculated. Fringe displacement versus radial distance is plotted as a function of time (blue to red). Fit residuals are shown as a grayscale bitmap. Distribution plot shows a single species with $M_r = 177$ kDa.

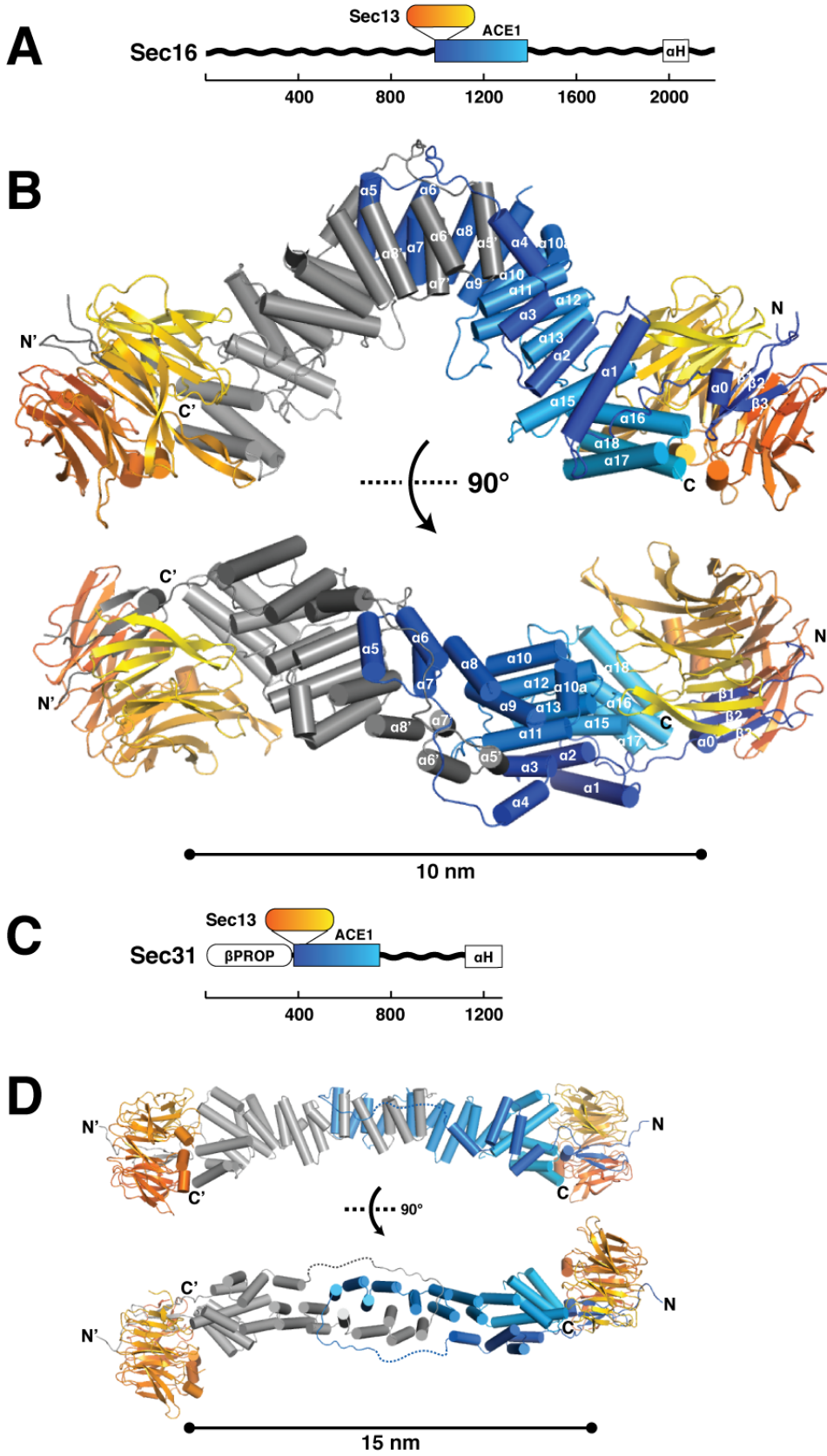


Figure 3-4 Structural Comparison of Sec16 and Sec31

- (A) Domain organization of Sec16. Unstructured regions (wavy black lines), central conserved domain (blue-cyan box) and C-terminal α -helical domain (white box, labeled α H) are shown. Scale bar shows number of amino acids residues. The β -propeller protein Sec13 binds Sec16 at the position indicated.
- (B) Crystal structure of Sec16 in complex with Sec13. Sec13 is colored orange to yellow from N to C terminus, as in A. One Sec16 monomer is colored blue to cyan, as in A, the other dark to light grey from N to C terminus. N and C termini are labeled, as well as β -strands β 1- β 3 and helices α 0- α 18. Helices α 5- α 7 of the Sec16 monomers domain swap at the homotypic interface. The lower view is rotated 90 degrees towards the viewer as indicated.
- (C) Domain organization of Sec31. Unstructured region (wavy black line), β -propeller (white oval, labeled β PROP), central structured domain (blue-cyan box) and C-terminal α -helical domain (white box, labeled α H) are shown. Scale bar shows number of amino acids residues. The β -propeller protein Sec13 binds Sec31 at the position indicated.
- (D) Structure of the Sec13•Sec31 tetramer. Color scheme as in B, with Sec31 coloring matching that of Sec16. The lower view is rotated 90 degrees towards the viewer as indicated.

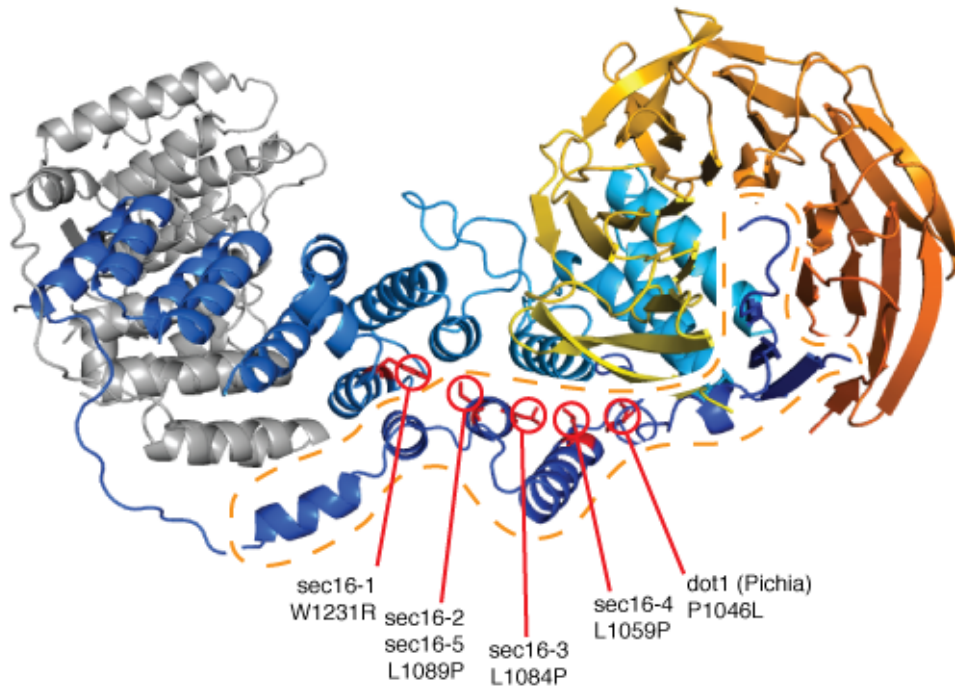


Figure 3-5 Structural Consequences of Temperature-Sensitive Alleles of Sec16

The known temperature sensitive alleles of Sec16 in *S. cerevisiae* (Espenshade, JCB 1995) and *P. pastoris* (Connerly, Current Biology 2005) are shown mapped to the structure of Sec13•Sec16. Sec16 is colored blue to cyan and Sec13 is colored orange to yellow from N to C terminus. Residues mutated in each temperature-sensitive allele are shown in red and labeled. Dashed line encircles the N-terminal portion of Sec16 central domain.

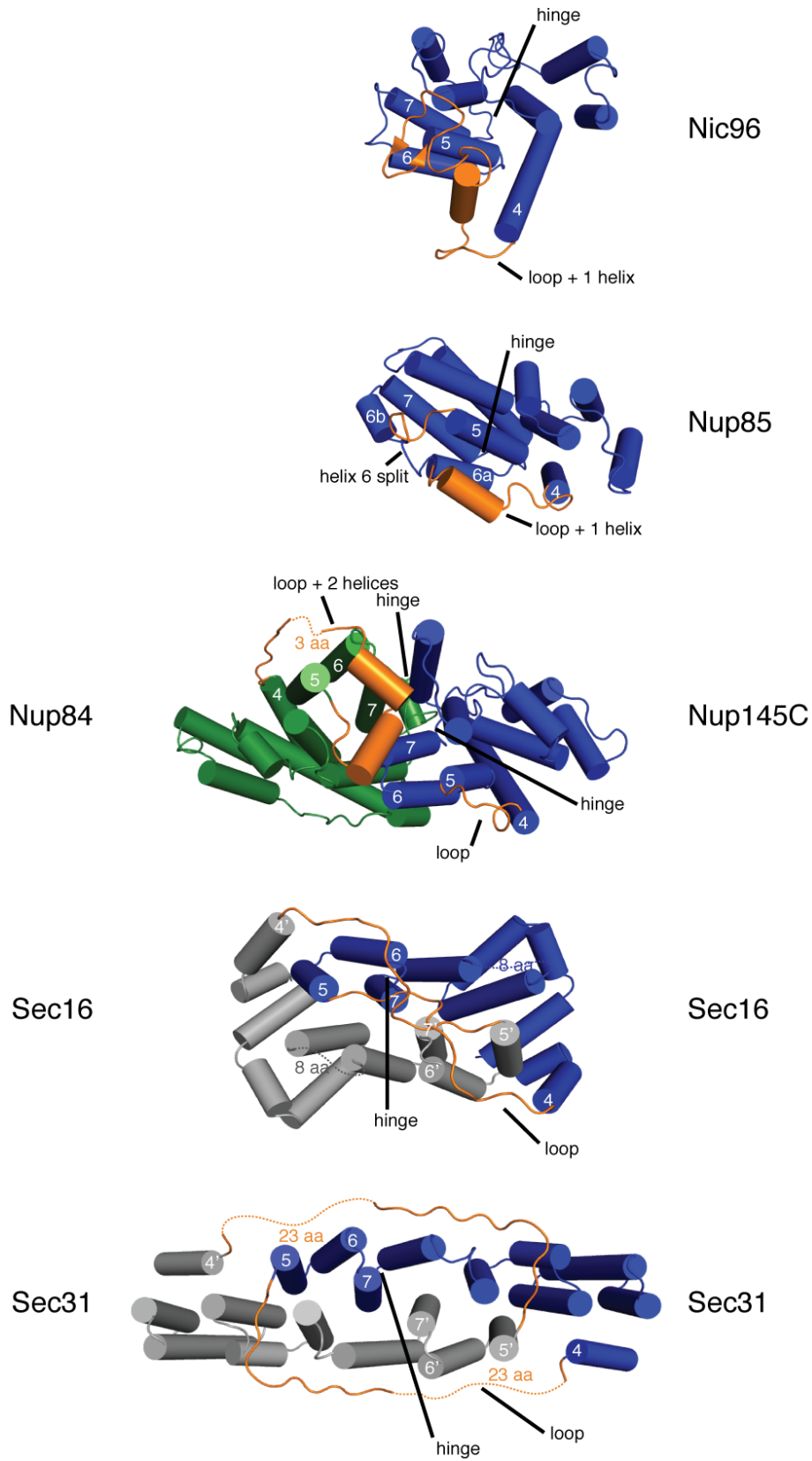


Figure 3-6 Interactions Formed by the ACE1 Crown

The crown domain of each ACE1 is shown colored blue, except Nup84, which is green. Nic96 and Nup85 are not known to dimerize. Nup84 and Nup145C form a heterodimer, and Sec16 and Sec31 form homodimers. The second copies of Sec16 and Sec31 are colored grey. Disordered loops are shown as dotted lines and labeled with the number of amino acids not observed (aa). Sec16 and Sec31 dimerize by domain-swapping. Helices $\alpha 5$ - $\alpha 7$ exchange positions with helices $\alpha 5'$ - $\alpha 7'$ in the binding partner. The domain swap requires extension of the swap loop (labeled “loop”) that connects helix $\alpha 4$ to $\alpha 5$, and rotation of the swap hinge (labeled “hinge”) that connects helix $\alpha 7$ to helix $\alpha 8$. The position of the corresponding loop and hinge are labeled in all ACE1s. Nic96, Nup85 and Nup84 have one or two α -helices inserted into this loop, (labeled “loop + n helix(ces)”)

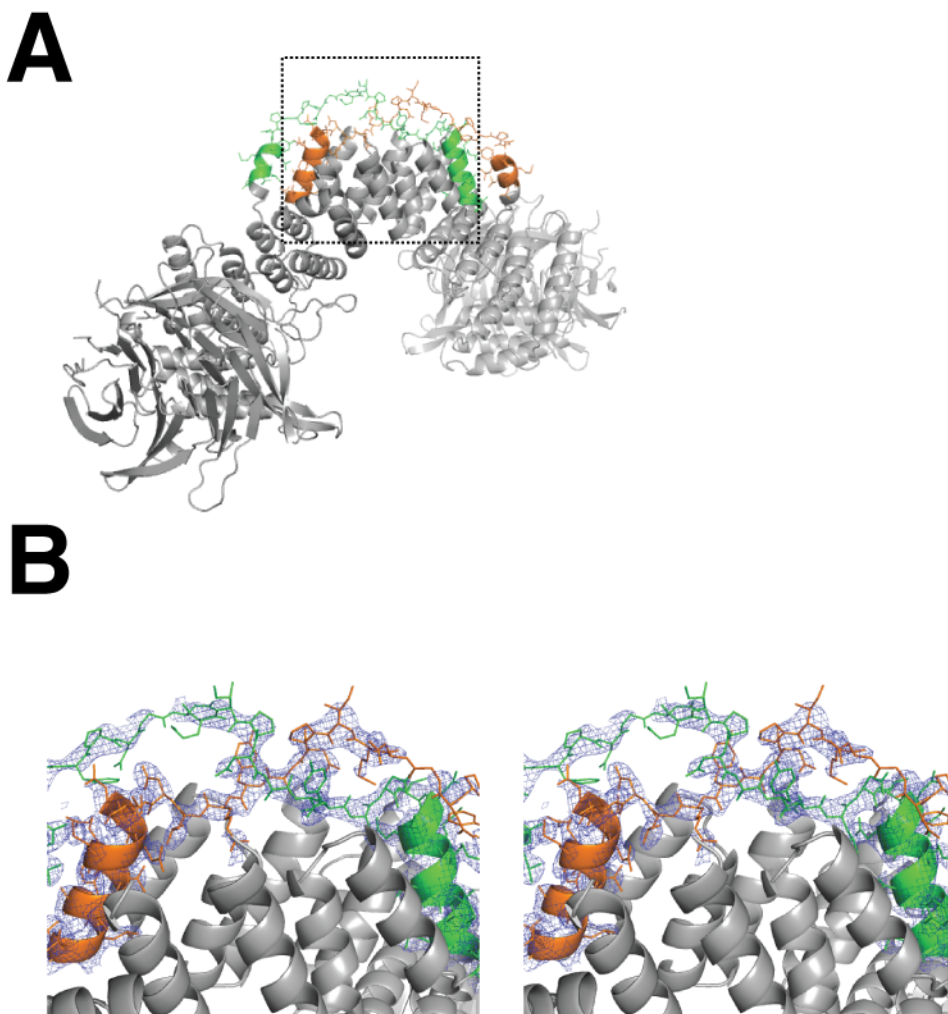


Figure 3-7 SA-omit Map of Sec16 Swap Loop

- (A) Crystal structure of Sec13•Sec16. Helix α_4 , the swap loop, and helix α_5 are colored green. The corresponding portion of the other Sec16 molecule is orange. The region enlarged in B and C is boxed.
- (B) Stereogram of the simulated-annealing omit map of the Sec16 swap loop. The $2F_o - F_c$ sa-omit map is contoured at 1.0σ . Although the loops are adjacent in space, they touch then continue over the opposite swap loop, rather than interlock (by passing underneath the opposite swap loop).

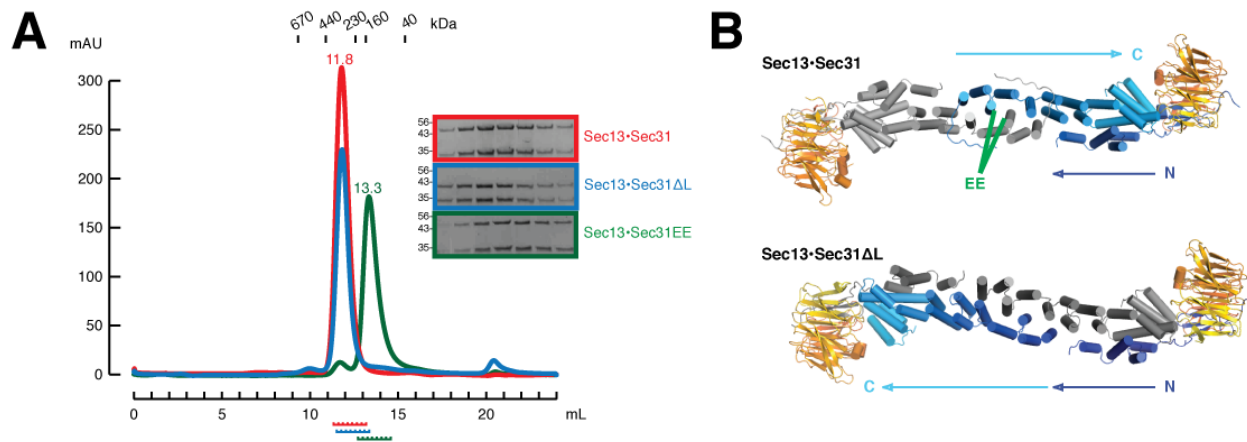


Figure 3-8 Solution Behavior and Crystal Structure of Sec13•Sec31 mutants

- (A) Sec13•Sec31 (red) compared to Sec13•Sec31 mutants Δ L (blue) and EE (green) by size exclusion chromatography. Sec13•Sec31 and Sec13•Sec31 Δ L are heterotetramers, whose structures are shown in B, with the same hydrodynamic radii. The EE mutation disrupts the crown interface. Sec13•Sec31EE is a heterodimer in solution. Elution volume in mL is plotted against absorbance at $\lambda = 280$ nm. Elution volumes for standard globular proteins are as indicated. SDS-PAGE analysis of each sample is shown, with fractions indicated below the x-axis.
- (B) Crystal structure of Sec13•Sec31 Δ L compared to Sec13•Sec31 (PDB ID: 2PM6). The tetramers form extended rods with the same 165° central angle. Due to deletion of the swap loop, Sec13•Sec31 Δ L forms a laminated structure, rather than form a U-turn, as indicated by arrows labeled N and C. Both copies of Sec31 are colored blue to cyan from N to C terminus. The green label EE indicates residues M540 and L544, in helices $\alpha 7$ and $\alpha 7'$, which were mutated to glutamic acid to generate Sec13•Sec31EE.

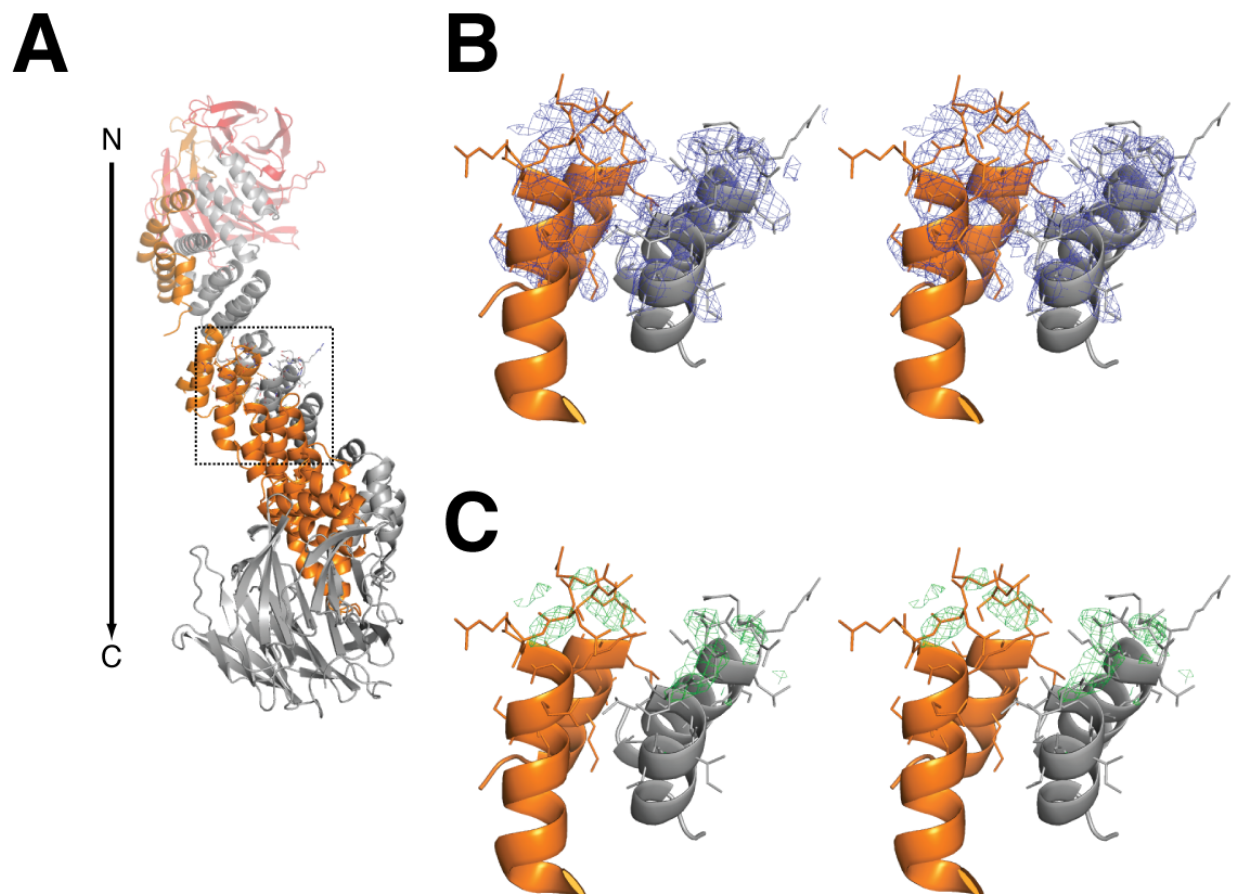


Figure 3-9 Electron Density at Sec31 Δ L Swap Hinge

- (A) Crystal structure of the Sec13•Sec31 Δ L. Sec13 is colored red or grey. Sec31 Δ L is colored orange or grey. The orange Sec31 Δ L runs top to bottom from N to C terminus, as labeled. The region enlarged in B and C is boxed.
- (B) Stereogram of swap hinges, connecting helices α 7- α 8 (orange) or connecting helices α 7'- α 8' (grey) of Sec31 Δ L. An electron density map ($2F_o-F_c$, contoured at 1.0σ) calculated before modeling the hinge is shown.
- (C) Stereogram as in B. Difference density (F_o-F_c , contoured at 3.0σ) is shown. The observed connectivity proves lamination of the Sec13•Sec31 Δ L tetramer. If Sec31 Δ L were not laminated, the swap hinge would connect helix α 7 to α 8' and helix α 7' to α 8.

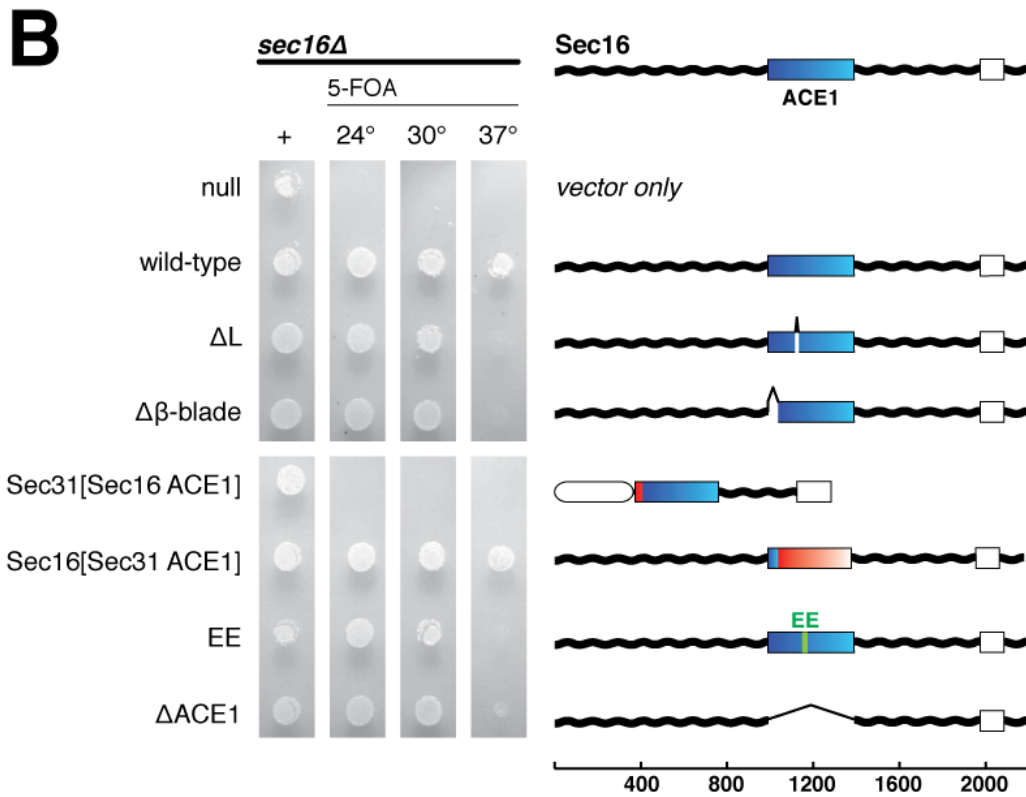
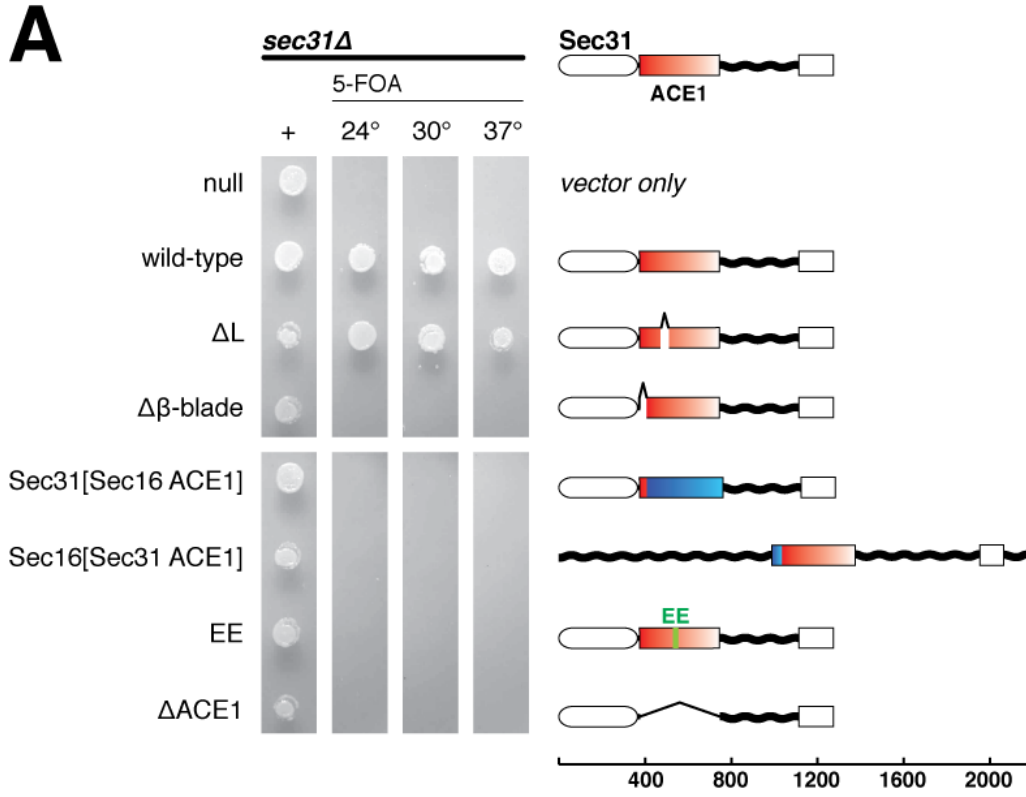


Figure 3-10 Complementation of Sec16 or Sec31 by Structure-Based Mutations

- (A) Structure-based mutants of Sec31 assayed by plasmid shuffle. A *sec31 Δ* plasmid shuffle strain was prepared using endogenous *SEC31* cloned into a URA3 plasmid. Mutations were introduced into *SEC31* on a LEU2 plasmid, transformed into the shuffle strain, spotted onto media lacking leucine (first lane) or lacking leucine and supplemented with 5-fluoroorotic acid (subsequent lanes), and grown for 36 hours at 24°C, 30°C, or 37°C. Sec31 domain architecture is diagrammed: N-terminal β -propeller (white oval), central insertion β -blade and ACE1 (red-white box), unstructured region (wavy black lines), and C-terminal α -helical domain (white box). Fragments of Sec16 used in chimeric genes are shown in blue-cyan.
- (B) Structure-based mutants of Sec16 assayed by plasmid shuffle. Mutations were introduced into *SEC16* on a LEU2 plasmid, and tested as in A. Genes are diagrammed: unstructured regions (wavy black lines), central conserved domain (blue-cyan box) and C-terminal α -helical domain (white box). Fragments of Sec31 used in chimeric genes are shown in red-white.

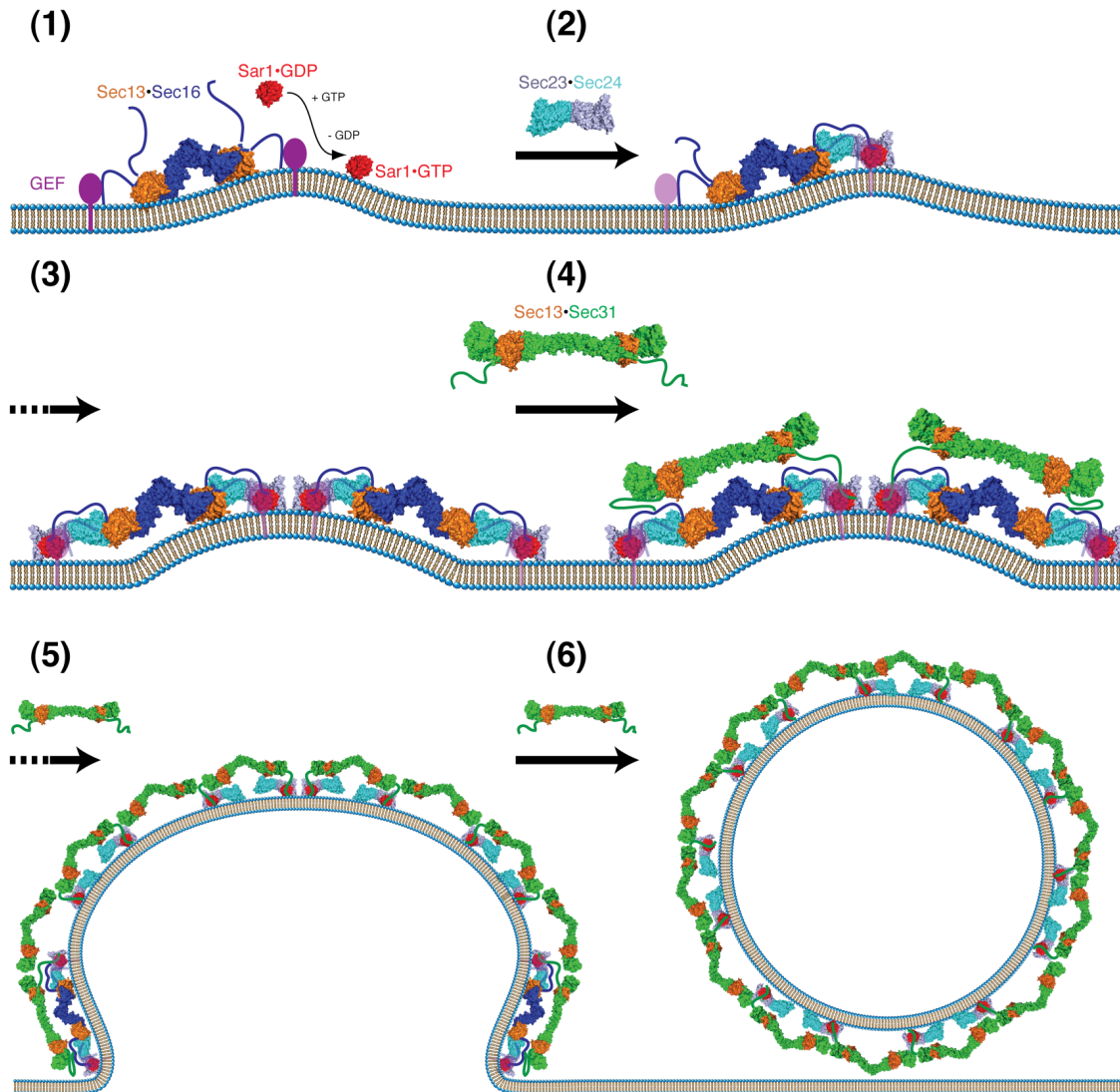


Figure 3-11 Model for Assembly of the COPII Coat Complex

The common model for assembly of the COPII coat complex is modified to include the role of Sec16. For simplicity, cargo molecules are omitted. (1) The Sec13•Sec16 tetramer is stably associated with the ER membrane and binds the integral membrane protein Sed4, or its homolog Sec12. Sar1 becomes associated with the membrane, when it is converted from GDP- to GTP-bound state. Concentration of membrane associated proteins begins to bend membrane. (2) Sec13•Sec16 and Sar1 collaborate to recruit the cargo adaptor Sec23•Sec24 dimer. (3) a pre-coat self-associates into higher-order oligomers. (4) Sec13•Sec16 and Sec23•Sec24•Sar1 form independent interactions with Sec13•Sec31, causing it to assemble near and/or in place of Sec16. (5) The forming coat contains progressively more Sec13•Sec31 and less Sec13•Sec16. Hand-off of Sec23•Sec24•Sar1 from Sec16 to Sec31 sets the stage for GTP hydrolysis by Sar1. (6) A final COPII coat is formed and vesicle budding is complete. Sec13•Sec16 remains mostly associated with the ER.

	Sec13•Sec16		Sec13•Sec31ΔL
	Selenomethionine	Native	Native
Data Collection			
Spacegroup	P 21	P 21 21 21	P 21
a, b, c (Å)	56.0, 144.1, 204.3	56.7, 139.0, 205.42	156.2, 46.6, 192.0
α, β, γ (°)	90, 90, 90	90, 90, 90	90, 93.5, 90
Wavelength (Å)	0.9792	0.9792	0.9792
Resolution range (Å)	30.0-2.70 (2.80-2.70)	30.0-2.65 (2.74-2.65)	30.0-2.80 (2.87-2.80)
Total reflections	430502	168736	396307
Unique reflections	88825	45333	69366
Completeness (%)	99.9 (100)	99.8 (99.4)	99.6(99.4)
Redundancy	3.6 (3.7)	3.7 (3.5)	5.7(5.5)
R _{merge} (%)	8.1 (56.0)	7.4 (65.3)	16.4(47.7)
R _{r.i.m.} (%)	9.9 (78.7)	8.6 (80.1)	18.1 (50.0)
R _{p.i.m.} (%)	4.5 (35.8)	4.4 (42.0)	7.3 (20.8)
I/σ	25.5 (2.7)	20.7 (1.9)	9.6 (3.3)
Wilson B	49.58	51.6	55.7
Refinement			
Resolution range (Å)		30.0-2.69	30.0-2.60
R _{work} (%)		19.4	26.7
R _{free} (%)		25.0	30.0
Twin law		n/a	-h,-k,l
Twin fraction		n/a	0.23
Number of reflections			
Total		44752	69353
Rfree		2158	1792
Number of atoms			
Protein		10476	19197
Water		184	0
Average B-factor (Å ²)			
Protein		102.8	51.8
Sec13 (molecule 1)		46.1	
Sec16 (molecule 2)		79.7	
Sec16 (molecule 3)		105.9	
Sec13 (molecule 4)		185.2	
Water		51.2	n/a
Ramachandran analysis (%)			
Favored		95.5	94.4
Allowed		4.2	5.1
Disallowed		0.3	0.5

R_{merge} is the merging R factor.

R_{r.i.m.} is the redundancy independent merging R factor.

R_{p.i.m.} is the precision-indicating merging R factor.

For definitions, see: Weiss, MS. J Appl Cryst. (2001) 34: 130-135

Table 3-1 Data Collection and Refinement Statistics

CHAPTER 4 Prospectus

Summary

This thesis presents five crystal structures of proteins or protein complexes from the NPC and the COPII vesicle coat, along with supporting biophysical and *in vivo* data. These provide structural information for 15% of the NPC scaffold. They complete the structure of Nup133 (in complex with Nup107), part of the Y-complex of the NPC, and show definitively that Nup133 forms a novel type of α -helical stack, unlike regular α -solenoids, or other nucleoporins or coat proteins. The helical domain of Nup170 shows that Nup170 is structurally homologous to Nup133. These structures prove that at least two classes of architectural nucleoporin (ACE1 and Nup130/Nup170-type) derived by duplication and diversification from elements of a simpler complex. The observation that Sec16 is an ACE1, and forms a heterotetramer with Sec13, which is similar to the Sec13•Sec31 edge element, proves that duplication has also occurred in the development of the COPII coat system. Indeed, despite only 15% sequence identity, the ACE1 of Sec31 can function in place of the ACE1 of Sec16. Together, these results suggest considering Sec16 a template for assembly of COPII.

Future Directions

Nup107•Nup133 and Nup170

The structures of Nup107•Nup133 and Nup170 suggest a few future avenues of research:

The identification of the ACE1 was a milestone in the study of the NPC, because it definitively linked the evolutionary origins of the NPC and COPII vesicle coat (Brohawn et al., 2008). If one could identify a similar link between Nup133/Nup170 and some other set of architectural proteins, that link likewise might shed light on the origin and function of this class of nucleoporin. The β -propeller/ α -helical tandem arrangement

occurs in several proteins whose structures have not been solved, and some of these are coat-related proteins. It is likely that Nup133 and Nup170 are structurally similar to one or more of these coat-related proteins. Sec39, a component of the Dsl1 vesicle tethering complex, makes an irregular helical stack with the same twist at the hinge before the C-terminal lobe observed in Nup133 and Nup170 (Ren et al., 2009). Sec39 might be distantly related to Nup133 and Nup170. It is interesting to note that Sec39 interacts with Dsl1 through its C-terminal lobe. The C-terminal lobes of Nup133 and Nup170 are a conserved feature of this family, but no function is yet attributed to them. The C-terminal lobes of Nup133 and Nup170 might form interactions analogous to Sec39•Dsl1. It might be appropriate to call Nup133 and Nup170 “tethering” proteins for the NPC. Consistent with that designation, Nup170 links several scaffold nucleoporins to integral membrane nucleoporins through Nup53 (Flemming et al., 2009; Makio et al., 2009; Onischenko et al., 2009), and the N-terminal β -propeller of Nup133 interacts directly with membrane (Drin et al., 2007).

The molecular mechanism by which Nup170 integrates into the Nic96-complex is not yet clear. As suggest in Chapter 2, one section of the α -helical domain of Nup170 corresponds to the section of Nup133 that binds the ACE1 nucleoporin Nup107. If Nup170 binds a protein by this surface, it might bind Nic96, the only ACE1 in the Nic96-complex. Like the C terminus of Nup107, which forms the interface to Nup133, the C terminus of Nic96 is hydrophobic and conserved, suggesting it forms a protein-protein interface—perhaps to Nup170. We have not yet been able to detect a Nup170•Nic96 interaction *in vitro* (by gel filtration or isothermal titration calorimetry), but it may be worthwhile to test for this interaction more thoroughly. In general, the Nic96-complex has proven difficult to reconstitute *in vitro*. Binary interactions among its components may be weaker than in the Y-complex. Perhaps only ternary complexes are stable. To this end, we have begun efforts to reconstitute recombinant Nic96, Nup170, Nup53, and Ndc1 into complexes. Two further members of the

Nic96-complex also should not be forgotten: Nup188 and Nup192 alone compose about 10% the mass of the NPC—one-fifth the scaffold. Secondary structure predictions suggest that each forms two all α -helical domains separated by a short linker region. Since the Nic96-complex constitutes two-thirds the scaffold of the NPC, the structure of this complex will be important for a complete reconstruction of the molecular architecture of the NPC.

It will be interesting to study further the β -propeller domains of Nup133 and Nup170. In both proteins, only the α -helical domain is required for targeting to the nuclear rim—the β -propeller domain does not integrate independently into the NPC (Berke et al., 2004; Flemming et al., 2009). The functions of these β -propeller domains have not been fully explored. In Nup133, the β -propeller domain binds and senses the curvature of membranes. How curvature sensing contributes to NPC assembly has not yet been explained fully. Although it seems the Nup133 N-terminal domain prefers liposomes with a curvature similar to what may be found at the nuclear pore (external diameter ~35 nm), one can only speculate how this affects NPC assembly (Drin et al., 2007). This sensing may be the primary function of the N-terminal domain of Nup133, but there are also indications that this domain forms protein-protein interactions (Seo et al., 2009). In Nup170, no molecular function is assigned to the β -propeller, but the R391H mutation in the human gene falls in the β -propeller and causes an inherited atrial fibrillation syndrome (Zhang et al., 2008). If a structure of the β -propeller of Nup170 were solved, it might suggest why this mutation is so damaging. This arginine (R) is strongly conserved as arginine or lysine, and found at the end of a predicted β -sheet, next to two prolines that start a loop. It might be surface exposed, and perhaps it is involved in an important protein-protein interaction. The Nup170 homolog Nup157 binds the Y-complex, probably through Nup120 (Lutzmann et al., 2005). Nup170 may form an analogous interaction, perhaps mediated by its β -propeller.

Sec16 in Assembly of the COPII coat

The structure of the Sec13•Sec16 edge element suggests that Sec16 templates assembly of the COPII coat. In Chapter 3, I put forward one model for its role. The proposal that Sec16 forms a template for the COPII coat could be substantiated either by showing that Sec16 can self-assemble into some higher order structure, or that the Sec13•Sec16 edge element can align the Sec13•Sec31 edge element in the right position for assembly of the outer coat. It is not yet clear how much Sec16 is present compared to other components at ER exit sites, how and when Sec16 assembles, and whether Sec16 enters the completed coat, or remains behind.

It might be possible to set up an *in vitro* system to answer some of these questions. Kirchhausen and colleagues have used total internal reflection (TIR) microscopy to monitor the kinetics of clathrin-mediated endocytosis from the basal surface of adherent cells (Saffarian et al., 2009). Their experiment traces fluorescently labeled proteins simultaneously with wide field (WF) and TIR microscopy. The WF signal and the TIR/WF ratio together give, respectively, the quantity of the protein and its average distance from the cell surface, at each position in the image. Establishing a similar experimental system for COPII transport may prove more difficult, because COPII budding happens at the ER rather than from the surface of the cell. An *in vitro* system will be needed. COPII coating can be reconstituted *in vitro* on artificial membranes in suspension using recombinant protein, without addition of cargo. It might be possible to flatten these artificial membranes against a microscope slide and monitor budding from them using TIR microscopy. One should see recruitment of Sec16 to the membrane prior to other components of the system, be able to measure kinetics of Sec16's arrival and departure, and see whether Sec16 moves away from the surface as budding occurs (with the coat) or remains at the membrane surface.

It has been suggested that Sec16 modulates the GTPase activity of Sar1, but it is not clear how (Supek et al., 2002). One would expect Sec16 to decrease the rate of hydrolysis in order to promote coat assembly. When Sec31 assembles, it activates Sar1 by inserting a peptide from its proline-rich unstructured region into a groove on the surface of the Sec23•Sar1 dimer (Bi et al., 2007). This Sec31 peptide positions active site residues near the substrate GTP. Based on the similarity of Sec16 and Sec31 ACE1 domains, I suspect that an analogous peptide in the unstructured region of Sec16 may insert into the same groove, blocking Sec31. In other words, Sec16 might be a competitive inhibitor of Sec31. Although Sec16 does not inhibit the GTPase activity of purified Sec23•Sar1 (Supek et al., 2002), no one has reported testing for competitive inhibition when Sec31 is present.

Both the Sec16 ACE1 and the Sec31 ACE1 lack the tail module observed in the nucleoporin ACE1s. Instead, each protein has an unstructured extension followed by a predicted, C-terminal α -helical domain. It is not clear whether this C-terminal α -helical domains fold against the ACE1, or forms a separate, detached domain. In each protein, this domain forms crucial protein-protein interactions: the C-terminal domain of Sec16 binds Sed4, an integral membrane protein that regulates Sar1 (Gimeno et al., 1995), and the C-terminal domain of Sec31 binds Sec16 (Shaywitz et al., 1997). Crystal structures of the C-terminal α -helical domains in complex with their binding partners would be useful for studying COPII assembly, and would show whether the C-terminal domains are the missing “trunk” modules for their respective ACE1s, or adopt some other structure.

Conclusion

These structures of large architectural nucleoporins and coat proteins contribute to our increasing knowledge of protein complexes that interact peripherally with membranes to coat, organize and shape them. Further research will better define the overall architecture of the complexes to which they belong—the nuclear pore complex and COPII vesicle coat—and clarify how their structures act to establish and maintain the internal morphology of the eukaryotic cell

References

- Adams, P., R. Grosse-Kunstleve, L. Hung, T. Ioerger, A. McCoy, N. Moriarty, R. Read, J. Sacchettini, N. Sauter, and T. Terwilliger. 2002. PHENIX: building new software for automated crystallographic structure determination. *Acta Cryst.* D58:1948-54.
- Aitchison, J.D., M.P. Rout, M. Marelli, G. Blobel, and R.W. Wozniak. 1995. Two novel related yeast nucleoporins Nup170p and Nup157p: complementation with the vertebrate homologue Nup155p and functional interactions with the yeast nuclear pore-membrane protein Pom152p. *J. Cell Biol.* 131:1133-48.
- Akey, C.W., and M. Radermacher. 1993. Architecture of the *Xenopus* nuclear pore complex revealed by three-dimensional cryo-electron microscopy. *J. Cell Biol.* 122:1-19.
- Alber, F., S. Dokudovskaya, L.M. Veenhoff, W. Zhang, J. Kipper, D. Devos, A. Suprpto, O. Karni-Schmidt, R. Williams, B.T. Chait, M.P. Rout, and A. Sali. 2007. Determining the architectures of macromolecular assemblies. *Nature.* 450:683-94.
- Andrade, M.A., C. Perez-Iratxeta, and C.P. Ponting. 2001a. Protein repeats: structures, functions, and evolution. *J. Struct. Biol.* 134:117-31.
- Andrade, M.A., C. Petosa, S.I. O'Donoghue, C.W. Müller, and P. Bork. 2001b. Comparison of ARM and HEAT protein repeats. *J. Mol. Biol.* 309:1-18.
- Antonny, B., P. Gounon, R. Schekman, and L. Orci. 2003. Self-assembly of minimal COPII cages. *EMBO Rep.* 4:419-24.
- Antonny, B., D. Madden, S. Hamamoto, L. Orci, and R. Schekman. 2001. Dynamics of the COPII coat with GTP and stable analogues. *Nat. Cell Biol.* 3:531-7.
- Antonny, B., and R. Schekman. 2001. ER export: public transportation by the COPII coach. *Curr. Opin. Cell Biol.* 13:438-43.

- Baï, S.W., J. Rouquette, M. Umeda, W. Faigle, D. Loew, S. Sazer, and V. Doye. 2004. The fission yeast Nup107-120 complex functionally interacts with the small GTPase Ran/Spi1 and is required for mRNA export, nuclear pore distribution, and proper cell division. *Mol. Cell. Biol.* 24:6379-92.
- Bailey, S. 1994. The Ccp4 Suite - Programs for Protein Crystallography. *Acta Crystallographica Section D-Biological Crystallography.* 50:760-763.
- Baker, N.A., D. Sept, S. Joseph, M.J. Holst, and J.A. McCammon. 2001. Electrostatics of nanosystems: application to microtubules and the ribosome. *Proc. Natl. Acad. Sci. U.S.A.* 98:10037-41.
- Barlowe, C., L. Orci, T. Yeung, M. Hosobuchi, S. Hamamoto, N. Salama, M.F. Rexach, M. Ravazzola, M. Amherdt, and R. Schekman. 1994. COPII: a membrane coat formed by Sec proteins that drive vesicle budding from the endoplasmic reticulum. *Cell.* 77:895-907.
- Bayliss, R., T. Littlewood, and M. Stewart. 2000. Structural basis for the interaction between FxFG nucleoporin repeats and importin- β in nuclear trafficking. *Cell.* 102:99-108.
- Bayliss, R., K. Ribbeck, D. Akin, H.M. Kent, C.M. Feldherr, D. Görlich, and M. Stewart. 1999. Interaction between NTF2 and xFxFG-containing nucleoporins is required to mediate nuclear import of RanGDP. *J. Mol. Biol.* 293:579-93.
- Beck, M., F. Förster, M. Ecke, J.M. Plitzko, F. Melchior, G. Gerisch, W. Baumeister, and O. Medalia. 2004. Nuclear pore complex structure and dynamics revealed by cryoelectron tomography. *Science.* 306:1387-90.
- Beck, M., V. Lucić, F. Förster, W. Baumeister, and O. Medalia. 2007. Snapshots of nuclear pore complexes in action captured by cryo-electron tomography. *Nature.* 449:611-5.
- Beck, R., M. Rawet, M. Ravet, F.T. Wieland, and D. Cassel. 2009. The COPI system: molecular mechanisms and function. *FEBS Letters.* 583:2701-9.
- Bednenko, J., G. Cingolani, and L. Gerace. 2003. Importin β contains a COOH-terminal nucleoporin binding region important for nuclear transport. *J. Cell Biol.* 162:391-401.
- Belgareh, N., G. Rabut, S.W. Baï, M. van Overbeek, J. Beaudouin, N. Daigle, O.V. Zatsepina, F. Pasteau, V. Labas, M. Fromont-Racine, J. Ellenberg, and V. Doye. 2001. An evolutionarily conserved NPC subcomplex, which redistributes in part to kinetochores in mammalian cells. *J. Cell Biol.* 154:1147-60.
- Bennett, M.J., M.P. Schlunegger, and D. Eisenberg. 1995. 3D domain swapping: a mechanism for oligomer assembly. *Protein Sci.* 4:2455-68.
- Berke, I.C., T. Boehmer, G. Blobel, and T.U. Schwartz. 2004. Structural and functional analysis of Nup133 domains reveals modular building blocks of the nuclear pore complex. *J. Cell Biol.* 167:591-7.
- Bhattacharyya, D., and B. Glick. 2007. Two Mammalian Sec16 Homologues Have Nonredundant Functions in Endoplasmic Reticulum (ER) Export and Transitional ER Organization. *Mol. Biol. Cell.* 18:839-49.
- Bi, X., R.A. Corpina, and J. Goldberg. 2002. Structure of the Sec23/24-Sar1 pre-budding complex of the COPII vesicle coat. *Nature.* 419:271-7.

- Bi, X., J.D. Mancias, and J. Goldberg. 2007. Insights into COPII coat nucleation from the structure of Sec23.Sar1 complexed with the active fragment of Sec31. *Dev Cell*. 13:635-45.
- Boehmer, T., J. Enninga, S. Dales, G. Blobel, and H. Zhong. 2003. Depletion of a single nucleoporin, Nup107, prevents the assembly of a subset of nucleoporins into the nuclear pore complex. *Proc. Natl. Acad. Sci. U.S.A.* 100:981-5.
- Boehmer, T., S. Jeudy, I.C. Berke, and T. Schwartz. 2008. Structural and Functional Studies of Nup107/Nup133 Interaction and Its Implications for the Architecture of the Nuclear Pore Complex. *Mol. Cell*. 30:721-731.
- Bond, C.S., and A.W. Schüttelkopf. 2009. ALINE: a WYSIWYG protein-sequence alignment editor for publication-quality alignments. *Acta Cryst.* D65:510-2.
- Bonifacino, J.S., and B.S. Glick. 2004. The mechanisms of vesicle budding and fusion. *Cell*. 116:153-66.
- Bonner, W.M. 1975. Protein migration into nuclei. I. Frog oocyte nuclei in vivo accumulate microinjected histones, allow entry to small proteins, and exclude large proteins. *J. Cell Biol.* 64:421-30.
- Brohawn, S.G., N.C. Leksa, E.D. Spear, K.R. Rajashankar, and T.U. Schwartz. 2008. Structural evidence for common ancestry of the nuclear pore complex and vesicle coats. *Science*. 322:1369-73.
- Brohawn, S.G., J.R. Partridge, J.R.R. Whittle, and T.U. Schwartz. 2009. The nuclear pore complex has entered the atomic age. *Structure*. 17:1156-68.
- Brohawn, S.G., and T.U. Schwartz. 2009a. A lattice model of the nuclear pore complex. *Commun. Integr. Biol.* 2:205-7.
- Brohawn, S.G., and T.U. Schwartz. 2009b. Molecular architecture of the Nup84-Nup145C-Sec13 edge element in the nuclear pore complex lattice. *Nat. Struct. Mol. Biol.* 16:1173-7.
- Brunger, A.T., B. Delabarre, J.M. Davies, and W.I. Weis. 2009. X-ray structure determination at low resolution. *Acta Cryst.* D65:128-33.
- Byrne, K.P., and K.H. Wolfe. 2005. The Yeast Gene Order Browser: combining curated homology and syntenic context reveals gene fate in polyploid species. *Genome Res.* 15:1456-61.
- Carmody, S., and S. Wenthe. 2009. mRNA nuclear export at a glance. *J. Cell. Sci.* 122:1933.
- Chaudhuri, I., J. Söding, and A.N. Lupas. 2008. Evolution of the β -propeller fold. *Proteins*. 71:795-803.
- Chiu, W., M.L. Baker, and S.C. Almo. 2006. Structural biology of cellular machines. *Trends Cell Biol.* 16:144-50.
- Chook, Y.M., and G. Blobel. 2001. Karyopherins and nuclear import. *Curr. Opin. Struct. Biol.* 11:703-15.
- Cronshaw, J.M., A.N. Krutchinsky, W. Zhang, B.T. Chait, and M.J. Matunis. 2002. Proteomic analysis of the mammalian nuclear pore complex. *J. Cell Biol.* 158:915-27.
- Connerly, P., M. Esaki, E. Montegna, D. Strongin, S. Levi, J. Soderholm, and B. Glick. 2005. Sec16 is a Determinant of Transitional ER Organization. *Curr. Biol.* 15:1439-1447.

- Conti, E., C.W. Müller, and M. Stewart. 2006. Karyopherin flexibility in nucleocytoplasmic transport. *Curr. Opin. Struct. Biol.* 16:237-44.
- Cook, A., F. Bono, M. Jinek, and E. Conti. 2007. Structural biology of nucleocytoplasmic transport. *Annu. Rev. Biochem.* 76:647-71.
- Cook, A., E. Fernandez, D. Lindner, J. Ebert, G. Schlenstedt, and E. Conti. 2005. The structure of the nuclear export receptor Cse1 in its cytosolic state reveals a closed conformation incompatible with cargo binding. *Mol. Cell.* 18:355-67.
- Cook, A.G., N. Fukuhara, M. Jinek, and E. Conti. 2009. Structures of the tRNA export factor in the nuclear and cytosolic states. *Nature.* 461:60-5.
- Cordes, V.C., S. Reidenbach, and W.W. Franke. 1995. High content of a nuclear pore complex protein in cytoplasmic annulate lamellae of *Xenopus* oocytes. *Eur. J. Cell Biol.* 68:240-55.
- Cronshaw, J., A. Krutchinsky, W. Zhang, and B. Chait. 2002. Proteomic analysis of the mammalian nuclear pore complex. *J. Cell Biol.* 158:915-27.
- D'Angelo, M., and M. Hetzer. 2008. Structure, dynamics and function of nuclear pore complexes. *Trends Cell Biol.* 18:456-466.
- D'souza-Schorey, C., and P. Chavrier. 2006. ARF proteins: roles in membrane traffic and beyond. *Nat. Rev. Mol. Cell Biol.* 7:347-58.
- Dacks, J.B., and M.C. Field. 2007. Evolution of the eukaryotic membrane-trafficking system: origin, tempo and mode. *J. Cell. Sci.* 120:2977-85.
- Debler, E., Y. Ma, H. Seo, K. Hsia, T. Noriega, G. Blobel, and A. Hoelz. 2008. A Fence-like Coat for the Nuclear Pore Membrane. *Mol. Cell.* 32:815-826.
- Denning, D.P., S.S. Patel, V. Uversky, A.L. Fink, and M. Rexach. 2003. Disorder in the nuclear pore complex: the FG repeat regions of nucleoporins are natively unfolded. *Proc. Natl. Acad. Sci. U.S.A.* 100:2450-5.
- Denning, D.P., and M.F. Rexach. 2007. Rapid evolution exposes the boundaries of domain structure and function in natively unfolded FG nucleoporins. *Mol. Cell Proteomics.* 6:272-82.
- Devos, D., S. Dokudovskaya, F. Alber, R. Williams, B.T. Chait, A. Sali, and M.P. Rout. 2004. Components of coated vesicles and nuclear pore complexes share a common molecular architecture. *PLoS Biol.* 2:e380.
- Devos, D., S. Dokudovskaya, R. Williams, F. Alber, N. Eswar, B.T. Chait, M.P. Rout, and A. Sali. 2006. Simple fold composition and modular architecture of the nuclear pore complex. *Proc. Natl. Acad. Sci. U.S.A.* 103:2172-7.
- Dolinsky, T.J., J.E. Nielsen, J.A. McCammon, and N.A. Baker. 2004. PDB2PQR: an automated pipeline for the setup of Poisson-Boltzmann electrostatics calculations. *Nucleic Acids Res.* 32:W665-7.
- Doye, V., and E. Hurt. 1997. From nucleoporins to nuclear pore complexes. *Curr. Opin. Cell Biol.* 9:401-11.
- Doye, V., R. Wepf, and E.C. Hurt. 1994. A novel nuclear pore protein Nup133p with distinct roles in poly(A)⁺ RNA transport and nuclear pore distribution. *EMBO J.* 13:6062-75.
- Drin, G., J.-F. Casella, R. Gautier, T. Boehmer, T.U. Schwartz, and B. Antony. 2007. A general amphipathic α -helical motif for sensing membrane curvature. *Nat. Struct. Mol. Biol.* 14:138-46.

- Dultz, E., E. Zanin, C. Wurzenberger, M. Braun, G. Rabut, L. Sironi, and J. Ellenberg. 2008. Systematic kinetic analysis of mitotic dis- and reassembly of the nuclear pore in living cells. *J. Cell Biol.* 180:857-65.
- Edeling, M.A., C. Smith, and D. Owen. 2006. Life of a clathrin coat: insights from clathrin and AP structures. *Nat. Rev. Mol. Cell Biol.* 7:32-44.
- Edgar, R.C. 2004. MUSCLE: multiple sequence alignment with high accuracy and high throughput. *Nucleic Acids Res.* 32:1792-7.
- Elad, N., T. Maimon, D. Frenkiel-Krispin, R.Y.H. Lim, and O. Medalia. 2009. Structural analysis of the nuclear pore complex by integrated approaches. *Curr. Opin. Struct. Biol.* 19:226-32.
- Emsley, P., and K. Cowtan. 2004. Coot: model-building tools for molecular graphics. *Acta Cryst.* D60:2126-32.
- Espenshade, P., R.E. Gimeno, E. Holzmacher, P. Teung, and C.A. Kaiser. 1995. Yeast SEC16 gene encodes a multidomain vesicle coat protein that interacts with Sec23p. *J. Cell Biol.* 131:311-24.
- Eswar, N., B. Webb, M.A. Marti-Renom, M.S. Madhusudhan, D. Eramian, M.-Y. Shen, U. Pieper, and A. Sali. 2007. Comparative protein structure modeling using MODELLER. *Current protocols in protein science*. Chapter 2:Unit 2.9.
- Fabre, E., and E. Hurt. 1997. Yeast genetics to dissect the nuclear pore complex and nucleocytoplasmic trafficking. *Annu Rev Genet.* 31:277-313.
- Fahrenkrog, B., J.P. Aris, E.C. Hurt, N. Panté, and U. Aebi. 2000. Comparative spatial localization of protein-A-tagged and authentic yeast nuclear pore complex proteins by immunogold electron microscopy. *J. Struct. Biol.* 129:295-305.
- Fahrenkrog, B., J. Koser, and U. Aebi. 2004. The nuclear pore complex: a jack of all trades. *Trends Biochem. Sci.* 29:175-182.
- Fane, B.A., and P.E. Prevelige. 2003. Mechanism of scaffolding-assisted viral assembly. *Adv Protein Chem.* 64:259-99.
- Fath, S., J.D. Mancias, X. Bi, and J. Goldberg. 2007. Structure and Organization of Coat Proteins in the COPII Cage. *Cell.* 129:1325-1336.
- Field, M.C., and J.B. Dacks. 2009. First and last ancestors: reconstructing evolution of the endomembrane system with ESCRTs, vesicle coat proteins, and nuclear pore complexes. *Curr. Opin. Cell Biol.* 21:4-13.
- Flemming, D., P. Sarges, P. Stelter, A. Hellwig, B. Bottcher, and E. Hurt. 2009. Two structurally distinct domains of the nucleoporin Nup170 cooperate to tether a subset of nucleoporins to nuclear pores. *J. Cell Biol.* 185:387-95.
- Fontes, M.R., T. Teh, and B. Kobe. 2000. Structural basis of recognition of monopartite and bipartite nuclear localization sequences by mammalian importin- α . *J. Mol. Biol.* 297:1183-94.
- Fornerod, M., M. Ohno, M. Yoshida, and I.W. Mattaj. 1997. CRM1 is an export receptor for leucine-rich nuclear export signals. *Cell.* 90:1051-60.
- Fotin, A., Y. Cheng, N. Grigorieff, T. Walz, S.C. Harrison, and T. Kirchhausen. 2004a. Structure of an auxilin-bound clathrin coat and its implications for the mechanism of uncoating. *Nature.* 432:649-53.

- Fotin, A., Y. Cheng, P. Sliz, N. Grigorieff, S.C. Harrison, T. Kirchhausen, and T. Walz. 2004b. Molecular model for a complete clathrin lattice from electron cryomicroscopy. *Nature*. 432:573-9.
- Franz, C., P. Askjaer, W. Antonin, C.L. Iglesias, U. Haselmann, M. Schelder, A. de Marco, M. Wilm, C. Antony, and I.W. Mattaj. 2005. Nup155 regulates nuclear envelope and nuclear pore complex formation in nematodes and vertebrates. *EMBO J*. 24:3519-31.
- Franz, C., R. Walczak, S. Yavuz, R. Santarella, M. Gentzel, P. Askjaer, V. Galy, M. Hetzer, I.W. Mattaj, and W. Antonin. 2007. MEL-28/ELYS is required for the recruitment of nucleoporins to chromatin and postmitotic nuclear pore complex assembly. *EMBO Rep*. 8:165-72.
- Frey, S., and D. Görlich. 2007. A Saturated FG-Repeat Hydrogel Can Reproduce the Permeability Properties of Nuclear Pore Complexes. *Cell*.
- Frey, S., and D. Görlich. 2009. FG/FxFG as well as GLFG repeats form a selective permeability barrier with self-healing properties. *EMBO J*. 28:2554-67.
- Frey, S., R.P. Richter, and D. Görlich. 2006. FG-rich repeats of nuclear pore proteins form a three-dimensional meshwork with hydrogel-like properties. *Science*. 314:815-7.
- Fromme, J.C., and R. Schekman. 2005. COPII-coated vesicles: flexible enough for large cargo? *Curr. Opin. Cell Biol*. 17:345-52.
- Fukuda, M., S. Asano, T. Nakamura, M. Adachi, M. Yoshida, M. Yanagida, and E. Nishida. 1997. CRM1 is responsible for intracellular transport mediated by the nuclear export signal. *Nature*. 390:308-11.
- Galy, V., I.W. Mattaj, and P. Askjaer. 2003. *Caenorhabditis elegans* nucleoporins Nup93 and Nup205 determine the limit of nuclear pore complex size exclusion in vivo. *Mol. Biol. Cell*. 14:5104-15.
- Gao, H., N. Sumanaweera, S.M. Bailer, and U. Stochaj. 2003. Nuclear accumulation of the small GTPase Gsp1p depends on nucleoporins Nup133p, Rat2p/Nup120p, Nup85p, Nic96p, and the acetyl-CoA carboxylase Acc1p. *J. Biol. Chem*. 278:25331-40.
- García De La Torre, J., M.L. Huertas, and B. Carrasco. 2000. Calculation of hydrodynamic properties of globular proteins from their atomic-level structure. *Biophys. J*. 78:719-30.
- Gigliotti, S., G. Callaini, S. Andone, M.G. Riparbelli, R. Pernas-Alonso, G. Hoffmann, F. Graziani, and C. Malva. 1998. Nup154, a new *Drosophila* gene essential for male and female gametogenesis is related to the nup155 vertebrate nucleoporin gene. *J. Cell Biol*. 142:1195-207.
- Gimeno, R., P. Espenshade, and C. Kaiser. 1996. COPII coat subunit interactions: Sec24p and Sec23p bind to adjacent regions of Sec16p. *Mol. Biol. Cell*. 7:1815-23.
- Gimeno, R.E., P. Espenshade, and C.A. Kaiser. 1995. SED4 encodes a yeast endoplasmic reticulum protein that binds Sec16p and participates in vesicle formation. *J. Cell Biol*. 131:325-38.

- Glavy, J.S., A.N. Krutchinsky, I.M. Cristea, I.C. Berke, T. Boehmer, G. Blobel, and B.T. Chait. 2007. Cell-cycle-dependent phosphorylation of the nuclear pore Nup107-160 subcomplex. *Proc. Natl. Acad. Sci. U.S.A.* 104:3811-6.
- Görlich, D., P. Henklein, R.A. Laskey, and E. Hartmann. 1996a. A 41 amino acid motif in importin- α confers binding to importin- β and hence transit into the nucleus. *EMBO J.* 15:1810-7.
- Görlich, D., S. Kostka, R. Kraft, C. Dingwall, R.A. Laskey, E. Hartmann, and S. Prehn. 1995. Two different subunits of importin cooperate to recognize nuclear localization signals and bind them to the nuclear envelope. *Curr. Biol.* 5:383-92.
- Görlich, D., and U. Kutay. 1999. Transport between the cell nucleus and the cytoplasm. *Annu. Rev. Cell Dev. Biol.* 15:607-60.
- Görlich, D., N. Panté, U. Kutay, U. Aebi, and F.R. Bischoff. 1996b. Identification of different roles for RanGDP and RanGTP in nuclear protein import. *EMBO J.* 15:5584-94.
- Grandi, P., T. Dang, N. Pané, A. Shevchenko, M. Mann, D. Forbes, and E. Hurt. 1997. Nup93, a vertebrate homologue of yeast Nic96p, forms a complex with a novel 205-kDa protein and is required for correct nuclear pore assembly. *Mol. Biol. Cell.* 8:2017-38.
- Grandi, P., V. Doye, and E.C. Hurt. 1993. Purification of NSP1 reveals complex formation with 'GLFG' nucleoporins and a novel nuclear pore protein NIC96. *EMBO J.* 12:3061-71.
- Grandi, P., N. Schlaich, H. Tekotte, and E.C. Hurt. 1995. Functional interaction of Nic96p with a core nucleoporin complex consisting of Nsp1p, Nup49p and a novel protein Nup57p. *EMBO J.* 14:76-87.
- Gronenborn, A.M. 2009. Protein acrobatics in pairs--dimerization via domain swapping. *Curr. Opin. Struct. Biol.* 19:39-49.
- Gürkan, C., S.M. Stagg, P. Lapointe, and W.E. Balch. 2006. The COPII cage: unifying principles of vesicle coat assembly. *Nat. Rev. Mol. Cell Biol.* 7:727-738.
- Handa, N., M. Kukimotoniino, R. Akasaka, S. Kishishita, K. Murayama, T. Terada, M. Inoue, T. Kigawa, S. Kose, and N. Imamoto. 2006. The Crystal Structure of Mouse Nup35 Reveals Atypical RNP Motifs and Novel Homodimerization of the RRM Domain. *J. Mol. Biol.* 363:114-124.
- Harel, A., A.V. Orjalo, T. Vincent, A. Lachish-Zalait, S. Vasu, S. Shah, E. Zimmerman, M. Elbaum, and D.J. Forbes. 2003. Removal of a single pore subcomplex results in vertebrate nuclei devoid of nuclear pores. *Mol. Cell.* 11:853-64.
- Hawryluk-Gara, L.A., M. Platani, R. Santarella, R.W. Wozniak, and I.W. Mattaj. 2008. Nup53 is required for nuclear envelope and nuclear pore complex assembly. *Mol. Biol. Cell.* 19:1753-62.
- Hawryluk-Gara, L.A., E.K. Shibuya, and R.W. Wozniak. 2005. Vertebrate Nup53 interacts with the nuclear lamina and is required for the assembly of a Nup93-containing complex. *Mol. Biol. Cell.* 16:2382-94.
- Heath, C.V., C.S. Copeland, D.C. Amberg, V. Del Priore, M. Snyder, and C.N. Cole. 1995. Nuclear pore complex clustering and nuclear accumulation of poly(A)⁺ RNA associated with mutation of the *Saccharomyces cerevisiae* RAT2/NUP120 gene. *J. Cell Biol.* 131:1677-97.

- Hinshaw, J.E., B.O. Carragher, and R.A. Milligan. 1992. Architecture and design of the nuclear pore complex. *Cell*. 69:1133-41.
- Holm, L., S. Kääriäinen, P. Rosenström, and A. Schenkel. 2008. Searching protein structure databases with DaliLite v.3. *Bioinformatics*. 24:2780-1.
- Hsia, K.-C., P. Stavropoulos, G. Blobel, and A. Hoelz. 2007. Architecture of a coat for the nuclear pore membrane. *Cell*. 131:1313-26.
- Hsu, V.W., and J.-S. Yang. 2009. Mechanisms of COPI vesicle formation. *FEBS Lett*. 583:3758-63.
- Hughes, H., A. Budnik, K. Schmidt, K.J. Palmer, J. Mantell, C. Noakes, A. Johnson, D.A. Carter, P. Verkade, P. Watson, and D.J. Stephens. 2009. Organisation of human ER-exit sites: requirements for the localisation of Sec16 to transitional ER. *J. Cell Sci*. 122:2924-34.
- Hughes, H., and D.J. Stephens. 2008. Assembly, organization, and function of the COPII coat. *Histochem Cell Biol*. 129:129-51.
- Hurt, E.C. 1988. A novel nucleoskeletal-like protein located at the nuclear periphery is required for the life cycle of *Saccharomyces cerevisiae*. *EMBO J*. 7:4323-34.
- Iovine, M.K., J.L. Watkins, and S.R. Wentz. 1995. The GLFG repetitive region of the nucleoporin Nup116p interacts with Kap95p, an essential yeast nuclear import factor. *J. Cell Biol*. 131:1699-713.
- Ivan, V., G. De Voer, D. Xanthakis, K. Spoorendonk, V. Kondylis, and C. Rabouille. 2008. Drosophila Sec16 Mediates the Biogenesis of tER Sites Upstream of Sar1 through an Arginine-Rich Motif. *Mol. Biol. Cell*. 19:4352-65.
- Judy, S., and T.U. Schwartz. 2007. Crystal structure of nucleoporin Nic96 reveals a novel, intricate helical domain architecture. *J. Biol. Chem*. 282:34904-12.
- Jovanovic-Talisman, T., J. Tetenbaum-Novatt, A.S. McKenney, A. Zilman, R. Peters, M.P. Rout, and B.T. Chait. 2009. Artificial nanopores that mimic the transport selectivity of the nuclear pore complex. *Nature*. 457:1023-7.
- Kabsch, W. 2010. XDS. *Acta Crystallogr D Biol Crystallogr*. 66:125-32.
- Kaiser, C.A., and R. Schekman. 1990. Distinct sets of SEC genes govern transport vesicle formation and fusion early in the secretory pathway. *Cell*. 61:723-33.
- Kalab, P., K. Weis, and R. Heald. 2002. Visualization of a Ran-GTP Gradient in Interphase and Mitotic *Xenopus* Egg Extracts. *Science*. 295:2452-6.
- Kalverda, B., and M. Fornerod. 2007. The nuclear life of nucleoporins. *Dev. Cell*. 13:164-5.
- Kampmann, M., and G. Blobel. 2009. Three-dimensional structure and flexibility of a membrane-coating module of the nuclear pore complex. *Nat. Struct. Mol. Biol*. 16:782-8.
- Kenna, M.A., J.G. Petranka, J.L. Reilly, and L.I. Davis. 1996. Yeast N1e3p/Nup170p is required for normal stoichiometry of FG nucleoporins within the nuclear pore complex. *Mol. Cell. Biol*. 16:2025-36.
- Kerscher, O., P. Hieter, M. Winey, and M. Basrai. 2001. Novel Role for a *Saccharomyces cerevisiae* Nucleoporin, Nup170p, in Chromosome Segregation. *Genetics*. 157:1543-53.

- Kiger, A.A., S. Gigliotti, and M.T. Fuller. 1999. Developmental genetics of the essential *Drosophila* nucleoporin nup154: allelic differences due to an outward-directed promoter in the P-element 3' end. *Genetics*. 153:799-812.
- King, M.C., C.P. Lusk, and G. Blobel. 2006. Karyopherin-mediated import of integral inner nuclear membrane proteins. *Nature*. 442:1003-7.
- Kiseleva, E., T.D. Allen, S. Rutherford, M. Bucci, S.R. Wentz, and M.W. Goldberg. 2004. Yeast nuclear pore complexes have a cytoplasmic ring and internal filaments. *J. Struct. Biol.* 145:272-88.
- Kiseleva, E., M.W. Goldberg, J. Cronshaw, and T.D. Allen. 2000. The nuclear pore complex: structure, function, and dynamics. *Crit Rev Eukaryot Gene Expr.* 10:101-12.
- Kobe, B., and A.V. Kajava. 2000. When protein folding is simplified to protein coiling: the continuum of solenoid protein structures. *Trends Biochem. Sci.* 25:509-15.
- Kosova, B., N. Panté, C. Rollenhagen, and E. Hurt. 1999. Nup192p is a conserved nucleoporin with a preferential location at the inner site of the nuclear membrane. *J. Biol. Chem.* 274:22646-51.
- Kramer, A., Y. Ludwig, V. Shahin, and H. Oberleithner. 2007. A pathway separate from the central channel through the nuclear pore complex for inorganic ions and small macromolecules. *J. Biol. Chem.* 282:31437-43.
- Krissinel, E., and K. Henrick. 2007. Inference of macromolecular assemblies from crystalline state. *J. Mol. Biol.* 372:774-97.
- Lee, M.C.S., L. Orci, S. Hamamoto, E. Futai, M. Ravazzola, and R. Schekman. 2005. Sar1p N-terminal helix initiates membrane curvature and completes the fission of a COPII vesicle. *Cell*. 122:605-17.
- Leksa, N.C., S.G. Brohawn, and T.U. Schwartz. 2009. The structure of the scaffold nucleoporin Nup120 reveals a new and unexpected domain architecture. *Structure*. 17:1082-91.
- Li, O., C. Heath, D. Amberg, T. Dockendorff, C. Copeland, M. Snyder, and C. Cole. 1995. Mutation or deletion of the *Saccharomyces cerevisiae* RAT3/NUP133 gene causes temperature-dependent nuclear accumulation of poly(A)⁺ RNA and constitutive clustering of nuclear pore complexes. *Mol. Biol. Cell*. 6:401-17.
- Lim, R.Y.H., B. Fahrenkrog, J. Köser, K. Schwarz-Herion, J. Deng, and U. Aebi. 2007. Nanomechanical basis of selective gating by the nuclear pore complex. *Science*. 318:640-3.
- Lim, R.Y.H., K.S. Ullman, and B. Fahrenkrog. 2008. Biology and biophysics of the nuclear pore complex and its components. *Int. Rev. Cell. Mol. Biol.* 267:299-342.
- Liu, Y., and D. Eisenberg. 2002. 3D domain swapping: As domains continue to swap. *Protein Sci.* 11:1285-99.
- Loiodice, I., A. Alves, G. Rabut, M. Van Overbeek, J. Ellenberg, J.-B. Sibarita, and V. Doye. 2004. The entire Nup107-160 complex, including three new members, is targeted as one entity to kinetochores in mitosis. *Mol. Biol. Cell*. 15:3333-44.
- Lupu, F., A. Alves, K. Anderson, V. Doye, and E. Lacy. 2008. Nuclear pore composition regulates neural stem/progenitor cell differentiation in the mouse embryo. *Dev. Cell*. 14:831-42.

- Lusk, C.P., G. Blobel, and M.C. King. 2007. Highway to the inner nuclear membrane: rules for the road. *Nat. Rev. Mol. Cell Biol.* 8:414-20.
- Lutzmann, M., R. Kunze, A. Buerer, U. Aebi, and E. Hurt. 2002. Modular self-assembly of a Y-shaped multiprotein complex from seven nucleoporins. *EMBO J.* 21:387-97.
- Lutzmann, M., R. Kunze, K. Stangl, P. Stelter, K.F. Tóth, B. Böttcher, and E. Hurt. 2005. Reconstitution of Nup157 and Nup145N into the Nup84-complex. *J. Biol. Chem.* 280:18442-51.
- Madej, T., J.F. Gibrat, and S.H. Bryant. 1995. Threading a database of protein cores. *Proteins.* 23:356-69.
- Makio, T., L.H. Stanton, C.-C. Lin, D.S. Goldfarb, K. Weis, and R.W. Wozniak. 2009. The nucleoporins Nup170p and Nup157p are essential for nuclear pore complex assembly. *J. Cell Biol.* 185:459-73.
- Mancias, J.D., and J. Goldberg. 2005. Exiting the endoplasmic reticulum. *Traffic.* 6:278-85.
- Mans, B., V. Anantharaman, L. Aravind, and E. Koonin. 2004. Comparative genomics, evolution and origins of the nuclear envelope and nuclear pore complex. *Cell Cycle.* 3-1612-37.
- Marelli, M., J.D. Aitchison, and R.W. Wozniak. 1998. Specific binding of the karyopherin Kap121p to a subunit of the nuclear pore complex containing Nup53p, Nup59p, and Nup170p. *J. Cell Biol.* 143:1813-30.
- Matsuoka, K. 1998. COPII-Coated Vesicle Formation Reconstituted with Purified Coat Proteins and Chemically Defined Liposomes. *Cell.* 93:263-275.
- Matsuoka, Y., M. Takagi, T. Ban, M. Miyazaki, T. Yamamoto, Y. Kondo, and Y. Yoneda. 1999. Identification and characterization of nuclear pore subcomplexes in mitotic extract of human somatic cells. *Biochem. Biophys. Res. Commun.* 254:417-23.
- Matsuura, Y., and M. Stewart. 2004. Structural basis for the assembly of a nuclear export complex. *Nature.* 432:872-7.
- McCoy, A., R. Grosse-Kunstleve, P. Adams, M. Winn, L. Storoni, and R. Read. 2007. Phaser crystallographic software. *J. Appl. Cryst.* 40:658-674.
- Miller, B.R., M. Powers, M. Park, W. Fischer, and D.J. Forbes. 2000. Identification of a new vertebrate nucleoporin, Nup188, with the use of a novel organelle trap assay. *Mol. Biol. Cell.* 11:3381-96.
- Miller, E., B. Antony, S. Hamamoto, and R. Schekman. 2002. Cargo selection into COPII vesicles is driven by the Sec24p subunit. *EMBO J.* 21:6105-13.
- Mishra, R.K., P. Chakraborty, A. Arnaoutov, B.M.A. Fontoura, and M. Dasso. 2010. The Nup107-160 complex and γ -TuRC regulate microtubule polymerization at kinetochores. *Nat. Cell Biol.* 12:164-9.
- Mohr, D., S. Frey, T. Fischer, T. Güttler, and D. Görlich. 2009. Characterisation of the passive permeability barrier of nuclear pore complexes. *EMBO J.* 28:2541-53.
- Monecke, T., T. Güttler, P. Neumann, A. Dickmanns, D. Görlich, and R. Ficner. 2009. Crystal structure of the nuclear export receptor CRM1 in complex with Snurportin1 and RanGTP. *Science.* 324:1087-91.

- Mossessova, E., L.C. Bickford, and J. Goldberg. 2003. SNARE selectivity of the COPII coat. *Cell*. 114:483-95.
- Murshudov, G.N., A.A. Vagin, and E.J. Dodson. 1997. Refinement of macromolecular structures by the maximum-likelihood method. *Acta Crystallogr D Biol Crystallogr*. 53:240-55.
- Nehrbass, U., M.P. Rout, S. Maguire, G. Blobel, and R.W. Wozniak. 1996. The yeast nucleoporin Nup188p interacts genetically and physically with the core structures of the nuclear pore complex. *J. Cell Biol*. 133:1153-62.
- Newmeyer, D.D., D.R. Finlay, and D.J. Forbes. 1986. In vitro transport of a fluorescent nuclear protein and exclusion of non-nuclear proteins. *J. Cell Biol*. 103:2091-102.
- Okada, C., E. Yamashita, S. Lee, S. Shibata, J. Katahira, A. Nakagawa, Y. Yoneda, and T. Tsukihara. 2009. A High-Resolution Structure of the Pre-microRNA Nuclear Export Machinery. *Science*. 326:1275-9.
- Onischenko, E., L.H. Stanton, A.S. Madrid, T. Kieselbach, and K. Weis. 2009. Role of the Ndc1 interaction network in yeast nuclear pore complex assembly and maintenance. *J. Cell Biol*. 185:475-91.
- Orjalo, A.V., A. Arnaoutov, Z. Shen, Y. Boyarchuk, S.G. Zeitlin, B. Fontoura, S. Briggs, M. Dasso, and D.J. Forbes. 2006. The Nup107-160 nucleoporin complex is required for correct bipolar spindle assembly. *Mol. Biol. Cell*. 17:3806-18.
- Ossareh-Nazari, B., F. Bachelerie, and C. Dargemont. 1997. Evidence for a role of CRM1 in signal-mediated nuclear protein export. *Science*. 278:141-4.
- Otwinowski, Z., and W. Minor. 1997. Processing of X-ray diffraction data collected in oscillation mode. *Macromolecular Crystallography, Pt A*. 276:307-326.
- Paine, P.L., L.C. Moore, and S.B. Horowitz. 1975. Nuclear envelope permeability. *Nature*. 254:109-14.
- Panté, N., and M. Kann. 2002. Nuclear pore complex is able to transport macromolecules with diameters of about 39 nm. *Mol. Biol. Cell*.
- Paoli, M. 2001. Protein folds propelled by diversity. *Prog. Biophys. Mol. Biol*. 76:103-30.
- Peters, R. 2009. Translocation through the nuclear pore: Kaps pave the way. *BioEssays*. 31:466-77.
- Powell, L., and B. Burke. 1990. Internuclear exchange of an inner nuclear membrane protein (p55) in heterokaryons: in vivo evidence for the interaction of p55 with the nuclear lamina. *J. Cell Biol*. 111:2225-34.
- Pryer, N.K., N.R. Salama, R. Schekman, and C.A. Kaiser. 1993. Cytosolic Sec13p complex is required for vesicle formation from the endoplasmic reticulum in vitro. *J. Cell Biol*. 120:865-75.
- Rabut, G., V. Doye, and J. Ellenberg. 2004a. Mapping the dynamic organization of the nuclear pore complex inside single living cells. *Nat. Cell Biol*. 6:1114:21
- Rabut, G., P. Lénárt, and J. Ellenberg. 2004b. Dynamics of nuclear pore complex organization through the cell cycle. *Curr. Opin. Cell Biol*. 16:314-21.
- Radu, A., G. Blobel, and R.W. Wozniak. 1993. Nup155 is a novel nuclear pore complex protein that contains neither repetitive sequence motifs nor reacts with WGA. *J. Cell Biol*. 121:1-9.

- Rasala, B.A., A.V. Orjalo, Z. Shen, S. Briggs, and D.J. Forbes. 2006. ELYS is a dual nucleoporin/kinetochore protein required for nuclear pore assembly and proper cell division. *Proc. Natl. Acad. Sci. U.S.A.* 103:17801-6.
- Rayala, H., F. Kendirgi, D. Barry, and P. Majerus. 2004. The mRNA Export Factor Human Gle1 Interacts with the Nuclear Pore Complex Protein Nup155. *Mol. Cell. Proteomics.* 3:145-55.
- Ren, Y., C.K. Yip, A. Tripathi, D. Huie, P.D. Jeffrey, T. Walz, and F.M. Hughson. 2009. A structure-based mechanism for vesicle capture by the multisubunit tethering complex Dsl1. *Cell.* 139:1119-29.
- Ribbeck, K., and D. Görlich. 2001. Kinetic analysis of translocation through nuclear pore complexes. *EMBO J.* 20:1320-30.
- Ribbeck, K., and D. Görlich. 2002. The permeability barrier of nuclear pore complexes appears to operate via hydrophobic exclusion. *EMBO J.* 21:2664-71.
- Ribbeck, K., G. Lipowsky, H.M. Kent, M. Stewart, and D. Görlich. 1998. NTF2 mediates nuclear import of Ran. *EMBO J.* 17:6587-98.
- Rost, B., G. Yachdav, and J. Liu. 2004. The PredictProtein server. *Nucleic Acids Res.* 32:W321-6.
- Rousseau, F., J.W.H. Schymkowitz, and L.S. Itzhaki. 2003. The unfolding story of three-dimensional domain swapping. *Structure.* 11:243-51.
- Rout, M., J.D. Aitchison, A. Suprpto, and K. Hjertaas. 2000a. The Yeast Nuclear Pore Complex Composition, Architecture, and Transport Mechanism. *J. Cell Biol.*
- Rout, M.P., J.D. Aitchison, M.O. Magnasco, and B.T. Chait. 2003. Virtual gating and nuclear transport: the hole picture. *Trends Cell Biol.* 13:622-8.
- Rout, M.P., J.D. Aitchison, A. Suprpto, K. Hjertaas, Y. Zhao, and B.T. Chait. 2000b. The yeast nuclear pore complex: composition, architecture, and transport mechanism. *J. Cell Biol.* 148:635-51.
- Rout, M.P., and G. Blobel. 1993. Isolation of the yeast nuclear pore complex. *J. Cell Biol.* 123:771-83.
- Saffarian, S., E. Cocucci, and T. Kirchhausen. 2009. Distinct dynamics of endocytic clathrin-coated pits and coated plaques. *PLoS Biol.* 7:e1000191.
- Salama, N.R., T. Yeung, and R.W. Schekman. 1993. The Sec13p complex and reconstitution of vesicle budding from the ER with purified cytosolic proteins. *EMBO J.* 12:4073-82.
- Sato, K., and A. Nakano. 2004. Reconstitution of coat protein complex II (COPII) vesicle formation from cargo-reconstituted proteoliposomes reveals the potential role of GTP hydrolysis by Sar1p in protein sorting. *J. Biol. Chem.* 279:1330-5.
- Scannell, D.R., G. Butler, and K.H. Wolfe. 2007. Yeast genome evolution--the origin of the species. *Yeast.* 24:929-42.
- Schrader, N., P. Stelter, D. Flemming, R. Kunze, E. Hurt, and I.R. Vetter. 2008. Structural basis of the nic96 subcomplex organization in the nuclear pore channel. *Mol. Cell.* 29:46-55.
- Schwartz, T.U. 2005. Modularity within the architecture of the nuclear pore complex. *Curr. Opin. Struct. Biol.* 15:221-6.

- Schwartz, T.U., D. Schmidt, S.G. Brohawn, and G. Blobel. 2006. Homodimerization of the G protein SR β in the nucleotide-free state involves proline cis/trans isomerization in the switch II region. *Proc. Natl. Acad. Sci. U.S.A.* 103:6823-8.
- Seo, H.-S., Y. Ma, E.W. Debler, D. Wacker, S. Kutik, G. Blobel, and A. Hoelz. 2009. Structural and functional analysis of Nup120 suggests ring formation of the Nup84-complex. *Proc. Natl. Acad. Sci. U.S.A.* 106:14281-6.
- Shaywitz, D.A. 1997. Towards an understanding of the role of COPII subunits in vesicle coat assembly. *Dissertation, M.I.T.*
- Shaywitz, D.A., P.J. Espenshade, R.E. Gimeno, and C.A. Kaiser. 1997. COPII subunit interactions in the assembly of the vesicle coat. *J. Biol. Chem.* 272:25413-6.
- Sheldrick, G.M. 2008. A short history of SHELX. *Acta Cryst.* A64:112-22.
- Shulga, N., N. Mosammaparast, R. Wozniak, and D. Goldfarb. 2000. Yeast Nucleoporins Involved in Passive Nuclear Envelope Permeability. *J. Cell Biol.* 149:1027-38
- Siegel, L., and K. Monty. 1966. Determination of molecular weights and frictional ratios of proteins in impure systems by use of gel filtration and density gradient centrifugation. Application to crude preparations of sulfite and hydroxylamine reductases. *Biochim. Biophys. Acta.* 112:346-362.
- Sikorski, R.S., and P. Hieter. 1989. A system of shuttle vectors and yeast host strains designed for efficient manipulation of DNA in *Saccharomyces cerevisiae*. *Genetics.* 122:19-27.
- Siniosoglou, S., M. Lutzmann, H. Santos-Rosa, K. Leonard, S. Mueller, U. Aebi, and E. Hurt. 2000. Structure and assembly of the Nup84p complex. *J. Cell Biol.* 149:41-54.
- Siniosoglou, S., C. Wimmer, M. Rieger, V. Doye, H. Tekotte, C. Weise, S. Emig, A. Segref, and E.C. Hurt. 1996. A novel complex of nucleoporins, which includes Sec13p and a Sec13p homolog, is essential for normal nuclear pores. *Cell.* 84:265-75.
- Smith, A., A. Brownawell, and I.G. Macara. 1998. Nuclear import of Ran is mediated by the transport factor NTF2. *Curr. Biol.* 8:1403-6.
- Stade, K., C.S. Ford, C. Guthrie, and K. Weis. 1997. Exportin 1 (Crm1p) is an essential nuclear export factor. *Cell.* 90:1041-50.
- Stagg, S., P. Lapointe, A. Razvi, C. Gurkan, C. Potter, B. Carragher, and W. Balch. 2008. Structural Basis for Cargo Regulation of COPII Coat Assembly. *Cell.* 134:474-484.
- Stagg, S.M., C. Gürkan, D.M. Fowler, P. Lapointe, T.R. Foss, C.S. Potter, B. Carragher, and W.E. Balch. 2006. Structure of the Sec13/31 COPII coat cage. *Nature.* 439:234-8.
- Stagg, S.M., P. Lapointe, and W.E. Balch. 2007. Structural design of cage and coat scaffolds that direct membrane traffic. *Curr. Opin. Struct. Biol.* 17:221-8.
- Stewart, M. 2007. Ratcheting mRNA out of the nucleus. *Mol. Cell.* 25:327-30.
- Stoffler, D., B. Feja, B. Fahrenkrog, J. Walz, D. Typke, and U. Aebi. 2003. Cryo-electron tomography provides novel insights into nuclear pore architecture: implications for nucleocytoplasmic transport. *J. Mol. Biol.* 328:119-30.

- Strasser, A., A. Dickmanns, R. Lührmann, and R. Ficner. 2005. Structural basis for m3G-cap-mediated nuclear import of spliceosomal UsnRNPs by snurportin1. *EMBO J.* 24:2235-43.
- Strawn, L.A., T. Shen, N. Shulga, D.S. Goldfarb, and S.R. Wentz. 2004. Minimal nuclear pore complexes define FG repeat domains essential for transport. *Nat. Cell Biol.* 6:197-206.
- Strong, M., M.R. Sawaya, S. Wang, M. Phillips, D. Cascio, and D. Eisenberg. 2006. Toward the structural genomics of complexes: crystal structure of a PE/PPE protein complex from *Mycobacterium tuberculosis*. *Proc. Natl. Acad. Sci. U.S.A.* 103:8060-5.
- Suhre, K., and Y.-H. Sanejouand. 2004. Elnemo: a normal mode web server for protein movement analysis and the generation of templates for molecular replacement. *Nucleic Acids Res.* 32:W610-4.
- Supek, F., D.T. Madden, S. Hamamoto, L. Orci, and R. Schekman. 2002. Sec16p potentiates the action of COPII proteins to bud transport vesicles. *J. Cell Biol.* 158:1029-38.
- Tang, B.L., Y. Wang, Y.S. Ong, and W. Hong. 2005. COPII and exit from the endoplasmic reticulum. *Biochim. Biophys. Acta.* 1744:293-303.
- ter Haar, E., S.C. Harrison, and T. Kirchhausen. 2000. Peptide-in-groove interactions link target proteins to the β -propeller of clathrin. *Proc. Natl. Acad. Sci. U.S.A.* 97:1096-100.
- ter Haar, E., A. Musacchio, S.C. Harrison, and T. Kirchhausen. 1998. Atomic structure of clathrin: a β propeller terminal domain joins an α zigzag linker. *Cell.* 95:563-73.
- Thuman-Commike, P.A., B. Greene, J.A. Malinski, J. King, and W. Chiu. 1998. Role of the scaffolding protein in P22 procapsid size determination suggested by T = 4 and T = 7 procapsid structures. *Biophys. J.* 74:559-68.
- Tran, E.J., and S.R. Wentz. 2006. Dynamic nuclear pore complexes: life on the edge. *Cell.* 125:1041-53.
- Vagin, A.A., and M.N. Isupov. 2001. Spherically averaged phased translation function and its application to the search for molecules and fragments in electron-density maps. *Acta Cryst.* D57:1451-6.
- Vasu, S., S. Shah, A. Orjalo, M. Park, W.H. Fischer, and D.J. Forbes. 2001. Novel vertebrate nucleoporins Nup133 and Nup160 play a role in mRNA export. *J. Cell Biol.* 155:339-54.
- Vonrhein, C., E. Blanc, P. Roversi, and G. Bricogne. 2007. Automated structure solution with autoSHARP. *Methods Mol. Biol.* 364:215-30.
- Walther, T.C., A. Alves, H. Pickersgill, I. Loiodice, M. Hetzer, V. Galy, B.B. Hülsmann, T. Köcher, M. Wilm, T. Allen, I.W. Mattaj, and V. Doye. 2003. The conserved Nup107-160 complex is critical for nuclear pore complex assembly. *Cell.* 113:195-206.
- Waterhouse, A.M., J.B. Procter, D.M.A. Martin, M. Clamp, and G.J. Barton. 2009. Jalview Version 2--a multiple sequence alignment editor and analysis workbench. *Bioinformatics.* 25:1189-91.

- Watson, P., A.K. Townley, P. Koka, K.J. Palmer, and D.J. Stephens. 2006. Sec16 defines endoplasmic reticulum exit sites and is required for secretory cargo export in mammalian cells. *Traffic*. 7:1678-87.
- Weis, K. 2003. Regulating access to the genome: nucleocytoplasmic transport throughout the cell cycle. *Cell*. 112:441-51.
- Weis, K. 2007. The Nuclear Pore Complex: Oily Spaghetti or Gummy Bear? *Cell*. 130:405-407.
- Weis, K., U. Ryder, and A.I. Lamond. 1996. The conserved amino-terminal domain of hSRP1 α is essential for nuclear protein import. *EMBO J*. 15:1818-25.
- Weiss, M. 2001. Global indicators of X-ray data quality. *Journal of Applied Crystallography*. 34:130-135.
- Wente, S.R., and G. Blobel. 1994. NUP145 encodes a novel yeast glycine-leucine-phenylalanine-glycine (GLFG) nucleoporin required for nuclear envelope structure. *J. Cell Biol*. 125:955-69.
- Will, C.L., and R. Lührmann. 2001. Spliceosomal UsnRNP biogenesis, structure and function. *Curr Opin Cell Biol*. 13:290-301.
- Winey, M., D. Yarar, T.H. Giddings, and D.N. Mastronarde. 1997. Nuclear pore complex number and distribution throughout the *Saccharomyces cerevisiae* cell cycle by three-dimensional reconstruction from electron micrographs of nuclear envelopes. *Mol. Biol. Cell*. 8:2119-32.
- Wlodawer, A., W. Minor, Z. Dauter, and M. Jaskolski. 2008. Protein crystallography for non-crystallographers, or how to get the best (but not more) from published macromolecular structures. *FEBS J*. 275:1-21.
- Wohlwend, D., A. Strasser, A. Dickmanns, and R. Ficner. 2007. Structural basis for RanGTP independent entry of spliceosomal U snRNPs into the nucleus. *J. Mol. Biol*. 374:1129-38.
- Wolfe, K.H., and D.C. Shields. 1997. Molecular evidence for an ancient duplication of the entire yeast genome. *Nature*. 387:708-13.
- Xing, Y., T. Böcking, M. Wolf, N. Grigorieff, T. Kirchhausen, and S.C. Harrison. 2010. Structure of clathrin coat with bound Hsc70 and auxilin: mechanism of Hsc70-facilitated disassembly. *EMBO J*. 29:655-65.
- Ybe, J., F. Brodsky, K. Hofmann, K. Lin, S. Liu., L. Chen, T. Earnest, R. Fletterick and P. Hwang. 1999. Clathrin self-assembly is mediated by a tandemly repeated superhelix. *Nature*. 399:371-5.
- Zabel, U., V. Doye, H. Tekotte, R. Wepf, P. Grandi, and E. Hurt. 1996. Nic96p is required for nuclear pore formation and functionally interacts with a novel nucleoporin, Nup188p. *J. Cell Biol*. 133:1141-52
- Zhang, X., S. Chen, S. Yoo, S. Chakrabarti, and T. Zhang. 2008. Mutation in Nuclear Pore Component NUP155 Leads to Atrial Fibrillation and Early Sudden Cardiac Death. *Cell*. 135:1017-27
- Zilman, D., S. Talia, B. Chait, M. Rout, and M. Magnasco. 2007. Efficiency, Selectivity, and Robustness of Nucleocytoplasmic Transport. *PLoS Comput Biol*. 3:e125.
- Zuccolo, M., A. Alves, V. Galy, S. Bolhy, E. Formstecher, V. Racine, J.-B. Sibarita, T. Fukagawa, R. Shiekhattar, T. Yen, and V. Doye. 2007. The human Nup107-160

- nuclear pore subcomplex contributes to proper kinetochore functions. *EMBO J.* 26:1853-64.
- Zuleger, N., N. Korfali, and E.C. Schirmer. 2008. Inner nuclear membrane protein transport is mediated by multiple mechanisms. *Biochem Soc Trans.* 36:1373-7.